ISSN 1173-5996

Experimental Fire Tests of Two-Way Concrete Slabs

Linus Lim
University of Canterbury

Colleen Wade
BRANZ Limited

University of Canterbury
Fire Engineering Research Report 02/12

September 2002

School of Engineering
University of Canterbury
Private Bag 4800
Christchurch, New Zealand

Phone 64 3 366-7001
Fax 64 3 364-2758

BRANZ Limited
Private Bag 50 908
Porirua City, New Zealand

Phone 64 4 237-1170
Fax 64 4 237-1171

Acknowledgments

This research project was conducted as part of a doctorate degree by the first author under the supervision of Associate Professors Andy Buchanan and Peter Moss of the Civil Engineering Department of the University of Canterbury, supported by a BHP NZ Steel doctoral scholarship.

The authors gratefully acknowledge the funding and contributions provided by the sponsors of this project. The financial sponsors of the project were the Heavy Engineering Research Association (HERA), BHP NZ Steel, Speedfloor Holdings, Dimond Industries, OneSteel and Nelson Stud Welding. Material contributions to the project were made by Firth Industries, Pacific Steel and Fletcher EasySteel. BRANZ Limited provided major sponsorship of the fire tests.

Many thanks to Mr. Geoff Bird from BHP NZ Steel and Mr. Charles Clifton from HERA for their support and advice, and providing the motivation for this project.

Thanks also to Mr. Des Bull and Mr. Jeff Matthews for their advice and help during the early stages of this project.

Finally, special thanks go to the technicians, Mr. Colin Bliss from the University of Canterbury and Mr. Rik Engel and Mr. Brett Millin from BRANZ Limited, for their help and technical expertise during the construction and testing of the slabs.

ABSTRACT

A series of full-scale fire tests conducted at the Cardington steel framed test building in the United Kingdom have shown that unprotected composite floor slabs do not collapse after a compartment burnout, despite suffering considerable deformations and very high measured steel temperatures. When the unprotected steel beams weakened, the load resistance progressively transferred from the beams to the slabs which resisted the loads by tensile membrane action. These tests have prompted extensive computer modelling by many researchers to simulate the behaviour of steel framed buildings and tensile membrane action of the slabs under fire conditions. However, there are no published fire tests of two-way concrete slabs in a controlled furnace environment

This report describes the fire tests of two-way concrete slabs conducted at the BRANZ fire resistance furnace. The tests were conducted to investigate the behaviour of unrestrained simply supported slabs in a controlled furnace environment. The test data can be used to verify current simple design methods and sophisticated computer models.

Six slabs were tested, comprising three reinforced concrete flat slabs and three composite steel-concrete slabs. The slabs measured 3.3m by 4.3m and had thicknesses ranging from 90mm to 130mm. The three flat slabs had different quantities of reinforcing steel to investigate their effect on controlling crack widths to prevent integrity failure. The slabs were simply supported on all four sides over the furnace with no horizontal restraint. The slabs were subjected to a live load of 3.0kPa and were heated on the underside with the gas time temperature curve following the ISO 834 standard fire for three hours.

The slabs performed very well in the fire tests, supporting the loads for the full duration of three hours without collapse. By three hours, the gas temperatures had reached 1100°C and high temperatures were measured across the depth of the slab. The temperatures of the reinforcing steel exceeded 700°C. All the slabs suffered extensive surface cracking and loss of moisture. Some of the slabs suffered large midspan deflections (up to 270mm) and full depth cracks which were associated with the yield line crack pattern. The slabs with higher steel contents and closer bar spacings suffered only surface cracking, while the slabs with the lower steel content suffered full-depth cracks. The cold-drawn mesh used in the tests performed well and did not fracture as might have been expected if such large strains had been imposed at ambient temperature; this is due to the increased ductility of the steel caused by the elevated temperatures.

The slabs resisted collapse even though the calculated ultimate load capacities had dropped significantly below the level of the applied loads. The structural fire resistance of the slabs in the tests exceeded the predictions of code recommendations. The tests illustrated the significant effect of tensile membrane action on the structural fire resistance of two-way slabs which resisted collapse despite significant loss of flexural strength.

CONTENTS

LIST OF FIGURES

LIST OF TABLES

1. INTRODUCTION

1.1. General

In recent years, real fires and full scale fire tests in multi-storey steel framed buildings have shown that unprotected steel beams and slabs do not collapse in real fires, despite suffering very large vertical deflections (Bailey et al, 1999). This is due to the high degree of redundancy of the structure which allows loads on the beams and slabs above the fire compartment to be redistributed to cooler parts of the structure. The loads supported by the heated beams, are transferred to the composite slabs and resisted by tensile membrane action.

This has led to intensive analytical and experimental research by many researchers to understand this mechanism in greater depth. An independent test was conducted at the Building Research Establishment (BRE) to simulate the behaviour of simply supported two-way slabs under fire conditions (Bailey et al, 2000). The test was conducted at ambient temperatures with the steel decking of the composite slab removed to represent the depleted strength of the steel decking under fire conditions. The test did not account for the thermal effects on the slab behaviour which include thermal bowing and expansion of the slab, and strength degradation of the steel and concrete. The need to determine the slab performance under representative severe fire conditions led to the fire tests of concrete slabs at BRANZ Limited (Building Research Association of New Zealand).

1.2. Objectives

The objectives of the fire tests were to:

- Investigate the behaviour of concrete and composite two-way floor slabs, in a controlled furnace test.
- Investigate the influence of tensile membrane action on the structural fire resistance of the slabs.
- Verify the SAFIR finite element program (Franssen et al, 2002) for further analyses of other slab configurations.
- Verify the current analytical design methods proposed by Bailey (2001) and Clifton et al (2001) for slabs under severe fire conditions.

1.3. Scope

This report describes the fire resistance tests of six concrete slabs using the BRANZ fire resistance furnace. The verification of the current analytical design methods by Bailey (2001) and Clifton et al (2001) and the SAFIR finite element program are presented by Lim (2003).

The slabs were simply supported on all four sides above the furnace and were horizontally unrestrained. The slabs were heated on the underside with the furnace gas time temperature following the prescribed in AS/NZS1530.4 (similar to ISO 834), while subjected to a constant uniformly distributed load. The floor slabs consisted of three reinforced concrete plain flat slabs and three different proprietary composite steel-concrete slabs. The opening of the furnace measured 3.0m by 4.0m and the slabs were constructed as 3.3m wide by 4.3m long to allow the edges of the slab to be supported over the furnace opening.

Different types of reinforcing mesh were used in the different slabs to determine the steel content required for crack control to prevent integrity failure. The performance of hard-drawn reinforcing mesh at elevated temperatures and the effect of the bar spacing of the mesh on the deformation capacity of the slabs were assessed.

1.4. Parties involved

The parties that were involved in this test were:

Researcher:	Linus Lim, University of Canterbury (Supported by the BHP New Zealand Steel scholarship)
Supervisors:	Associate Professor Andy Buchanan, University of Canterbury Associate Professor Peter Moss, University of Canterbury

Testing organisation:

BRANZ Limited	Colleen Wade, Merv Godkin, Paul Wong

Industry Partners:

The industry partners that provided financial contributions to the tests were:

Heavy Engineering Research Association (HERA)	Charles Clifton
BHP New Zealand Steel Limited	Geoff Bird
Speedfloor Holdings	Graeme Stubbing
Dimond Industries	Mike Klemick, Stuart Moore
OneSteel Australia	Anthony Ng
Nelson Stud Welding, Forgan Jones Structural Ltd.	Ian Welch

Construction materials for the tests were donated by:

Firth Industries Limited	Len McSaveney, Baldev Kesha
Fletcher Easysteel	Mark Janssens
Pacific Steel	Rajiva Kumar

Technicians

University of Canterbury	Collin Bliss, Russell McConchie, Mike Weavers
BRANZ	Rick Engel, Brett Millin

1.5. Organisation of the tests

The slabs were constructed between July and November 2001, at the Civil Engineering Laboratory of the University of Canterbury, Christchurch. After the slabs were constructed, they were stored in a warehouse at a separate location in Christchurch to cure and dry. In April 2002, the slabs were shipped to Wellington where they were stored at the BRANZ Fire Laboratory until the scheduled date of the tests. The fire tests were conducted at BRANZ during the period 21st June 2002 to 5th July 2002.

1.6. Organisation of this report

This report consists of 9 chapters. Chapter 1 gives an introduction to the project. Chapter 2 presents the theoretical background and past research which led to this project. Chapter 3 describes the slab specimens that were tested. Chapter 4 describes the set up of the test and chapter 5 covers the overall implementation of the project.

Chapter 6 discusses the results of the fire tests. The conclusions are presented in Chapter 7 and Chapter 8 provides the references that were used in this report. The appendices of the report are in the last chapter.

Data from the tests is available in electronic form from the authors.

2. BACKGROUND

2.1. Composite floor slab behaviour in fire

Composite slabs are normally designed as one-way spanning beams under ambient and fire conditions, resisting loads through bending action. To increase the strength of these slabs under fire conditions, fire emergency reinforcing bars are placed in the troughs of the composite slabs, to increase the flexural strength of the slabs during the fire. However, actual fires in steel buildings in England (Broadgate and Churchill Plaza) and full scale fire tests (Bailey et al, 1999) have shown that the unprotected composite slabs do not collapse during a severe fire. The slabs behaved as membranes during the fire, supported by the colder perimeter beams and protected columns, and resisted the applied loads by tensile membrane action.

2.2. Experimental studies of composite floor systems in fire

2.2.1. Cardington full scale fire tests

A series of full-scale fire tests were conducted at the 8 storey steel framed test building at the Cardington Large Building Test Facility in 1995/1996 (Bailey et al., 1999). The fire tests were conducted by British Steel and BRE, involving different compartment sizes and test configurations at different locations in the building. In the tests, the soffit of the trapezoidal composite deck and all the steel beams were unprotected but the columns were fully protected up to the soffit of the slabs. The maximum fire temperatures in the tests exceeded 1000°C. The composite floors suffered large deflections (~span/20) but there was no structural collapse. The tests showed that when the unprotected beams weakened at high temperatures, the load resistance was progressively transferred to the slabs, resisting the loads by tensile membrane action.

These tests have lead to extensive computer modelling by many researchers to understand the behaviour of steel framed structures and tensile membrane action in the slabs under fire conditions (Elghazouli et al, 2001; Huang et al, 1999a, 1999b, 2001; Lamont et al, 2001; Sanad et al, 1999).

2.2.2. BRE tests

Following the full scale tests at the Cardington steel building, a test was conducted at the BRE to show the effects of membrane action in slabs exposed to elevated temperatures (Bailey et al, 2000). The slab measured 9.5m x 6.5m and was built with a trapezoidal-shaped composite steel deck beneath it. The troughs of the steel deck were 60mm deep and the slab had an overall thickness of 150mm. After the slab was cast, the steel decking was later removed from beneath the slab, leaving the concrete slab reinforced only with the A142 mesh. The absence of the steel decking represented the depleted strength and stiffness to the slab during a real fire. The slab was vertically supported at the perimeter on beams and columns but it was

horizontally unrestrained. The test showed that a composite slab simply supported on four edges could carry loads considerably in excess of those predicted by conventional yield line design principles.

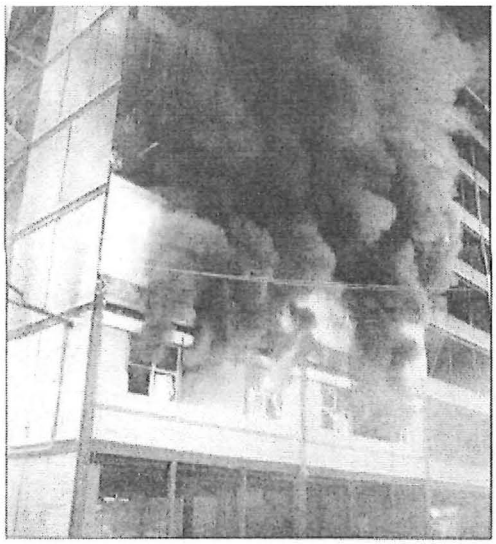

Figure 2-1: Fire tests at the Cardington steel building (Newman et al, 2000)

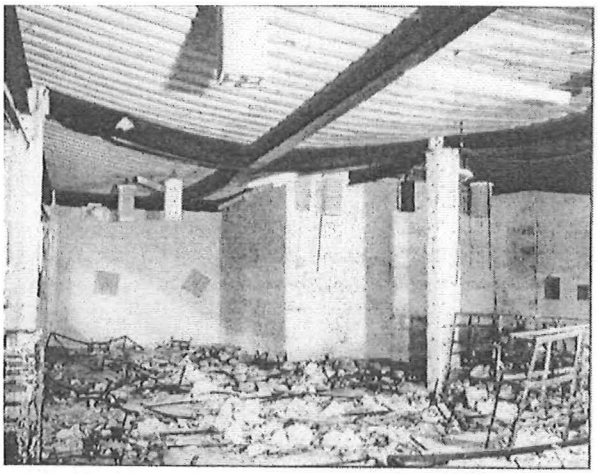

Figure 2-2: Large deflections of the composite slabs following the fire tests at the Cardington steel building (Newman et al, 2000)

2.3. Tensile membrane action

The actual collapse loads of reinforced concrete slabs have been shown by earlier researchers to be larger than predicted by yield line theory. Yield line theory assumes a flexural collapse mode and does not consider the effects of strain hardening of the reinforcement and membrane effects. Earlier tests have been conducted by Sawczuk et al (1965) and Hayes (1968) to investigate the effects of tensile membrane action on unrestrained two-way spanning slabs. These slabs were tested at ambient conditions and did not consider the effects of elevated temperatures. Based on these tests, analytical methods for considering membrane action in unrestrained slabs were presented by Sawczuk et al (1965) and Hayes (1968).

2.4. Design Methods

2.4.1. BRE design method

Following the tests conducted at the BRE, Bailey et al (2000a, 2000b) and Bailey (2001) have developed a method for determining the ultimate load carrying capacity of slabs incorporating the effects of tensile membrane enhancement under elevated temperatures. The new method considers the failure mode which has a crack in the middle of the slab. This failure mode differs from the failure mode presented by earlier researchers (Sawczuk et al, 1965 and Hayes, 1968) where full depth cracks formed at the intersection of the yield lines. This new method has shown excellent agreement with the results of the fire tests undertaken at the Cardington steel framed test (Bailey et al, 2000).

The postulated membrane behaviour is not yet fully understood, especially at elevated temperatures. Newman et al (2000) have applied this procedure to a limited range of

conditions involving low to moderate fire severity, in which the influence of elevated temperatures on the components is expected to be minor.

2.4.2. HERA design method

Clifton et al (2001) have extended the design method proposed by Bailey (2001) for application in New Zealand. This method considers higher fire severities compared to those specified for the UK application. This design method takes account of the effects of elevated temperatures on the load resisting components and the strength contributions of the secondary beams to the slabs.

3. SPECIMEN DETAILS

3.1. Slab configurations

Six slabs were tested at the BRANZ furnace. The slabs consisted of three flat slabs and three proprietary composite steel-concrete slabs. Each slab measured 3.3m wide by 4.3m long. The thicknesses of the slabs varied from 90mm to 130mm. The flat slabs were 100mm thick and differed from each other by the amount of reinforcing steel. The different amounts of reinforcing were intended to investigate its effect on controlling the size of the cracks in the slabs to prevent integrity failure.

The six configurations that were tested are shown in Table 1:

	Slab	Slab thickness	Reinforcing mesh	Concrete cover
1.	661 flat slab	100mm	661 mesh	25mm
2.	HD12 flat slab	100mm	HD12 bars	25mm
3.	D147 flat slab	100mm	D147	25mm
4.	130mm Hi-bond slab	130mm	D147	20mm above steel ribs.
5.	130mm Traydec slab	130mm	D147	15mm above steel ribs.
6.	Speedfloor	90mm	661 mesh	25mm

Table 1: Configuration of slabs that were tested

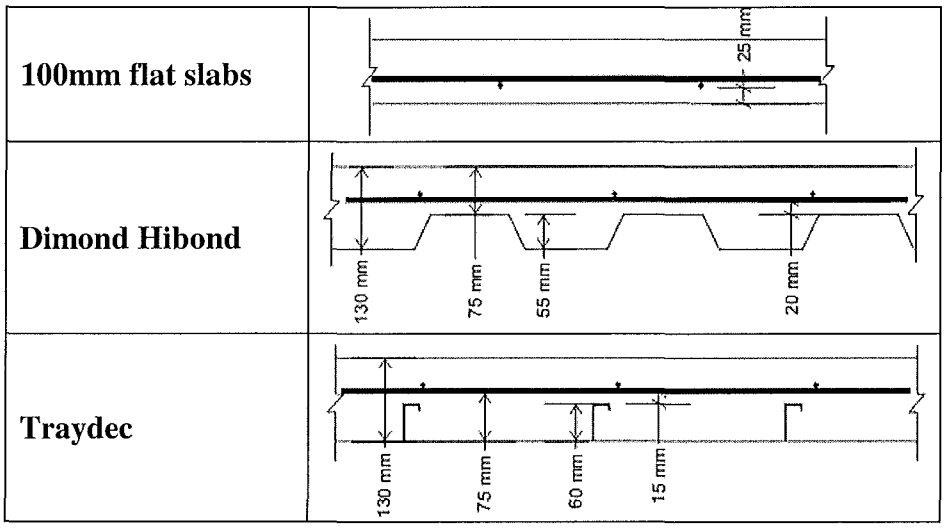

Speedfloor	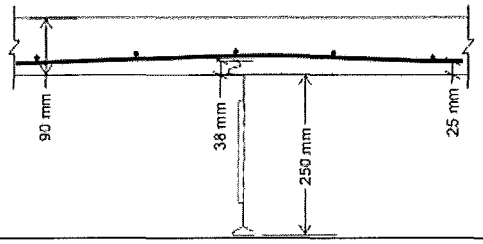

Table 2: Cross section of slabs that were tested

3.2. Reinforcement

Different types of reinforcing steel were used for the tests, which consisted of hard-drawn mesh and hot-rolled reinforcing bars (Table 3). The 25mm clear concrete cover to the reinforcement in the flat slabs provided a two-hour fire resistance stability rating, in accordance with the New Zealand Concrete Structures Standard (NZS, 1995). The reinforcement configurations for slabs 4 and 5 of Table 1 was chosen to obtain a uniform moment capacity for the two composite steel-concrete slabs, assuming the steel decking did not contribute to the bending strength in the fire.

The mesh in all the slabs was arranged so that the bars that spanned the short direction were placed below the bars that spanned in the long direction. This increased the lever arm of the bars spanning in the short direction to allow larger moments to be carried across the short direction. The ribs of the *Dimond Hi-bond* and *Tray-dec* steel decking and the joists of the Speedfloor slab spanned parallel to the long span of the furnace.

Reinforcing steel	Description	Bar diameter	Grid spacing	Yield stress*	Steel content	Strain limit*
D147 mesh	Cold drawn deformed mesh	8.7mm	300mm	565 MPa	198mm^2/m	2.3 %
661 mesh	Cold drawn plain mesh	7.5mm	150mm	568 MPa	295mm^2/m	3.2 %
HD12 bars	Hot rolled deformed bars	12mm	200mm	468 MPa	565mm^2/m	21 %

*Average of three samples

Table 3: Properties of the reinforcing steel used in the slabs (At ambient conditions).

Steel decking/ joists	Steel deck/joist thickness	Yield stress
Dimond Hibond	0.75mm	550 MPa
Traydec	0.75mm	550 MPa
Speedfloor	3mm	350 MPa

Table 4: Properties of the steel decking/joists of the composite slabs

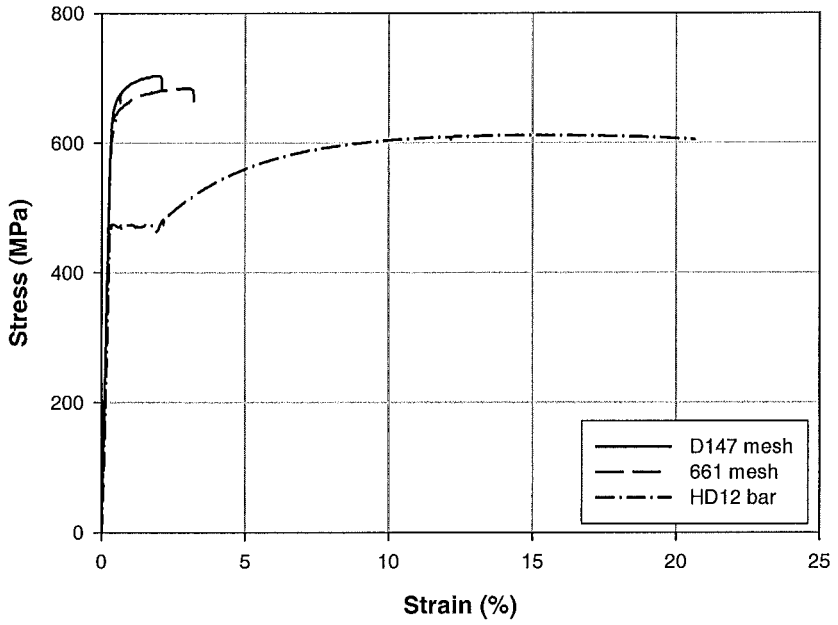

Figure 3-1: Stress strain curves of reinforcing steel at ambient conditions.

3.3. Concrete

The concrete that was used in the tests was normal weight concrete, supplied by *Firth Industries Ltd.* 19mm greywacke (siliceous) aggregates were used. The specified compressive strength of the concrete is 30MPa. The compressive strengths of the concrete were determined by cylinder crushing tests conducted 7 days and 28 days after the concrete was cast. Crushing tests were also conducted a week after the fire tests. The results of the crushing tests are shown in Table 5.

Pour No.	Slab	Curing time (days)	28 day stgh (MPa)	15 July 2002 (Fire test) (MPa)
Batch 1	Hibond	308	30.2	32.1
	Traydec	310	30.2	32.1
Batch 2	147 slab	293	32.8	36.6
	661 slab	287	32.8	36.6
Batch 3	HD12 slab	216	22.6	36.7
Batch 4	Speedfloor	214	31.5	37.6

Table 5: Compressive strengths of concrete

3.4. Strain gauge and thermocouple layouts

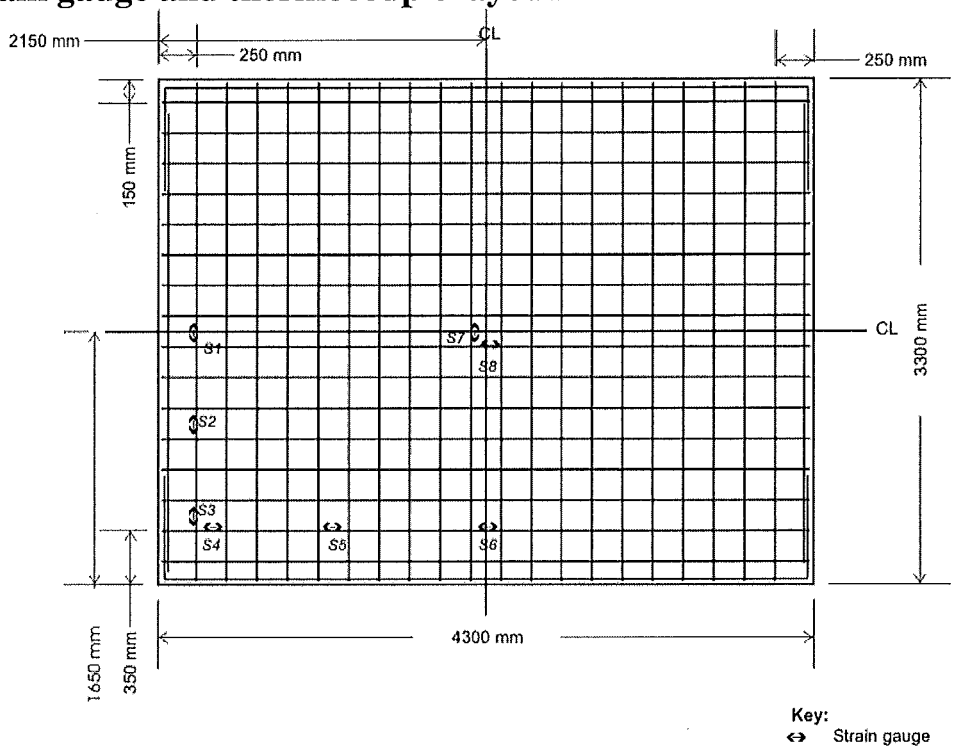

Figure 3-2: Typical layout of strain gauges in the slabs

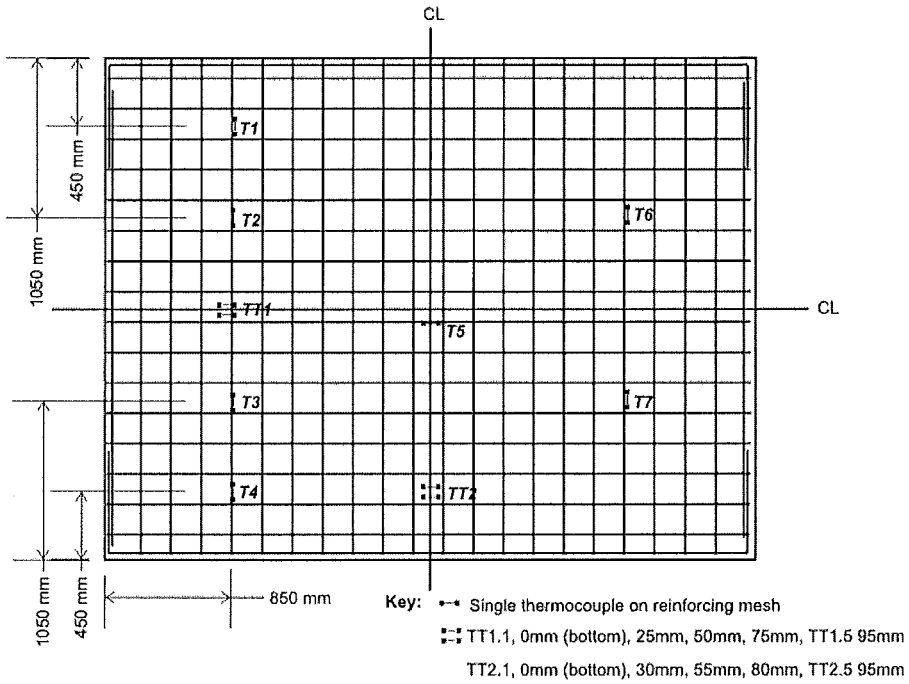

Figure 3-3: Typical layout of thermocouples in the slabs

Slab		No. of strain gauges	No. of thermocouples
1.	661 flat slab	8	7 thermocouples on reinforcing steel 5 key thermocouples
2.	HD12 flat slab	8	7 thermocouples on reinforcing steel 2 thermocouple trees 5 key thermocouples
3.	D147 flat slab	26	7 thermocouples on reinforcing steel 2 thermocouple trees 5 key thermocouples
4.	130mm Hi-bond slab	8	7 thermocouples on reinforcing steel 2 thermocouple trees 5 key thermocouples
5.	130mm Traydec slab	20	5 thermocouples on reinforcing steel 2 thermocouple trees 5 key thermocouples
6.	90mm flat slab on Speedfloor joists	14	5 thermocouples on reinforcing steel 2 thermocouple trees 5 key thermocouples

Table 6: Strain gauges and thermocouples in each slab.

Figure 3-2 shows the typical strain gauge layout in the slabs. This figure shows a slab with 8 strain gauges; arranged to measure the strains in the reinforcing steel in the middle and the edges of the slab. Some of the slabs were more heavily instrumented to measure the strains at other locations such as at the quarter spans of the slab or at the steel joists (in the Speedfloor slab). The layouts of the strain gauges for each of the slabs are located in the Appendix. Figure 3-3 shows the typical layout of thermocouples and thermocouple trees in a slab. The thermocouples placed at mid-height of the reinforcing bars are labelled as T1, T2, etc. The thermocouple trees are labelled as TT1 and TT2 and the key thermocouples placed on the unheated surface of the slab are labelled as K1 to K5. Table 6 shows the number of strain gauges and thermocouples in each slab.

3.4.1. Strain gauges

The strains in the reinforcing bars of the slabs were measured with high-temperature resistant strain gauges. ZFLA-6.350-11 strain gauges were used, obtained from Tokyo Sokki Kenkyujo, Japan. These strain gauges are accurate up to 300°C and have a maximum strain limit of 1% strain. The strain gauges were attached with high temperature resistant glue, water-proof coating and wires in order for the gauge to function up to its maximum operational temperature.

The wires from the strain gauges and thermocouples were laid so that they came out at three locations at one side of each slab. In order to minimise the usage (and the cost) of the high temperature wires for the strain gauges, normal wire was used to lead the connections of the strain gauges out of the slab. Long lengths of normal wire were connected to short lengths of high temperature resistant wire, which in turn were connected to the strain gauges. To prevent

the normal wires from being exposed to the high temperatures, they were suspended above the level of the strain gauges on high tensile wires. This increased the cover to the normal wires to ensure that the wires do not burn out and fail before the strain gauges.

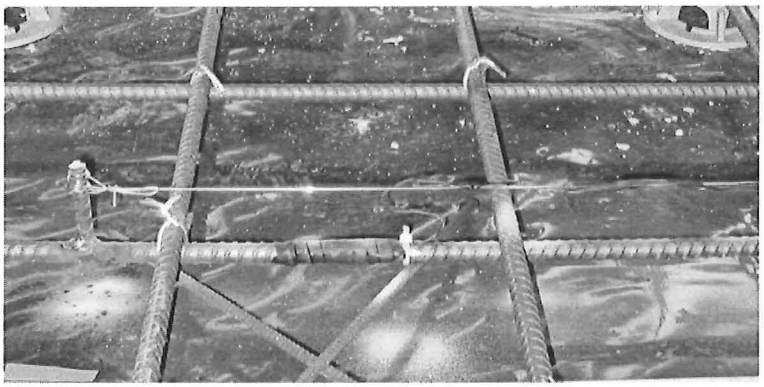

Figure 3-4: Strain gauge attached to reinforcing steel and sealed with water proofing. Note the strain gauge wires have been suspended above the strain gauges on a high tensile wire.

3.4.2. Specimen temperature measurement

All the specimens had type-K thermocouples on the reinforcing steel and thermocouple trees across the thickness of the slabs to measure the steel temperatures and temperature distributions across the slabs. The thermocouples on the reinforcing steel were placed at mid-height of the steel bars.

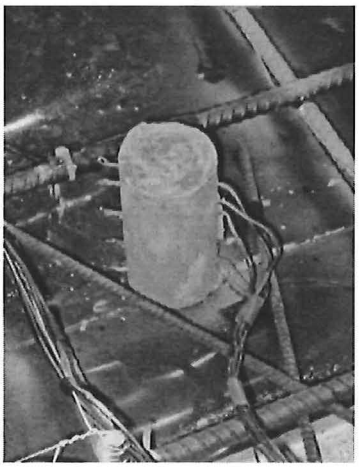

Figure 3-5: A thermocouple tree placed in one of the slabs prior to pouring of the concrete.

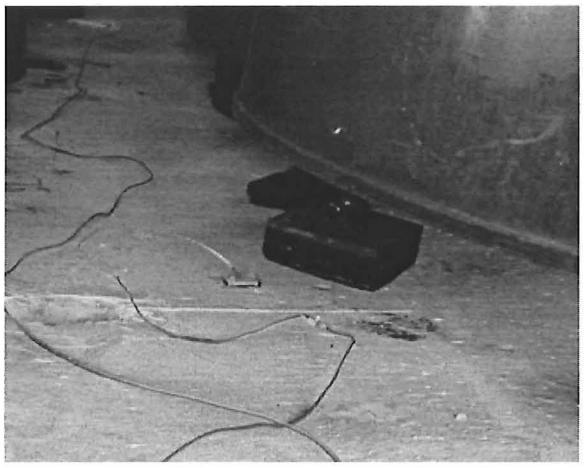

Figure 3-6: A key thermocouple for measuring temperatures on the unheated surface.

Figure 3-5 shows a typical thermocouple tree. Each thermocouple tree consisted of 5 thermocouples held in a mortar cylinder block. The trees were constructed by setting the thermocouples wires in a steel mould filled with mortar. When the mortar had set, the steel mould was removed and the tree was positioned in the slab. Five key thermocouples were placed on the unheated surface of each slab, with one thermocouple in the middle of the slab and the others in the four quadrants of the slab. Figure 3-6 shows one of the key thermocouples attached to the unheated side of the slab.

4. TEST CONFIGURATION

4.1. General

This section describes the slab loading and support conditions. It also describes the instrumentation used to measure the deflections and temperatures in the slab.

4.2. Testing standard

The fire tests were conducted on an oil-fired furnace. The fire curve that was used to heat the slabs was the ISO 834 standard fire curve. The three standard categories of failure in typical fire resistance tests are:

1. Structural stability
2. Integrity
3. Insulation

The tests were conducted to a maximum of three hours and were only terminated at an earlier time if the slab deformed to the point of imminent structural collapse which may lead to collapse and damage the furnace. The test would also be stopped before three hours if an integrity failure occurred, allowing a significant amount of flames to pass through the slab and damage the potentiometers.

4.3. Fire type

Figure 4-1 shows the time-temperature curve of the ISO 834 standard fire in the fire tests. The maximum duration of the tests was 3 hours.

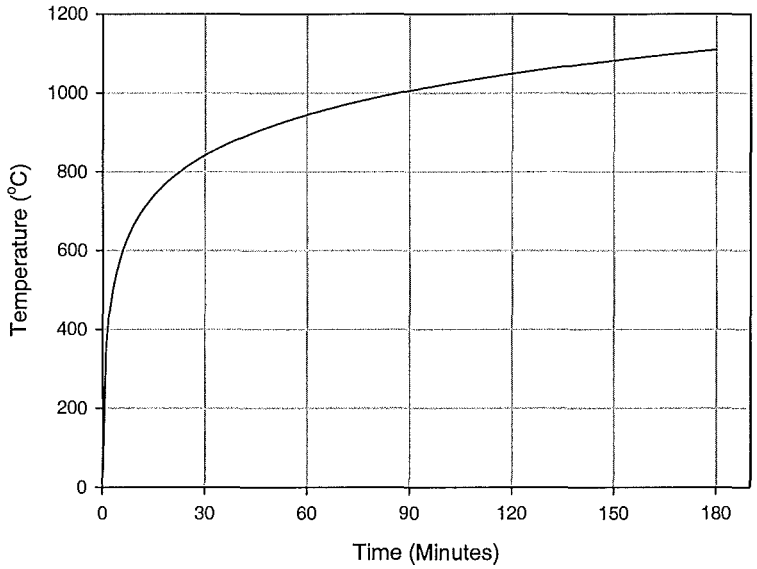

Figure 4-1: ISO 834 standard fire curve used in the tests.

4.4. Fire testing schedule

The slabs were tested in the sequence shown in Table 1. The flat slabs with medium (661 mesh) and high (HD12) levels of reinforcing were tested first to gauge whether or not the level of loading was appropriate for the weaker flat slab and composite slabs, and to detect

any problems with the data logging equipment for the subsequent slabs which had more instrumentation.

4.5. Support conditions

4.5.1. Vertical support

The slabs were simply supported on four edges and were unrestrained against horizontal movement. The slabs were supported over the furnace on a rectangular frame which was made of steel C-channels with a reinforced concrete beam lining the internal perimeter. The slab was directly supported on the concrete beam, which also prevents the outer steel frame from heating up.

The slabs were vertically supported on its four edges on top of the concrete beam on cylindrical rollers. The rollers allowed the slab to freely rotate and roll horizontally at the supports. The rollers were positioned around the perimeter of the steel frame on strips of 5mm thick steel plates which were placed on the concrete beam and welded to the steel frame (Figure 4-2). The steel plates formed a smooth rolling surface between the rollers and the concrete beam because the surface of the concrete beam was rough and would generate a lot of friction between the rollers.

A 16mm square rod was welded to the edge of the steel plates to stop the rollers from rolling into the furnace (Figure 4-10). The cylindrical rod was placed continuously around the perimeter of the supporting frame to simulate a continuous support. Mineral wool was glued to the vertical faces of the concrete beam (Figure 4-3 and Figure 4-10) to prevent the rollers from being directly exposed to the flames and to prevent the flames from coming out of the gap between the rollers and the slab.

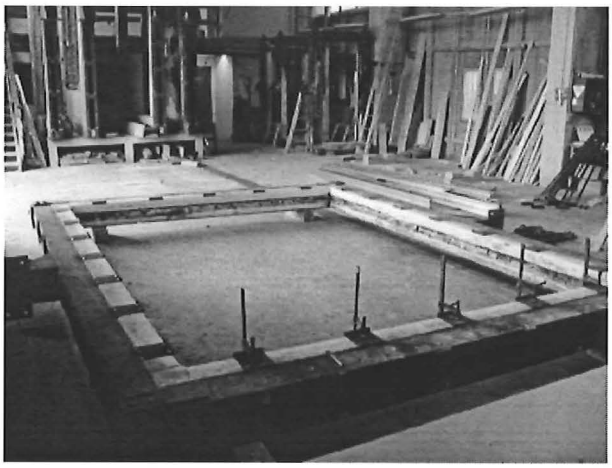

Figure 4-2: Rectangular frame used to support the slab over the furnace. Note the 150mm wide plates welded to the steel frame, over the concrete beam.

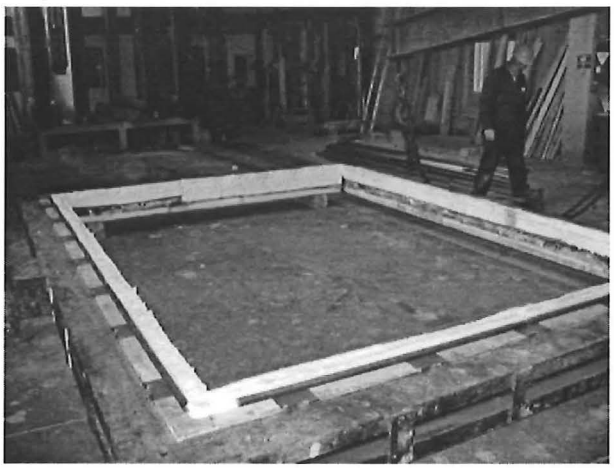

Figure 4-3: Steel rollers positioned on the frame with the mineral wool lining the internal perimeter.

A 150mm wide steel flashing was placed beneath the perimeter of each slab when they were constructed. This steel flashing minimised the friction between the bottom surface of the concrete slab and the rollers to allow the slab to slide freely. The steel flashing also prevented local crushing of the concrete when the slab was supported on the rollers. The slab was

positioned onto the steel frame and both the frame and slab were lifted simultaneously and placed on the furnace. Immediately after each test, the frame and slab were lifted off the furnace.

Figure 4-4: Steel flashing placed around the perimeter prior to pouring of the concrete.

Figure 4-5: Steel flashings at the bottom side of the slab.

4.5.2. Corner clamps

The corners of the first two tests (661 and HD12 flat slabs) were not clamped down and were free to lift. The amount of curling of the corners of the slabs seen during the first two tests was very large and would not represent the behaviour of a slab under realistic support conditions found in a typical building.

The corners of the slabs were clamped down with steel angles placed diagonally across the corners. The steel angles at two of the corners were welded to the supporting steel frame (Figure 4-6). These steel angles were welded with sufficient slack to accommodate the different slab thicknesses. Each slab was slid under the welded steel angles and the gap between the angle and the slab was filled with steel plates. The other two corners were clamped by bolting the steel angles to the supporting steel frame (Figure 4-7).

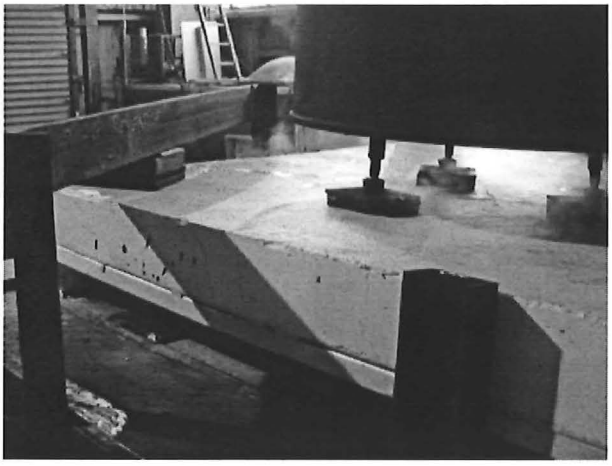

Figure 4-6: Steel angle welded to the supporting steel frame to clamp down the corners.

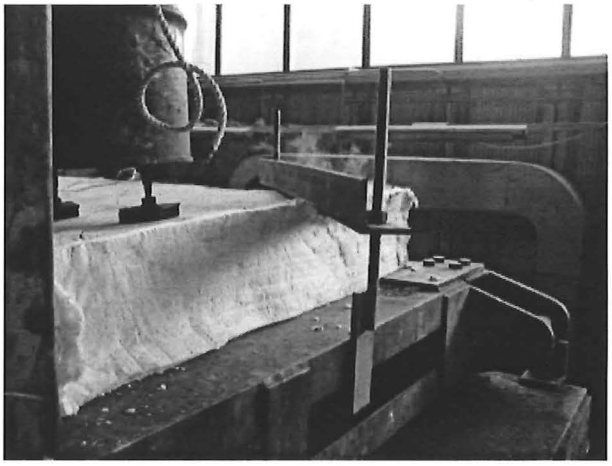

Figure 4-7: Steel angle bolted to the supporting steel frame to clamp down the corners.

4.5.3. Horizontal restraint

Although the outward expansion of the slabs was unrestrained, their inward horizontal travel was limited to prevent the edges of the slabs from moving inwards excessively when the slabs undergo large vertical deflections. Short lengths of steel C-channels were bolted to inserts which were cast into the sides of the slab. If the slab edges moved inwards excessively, the C-channels would catch the rollers, which in turn will catch the square sections welded to the edges of the steel strips, and prevent the slab from falling into the furnace.

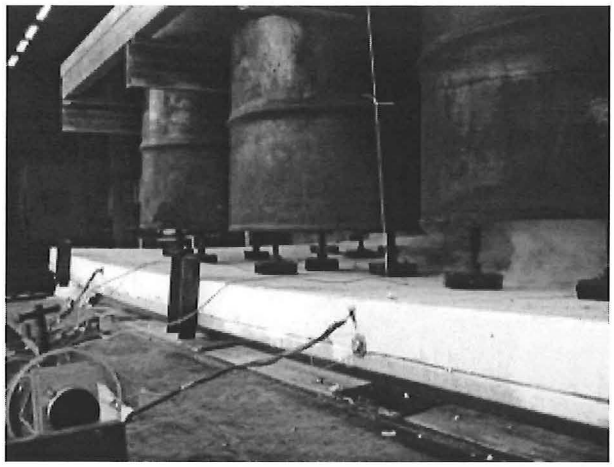

Figure 4-8: Steel C-channels bolted to the sides of each slab to prevent collapse of the slab into the furnace.

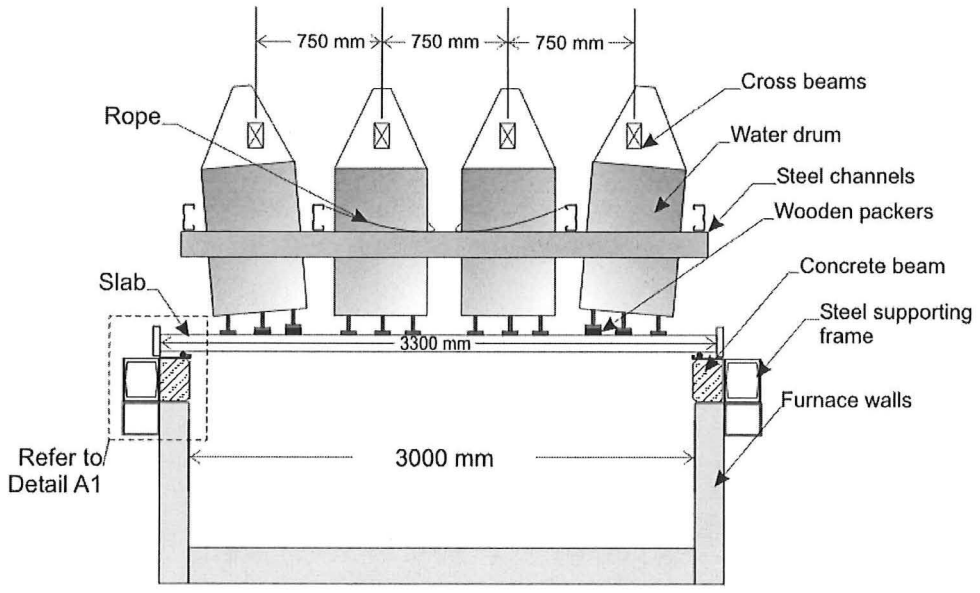

Figure 4-9: Section across the short span of the furnace.

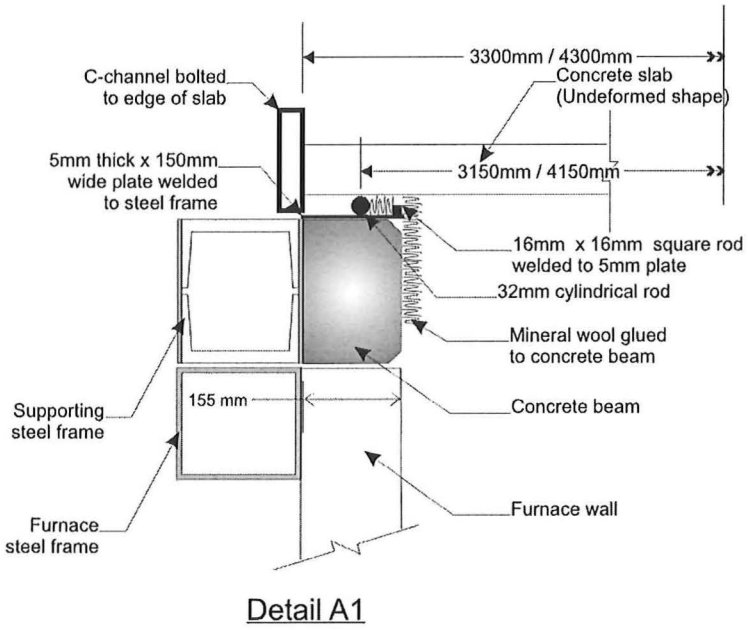

Figure 4-10: Detail A1 (Detail of slab support on the furnace)

4.6. Slab loading

A uniformly distributed load was applied on the slabs, in addition to the self weight of the slabs, to simulate live loads. Twenty 200-litre water drums placed on the slab to simulate the uniformly distributed load. The combined weight of the water and the steel drums was 200kg per drum, equivalent to a uniformly distributed load of 3.0kPa.

The drums were arranged in a uniform grid of four by five drums (Figure 4-11). The drums were lowered onto the slab by an overhead gantry crane. Each drum had a steel strap which allowed the drums to be hung off a series of parallel cross beams. The crane picked up the cross beams, which in turn, picked up the drums. When the drums were placed on the slab, the cross beams were lowered further to provide some slack to allow the drums to drop downwards when the slabs deflected underneath the drums. The cross beams also held the drums to prevent them from falling into the furnace if catastrophic collapse of the slab occurred. Each drum had three swivel feet and each foot had a contact surface made of a 100mm square particle board. The slab specimens were loaded an least an hour before each test.

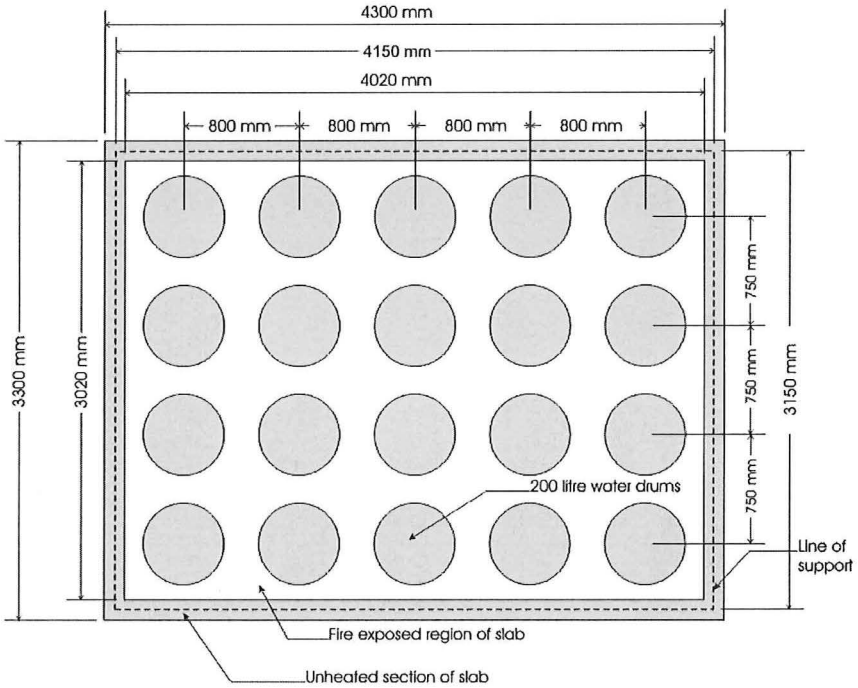

Figure 4-11: Position of the loading drums

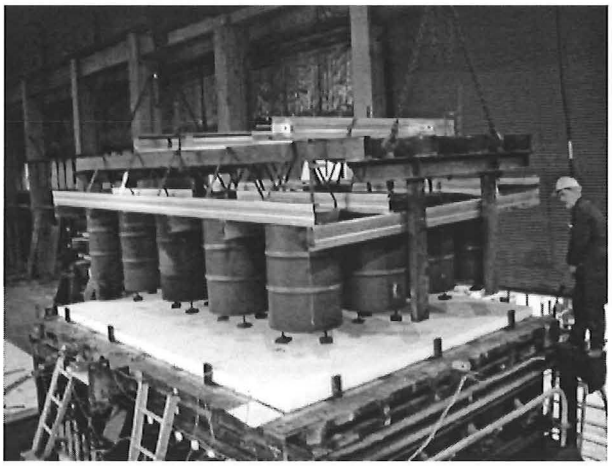

Figure 4-12: The twenty 200-litre water drums being lowered onto the slabs by a gantry crane.

	W_u (kPa)	Self weight, G (kPa)	Live load, Q (kPa)	Total load, G + Q (kPa)	Load ratio, r_{load}
Flat slab 661 mesh	20.0	2.40	3.0	5.40	0.27
Flat slab HD12 mesh	28.2	2.40	3.0	5.40	0.19
Flat slab D147 mesh	10.2	2.40	3.0	5.40	0.41
Hibond slab	69.1	2.52	3.0	5.52	0.079
Traydec slab	73.8	3.12	3.0	6.12	0.082
Speedfloor slab	55.1	2.16	3.0	5.16	0.094

Table 7: Applied loads on the slabs

Table 7 shows the applied loads on the slabs. The level of loads that were applied to the slabs during the fire tests are expressed by a load ratio, r_{load}. The load ratio is defined as the ratio of the applied loads on the structure, U^*_{fire}, to the loads that would cause collapse at ambient temperature, R_{cold}. The applied loads consisted of the self-weight of the slab (G) and the live loads from the water drums (Q). The slabs that were tested had different levels of strength, R_{cold}, due to the different quantities of reinforcing and the types of steel decking resulting in the load ratios ranging from 0.08 to 0.406.

$$r_{load} = \frac{U^*_{fire}}{R_{cold}} = \frac{(G + Q)}{W_u} \qquad \textbf{Equation 1}$$

For the two-way slabs, the strengths of the slabs were determined by the ultimate load, W_u, which is the lowest load level that will form yield line cracks in the slabs. The ultimate loads were calculated from yield line theory (Park et al, 2000).

In the calculation of the ultimate loads of the composite slabs and Speedfloor slab, the contributions of both the composite steel decking/joists and the steel mesh were included in the flexural strengths spanning in the longitudinal direction. In the transverse direction, only the contribution of the mesh was considered and the strength contribution of the steel decking was ignored.

4.6.1. Large differential deflections

When the slab undergoes large vertical deflections, the water drums would tilt onto each other and could interfere with the potentiometers which measure the vertical deflections. To address this problem, a steel grille was built around the drums to prevent them from tilting and to ensure they remain vertical (refer to Figure 4-12 and Figure 4-13). The grille was made of cold-formed steel channels, which were bolted together. The grille was bolted to the legs of the frame which supported the cross beams above the drums. Along the centrelines of the long and short directions of the slab, rope was substituted for the steel channels as the steel channels placed between the drums obstructed the potentiometers.

The outer drums were tilted to one side (leaning outwards) during the start of the test by chocking some of the feet of the drums with wooden packers (Figure 4-9). This was to prevent the load application changing from three feet to one or two feet when they leaned onto the steel grid, producing a point load rather than a distributed load. By chocking some of the feet, the drums would tilt inwards under large vertical deflections, and maintain the uniform load application on three feet.

4.7. Deflection measurements

The vertical and horizontal deflections of the slabs were measured during the fire test. The vertical deflections were measured across the centre of the slab in the long and short directions. Figure 4-13 shows the positions of the vertical and horizontal deflection measurements. The horizontal and vertical deflections were measured with rotary potentiometers. The rotary potentiometer consisted of a potentiometer attached to a perspex wheel with two strings travelling around the wheel in opposite directions (Figure 4-14 and Figure 4-15). One of the strings is attached to the slab while the other is attached to a

counterweight. When the slab deflected, it pulled the attached string, which turned the wheel. The rotation of the wheel is detected by the potentiometer which sends the signal to the data logger.

In order to measure the vertical deflections, the rotary potentiometers were supported on steel purlins. The steel purlins were clamped onto the cross beams located above the drums (Figure 4-14). The horizontal movement of the slabs were measured at the centres of the sides of the slabs. The potentiometers for measuring the horizontal deflections were clamped to the steel frame which supported the slab (Figure 4-15).

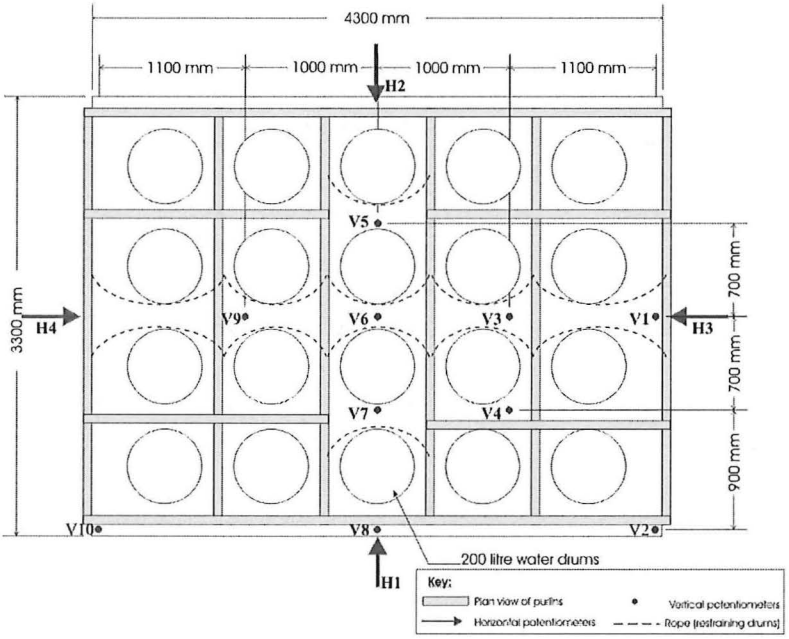

Figure 4-13: Plan view of the potentiometer layout and the steel grid used to prevent tilting of the drums.

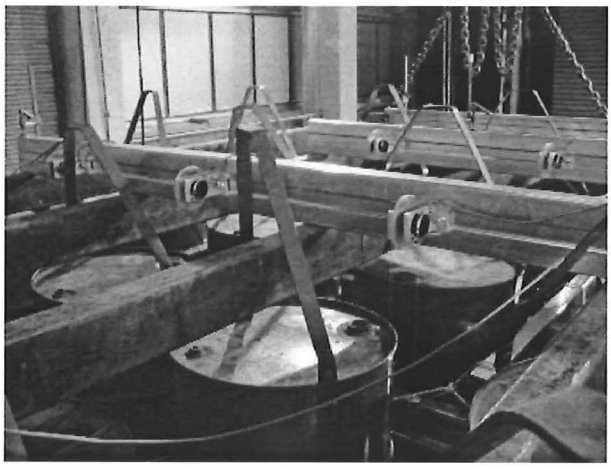

Figure 4-14: Potentiometers supported on the cross beams above the slab for measuring vertical deflections.

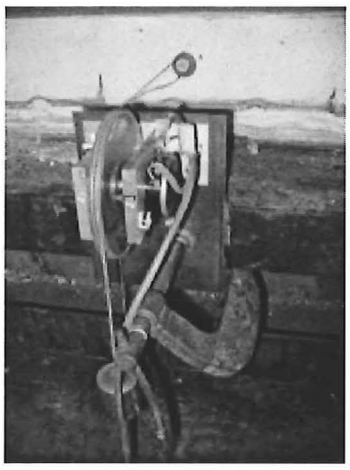

Figure 4-15: Potentiometer for measuring horizontal deflections, clamped to the supporting frame.

4.8. Furnace details

4.8.1. Furnace temperatures

The temperature in the furnace was measured with 12 chromel-alumel thermocouples distributed evenly on a horizontal plane approximately 400mm below the soffit of each specimen.

4.8.2. Furnace pressure

The pressure in the furnace was controlled to 18 Pa at 300 mm below the underside of the slab for all the tests. The test standard referenced in all the duties list was AS 1530 Part 4 (Standards Australia, 1997).

4.9. Data acquisition

The data acquisition equipment for the rotary potentiometers and strain gauges was supplied by the University of Canterbury. The data loggers for the strain gauges were specifically made to accommodate the correct resistances of the strain gauges. The strain gauges and rotary potentiometers were wired up in series to the data loggers which in turn, were connected to a serial box interface. The serial box interface was connected to a personal computer which recorded the strain and deflection measurements at 10 second intervals.

The temperatures from the thermocouples were recorded with the data logging equipment from BRANZ. The thermocouples for measuring the temperatures in the furnace and in the slabs were connected to a computer controlled data logger which recorded the temperatures at one minute intervals.

5. IMPLEMENTATION

5.1. Introduction

This section describes the construction process and the transportation of the slabs from Christchurch to BRANZ, Wellington. The slabs were constructed and temporarily stored in Christchurch, and later shipped to BRANZ, prior to the scheduled test dates.

5.2. Construction of the slabs

The slabs were constructed at the University of Canterbury between July and September 2001 and November 2001. The slabs were built and cast in pairs, starting with the Traydec and Hibond slabs. The steel decking of these composite slabs acted as formwork. The subsequent slabs were cast on top of these first two slabs. In order to cast the next pair of slabs on the already cast slabs, polyethylene sheets were stretched over the cast slabs to act as bond-breakers to prevent the concrete of the slab above from sticking to the concrete on the slab below.

The construction of each slab involved:

1. **Setting out and construction of formwork.**
   Hot-rolled steel angles were used as formwork. The formwork was built by bolting the steel angles together. The steel angles allowed the formwork to be easily detached from the already cast slab and rebuilt rapidly for the next slab without deformation after each use. The steel flashings, provided by *Dimond Industries*, were laid at the perimeter of each slab. The steel flashings served as a bearing surface for the slab on the rollers.

2. **Attachment of high temperature strain gauges and thermocouples to the reinforcing steel.**
   In order to attach the strain gauges, the reinforcing bars needed to have a smooth surface. Therefore, the deformations of the reinforcing bars were grinded off. The strain gauges were attached to the steel with high temperature resistant glue and water proofing compounds. This was a delicate and time consuming process. After the strain gauges were attached, the reinforcing mesh was placed in the formwork and the thermocouples were then attached to the reinforcing bars. The strain gauges were wired up with longer lengths of wire.

3. **Attachment of lifting inserts and concrete threaded inserts.**
   The slabs were lifted with Reid Short Foot Anchors. Four face lifting inserts were distributed equally across the top surface of the slab. Each lifting anchor had a 2.3 tonne capacity. Figure 5-1 and Figure 5-2 show the lifting anchors placed in the slabs, prior to casting. They also show the additional reinforcing bars tied to the anchors to prevent instantaneous failure by concrete rupture. Threaded inserts were placed at the top surface of the composite slabs to allow strong backs to be bolted to the slab. The composite slabs were very strong in bending about one axis but are weak in the perpendicular axis. Therefore, strongbacks had to be attached to the slabs to increase their flexural rigidity about the weak axis to prevent them from cracking when they were lifted. The strongbacks were positioned over the slabs on the steel formwork with the 16mm inserts bolted to them, to position the inserts during the casting process (Figure 5-1).

   12mm concrete inserts were placed horizontally at the edges around the perimeter of the slab (Figure 5-1 and Figure 5-2). They were used to bolt steel channels to the slabs to prevent the sides of the slabs from sliding into the furnace. Reinforcing bars were threaded

through the 16mm and 12mm inserts to increase their pull-out capacities and to prevent failure due to rupture of the concrete cone.

Figure 5-1: Hibond slab prior to casting.

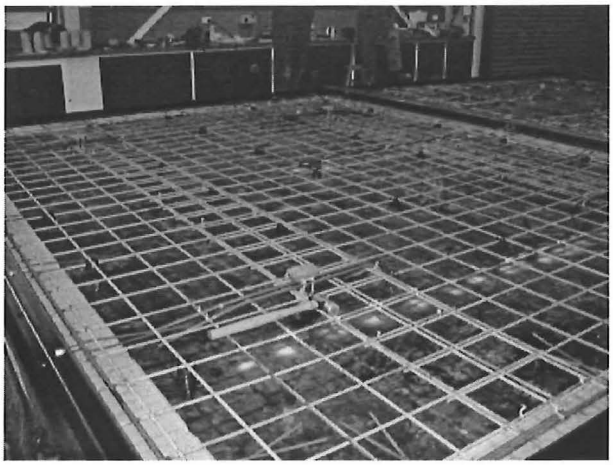

Figure 5-2: Flat slab (661 mesh) prior to casting.

4. Pouring of concrete.

The concrete was supplied by *Firth Industries*. Most of the slabs were cast in pairs, with the exception of the last two slabs which were cast individually. The concrete was supplied by mixer trucks to the Civil Engineering Laboratory which was then poured into the formwork with a skip (Figure 5-3). Needle vibrators were used to vibrate the concrete to prevent honey-combing. Concrete cylinder samples were made for each pour to be used for determining their strengths.

5. Curing of concrete

Figure 5-4 shows the slabs the day after the concrete was poured. Wet gunny sacks were placed over the slabs for several days to allow the slabs to cure. The sacks were covered with a large polyethylene sheet to prevent moisture lost by evaporation.

Figure 5-3: Concrete being poured into the formwork and vibrated.

Figure 5-4: Slabs covered with wet gunny sacks and polyethylene sheets the day after being cast.

6. Construction of the Speedfloor system

The Speedfloor system was built on a wooden box to raise the slab above the floor level because it had steel joists hanging below the slab (Figure 5-5). The joists were suspended

on the wooden box with lock-bars placed between the joists to laterally brace the joists. Plywood was placed on top of the lock bars for the formwork and steel flashings were placed around the edges of the slab.

Figure 5-5: Construction of the Speedfloor system.

5.3. Storage of slabs

When all the slabs had been cast, they were stored at a warehouse at a separate location in Christchurch. The warehouse storage of the slabs was contributed by *Smith's Crane and Construction*. When the 100mm plain flat slabs were lifted, there were lines of indentations at the bottom surface of the slabs. This was formed by the creases in the polyethylene sheets placed below the slabs as bond-breakers.

The slabs were stacked on an A-frame with three slabs on each side of the frame. Timber bearers were placed between the slabs to provide air circulation between the slabs to allow them to dry and cure. A tent was constructed over the slabs using polyethylene sheets to form an air-tight condition. A dehumidifier was placed in the tent to produce a dry condition in the tent to expedite the drying of the slabs. The concrete cylinders were also placed in the tent so that they would be exposed to the same conditions as the slabs.

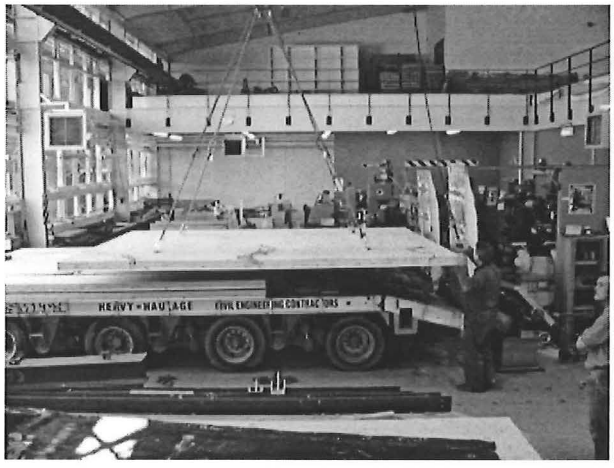

Figure 5-6: Transporting of the slabs out of the Civil Engineering Laboratory.

Figure 5-7: Slabs being stacked on an A-frame in a warehouse in Christchurch.

5.4. Shipping of slabs

The slabs were removed from the warehouse in Sockburn and shipped to BRANZ on the 16th April 2002. The slabs were transported to Lyttleton Harbour on trailers and were shipped from Lyttleton Harbour to BRANZ.

5.5. Testing procedure

The following procedure was carried out to set up the slabs before each test:

1. The rollers were aligned on the supporting frame and shielded with mineral wool.
2. The slab was weighed before placing it on the supporting frame.
3. Key thermocouples were glued to the top surface of the slab.
4. The positions of the rotary potentiometers were marked on the surface of the slab and concrete inserts were drilled at the marked positions.
5. The top surface of the slab was painted with white acrylic undercoat paint.
6. Steel C-channels were then bolted to the sides of the slabs.
7. The frame and the slab was lifted with the gantry crane and placed on the furnace frame.
8. The strain gauges and the thermocouples were wired up to their respective data loggers and their connections were tested.
9. The drums were then lifted using the steel cross beams and lowered onto the slab.
10. The strings from rotary potentiometers were tied to the drilled inserts on the slab and the rotary potentiometers were wired up to the data logger.
11. The rotary potentiometers and their connections were tested before the test.
12. The data loggers were activated and the instruments started recording data.
13. The test commenced when the furnace was switched on.

After each test, the following procedure was conducted:

1. The furnace was switched off.
2. The strain gauges, thermocouples and rotary potentiometers were detached from the slab.
3. The drums were lifted off and the slab and supporting frame were lifted off the furnace.
4. The slab was weighed the following day to determine the weight difference before and after the test.

6. RESULTS AND DISCUSSION

6.1. General overview

This section describes the results and observations of the tests. The deflections, temperatures and strains measured during the tests are presented. This section presents only part of the data recorded during the experiments. The remainder of the data and the layout of the instruments for each of the slabs are presented in the Appendices.

In the deflection plots, negative vertical deflections are downward and positive deflections are upward. For the horizontal deflections, positive deflections indicate outward deflection (expansion) while negative deflections indicate inward deflection (contraction). Tensile strains are measured as positive strains, while compressive strains are negative. For the purposes of discussion, the long span of the slab is referred as the longitudinal direction while the short span is referred as the transverse direction.

6.2. Test 1: 661 flat slab

6.2.1. General

The test was conducted on the 21st June 2002 at the BRANZ Fire Laboratory. The fire test started at 12.45pm and lasted for 3 hours.

6.2.2. Furnace temperature

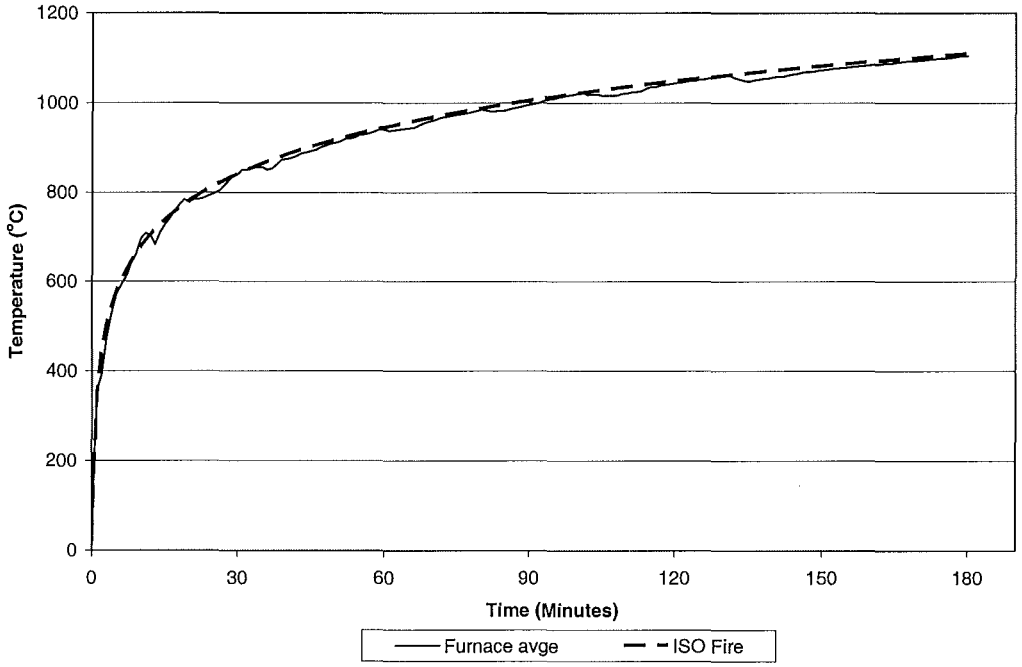

Figure 6-1: Furnace temperature during the 661 flat slab fire test.

Figure 6-1 shows the average temperature in the furnace during the fire test of the 661 flat slab. The temperature curve shown is the average of the twelve thermocouples in the furnace. The furnace was driven so that the temperature produced by the fire is identical to the temperatures of the ISO 834 standard fire curve.

6.2.3. Observations

Several minutes after the test started, some of the rotary potentiometers indicated some recording problems. As a result, the vertical deflections at some locations at the top of the slab and horizontal deflections of the edges of the slabs were not recorded. The test could not be aborted by then and had to proceed without those potentiometers.

After 15 minutes into the tests, the corners of the slabs started to curl upwards noticeably (Figure 6-2). Mineral wool was used to cover these openings to prevent the gases from escaping. Cracking at the top of the slab soon followed the curling of the slab corners. The first cracks appeared in the middle of the slab, running in the transverse direction. Water and steam then started to seep through cracks. The curling of the corners of the slab caused the water to accumulate in the middle of the slab, forming a large puddle (Figure 6-3). Water also accumulated in the recesses of the lifting inserts, which eventually boiled and evaporated. The cracks on the unheated side did not penetrate the full depth of the slab. Had a full depth crack formed in the middle of the slab, the water would seep through and flames would have passed through the cracks.

At about 1 hour and 25 minutes, the puddle level in the middle of the slab started to reside. There were no cracks visible on the bottom surface of the slab, seen through the viewing ports located on the east side of the furnace. At 2 hours 15 minutes, the corners of the slabs had lifted up to 119mm and the puddle of water in the middle of the slab had dried up. The first set of cracks which appeared on the unheated surface (running down the centre of the slab) had opened up to 5mm wide without flames passing through these cracks.

Figure 6-2: Curled corners of the slab.

Figure 6-3: Water puddle in the middle of the slab.

The furnace was turned off at 3 hours. By then, the midspan deflection had reached 210mm. The instruments were disconnected and the water drums were lifted off the slab with the crane. The slab was then lifted off the furnace with the supporting steel frame.

The bottom surface of the slab was very smooth and did not show any signs of cracking or spalling. The line indentations on the bottom surface of the slab were due to creases in the polyethylene sheets when the slab was cast and not due to the effects of the fire (Figure 6-5). The most visible cracks on the top surface were in the middle of the slab, running in the

transverse direction at a regular spacing of 300mm centres (Figure 6-6). These cracks had propagated outwards, from the centre of the slab to the supports. There were also diagonal cracks at the corners and horizontal cracks running in the longitudinal direction, located approximately 600mm from the edges of the slab.

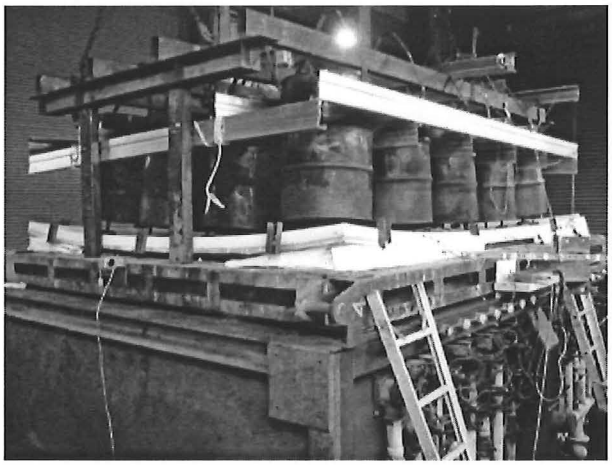

Figure 6-4: Fire test of the 661 flat slab underway.

Figure 6-5: Underside of the slab after the fire test.

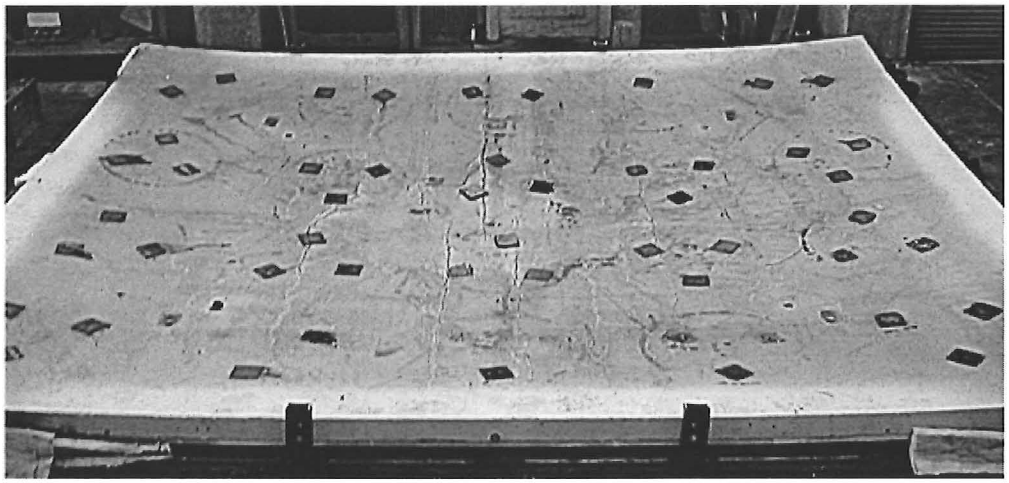

Figure 6-6: Top view of the slab after the test.

6.2.4. Deflections

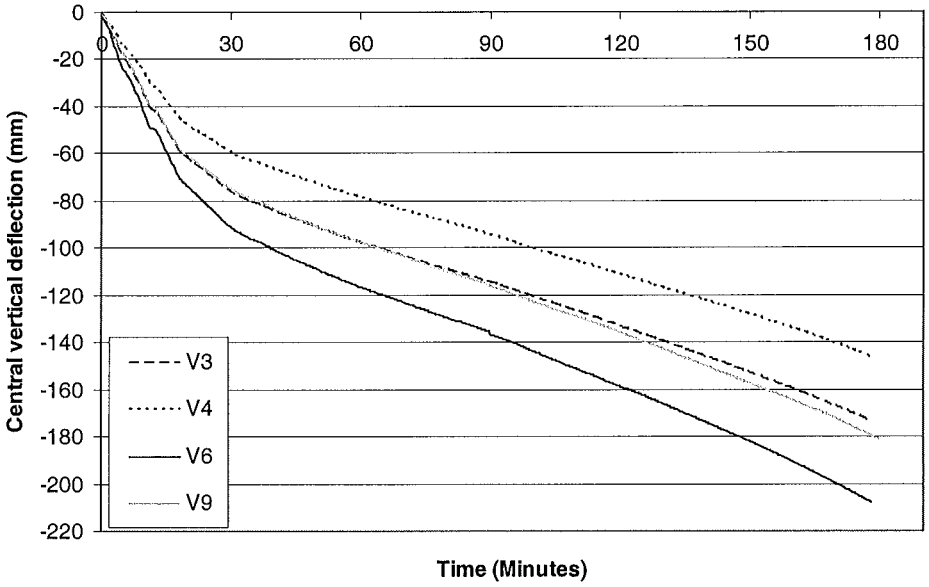

Figure 6-7: Central vertical deflections of the 661 flat slab.

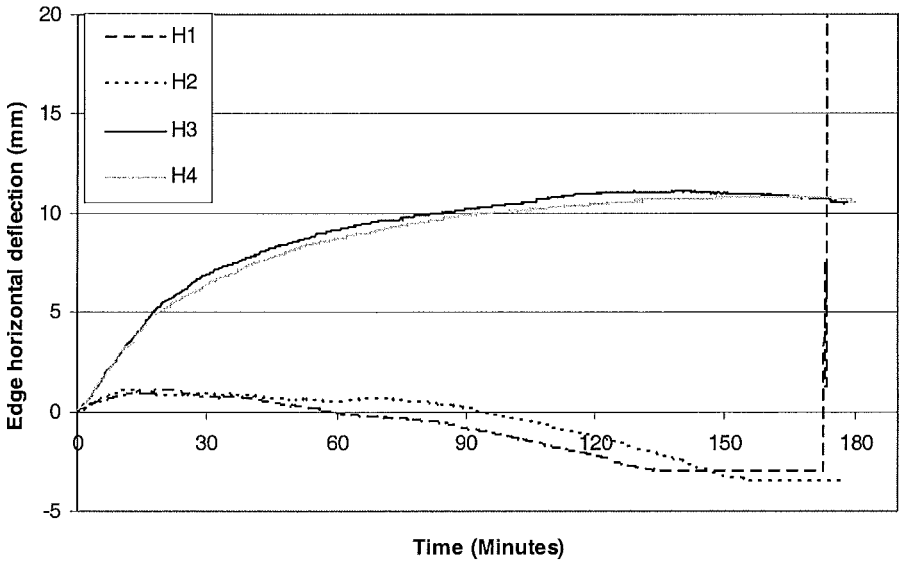

Figure 6-8: Edge horizontal deflections of the 661 flat slab.

Figure 6-7 shows the variation of the central vertical deflections of the slab during the fire. The deflections from the rotary potentiometers that worked properly were plotted while the

deflection readings from potentiometers V1, V2, V5, V7 and V8 did not function properly and were not plotted. Figure 6-7 shows that the slab deflected downwards very rapidly during the initial stage, reaching -74mm at midspan by 20 minutes, equal to a rate of -3.7mm per minute. After 30 minutes, the deflection rate of the slab decreased and deflected at a steady rate of approximately -0.8mm per minute for the remaining duration of the test. When the test was stopped at 180 minutes, the midspan deflection had reached -210mm.

Figure 6-8 shows the measured horizontal deflections of the slab. The horizontal deflections measured were due to the expansion and downward deflections in the centre region of the slab. H1 and H2 measured the horizontal deflections in the transverse direction of the slab; while H3 and H4 measured the deflections in the longitudinal direction (refer to Figure 4-13).

Figure 6-8 shows that in the transverse direction, the slab deflects outwards only very slightly during the initial stage, reaching a maximum of 1mm at 24 minutes. After this, it gradually deflected inwards until it reaches a minimum of -3mm and -3.45mm at H1 and H2, respectively. The horizontal deflections reached a plateau due to the potentiometers running out of travel. In the long direction, the slab expanded at a linear rate until 19.3 minutes and was followed by a slower non-linear increase. The outward deflection reached a maximum of 11.2mm at 143 minutes followed, by a gradual decrease of its deflection trend.

6.2.5. Slab temperatures

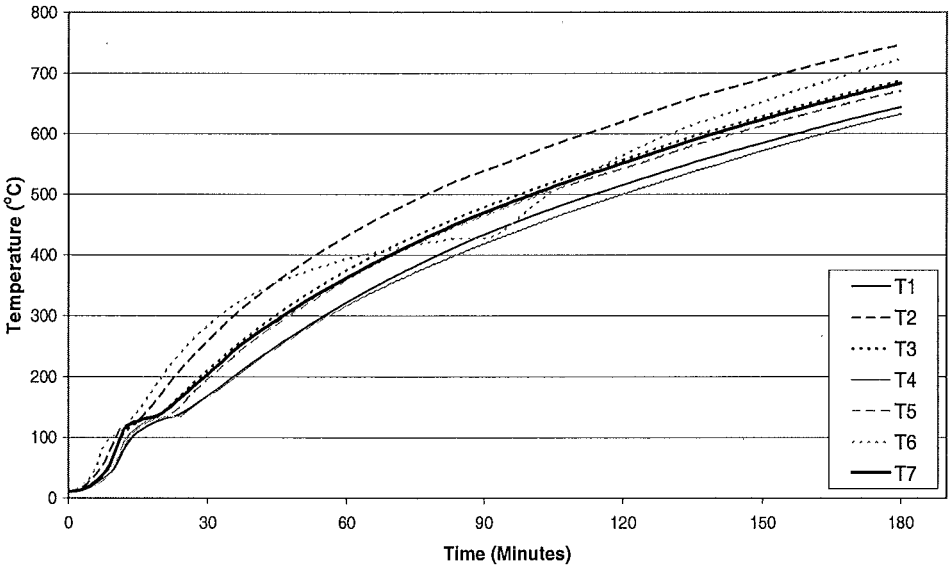

Figure 6-9: Temperatures of the reinforcing mesh in the 661 flat slab.

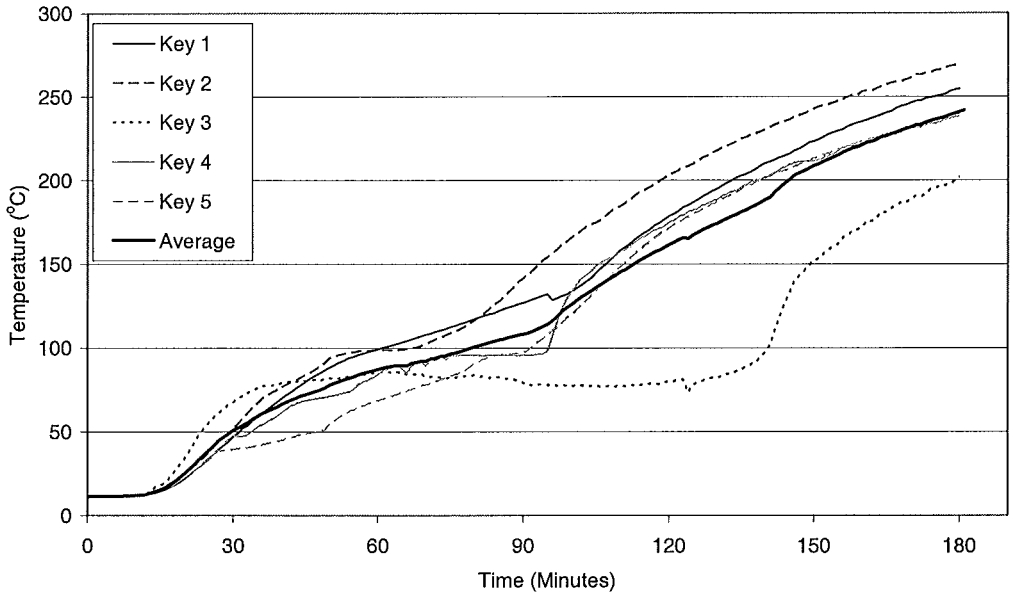

Figure 6-10: Temperatures of the unheated side of the 661 flat slab.

Figure 6-9 shows the temperature rise of the thermocouples attached to the reinforcing mesh. The thermocouples were attached at mid-height, at the sides of the reinforcing bars. The mesh had 25mm concrete cover to the bottom of the steel. Apart from a slight variation between the thermocouples, the temperatures show a consistent trend, rising from 12°C during the initial stage, up to a maximum of 746°C by the end of the test. The graph shows a plateau in the temperature rise between 14 and 20 minutes. This is attributed to the increase in moisture at the mesh level as the moisture in the slab is driven from the heated side of the slab to the unheated side.

Figure 6-10 shows the temperatures of the unexposed face of the slab. The initial temperature on the unexposed side was 12°C. The average temperature of the five thermocouples on the unheated side started to increase after 13 minutes. Between 39 and 95 minutes, the rate of temperature rise is lower compared to the other periods of the fire test. This is possibly due to the increase of moisture on the top surface, therefore reducing the rate of temperature rise. When the moisture on the top surface evaporated, the temperatures started to increase at a faster rate. Thermocouple number 3, located in the middle of the slab shows a temperature lag, remaining below 100°C until approximately 140 minutes had elapsed. The low temperature reading is due to the thermocouple being submerged in the puddle of water in the middle of the slab. After approximately 140 minutes, the puddle of water had evaporated and the temperature readings increased very rapidly.

The average temperature rise measured by the five thermocouples exceeded the failure criterion of the 140°C temperature rise at 114 minutes (152°C). The maximum temperature rise measured by any one of the five key thermocouples exceeded the criterion of the 180°C temperature rise at 114 minutes (192°C).

6.2.6. Strain gauge measurements

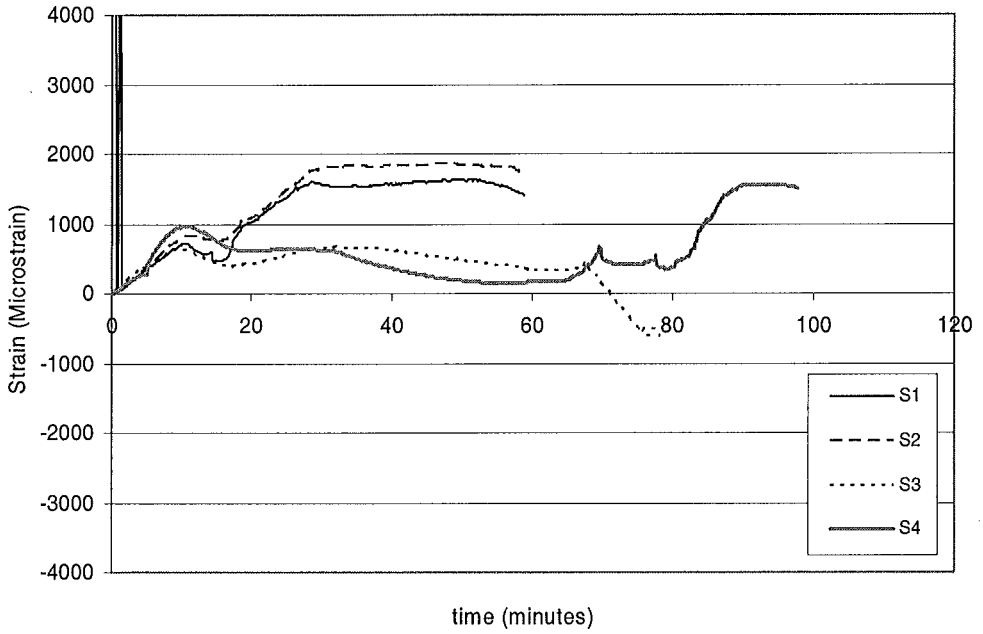

Figure 6-11: Strain gauge measurements in the 661 flat slab.

Figure 6-11 shows the strains measured by strain gauges S1 to S4. The plots for strain gauges S5 to S8 are in the Appendices. The graph shows that as the fire started, tensile strains in the steel started to increase until they eventually reached a plateau, which ranged from 500 to 1800 microstrain. After approximately 58 minutes, the tensile strains start to fluctuate between compression and tension. By this stage, the recorded temperatures of the mesh had exceeded 300°C, indicating the strain gauges or their connections had started to fail.

6.3. Test 2: HD12 flat slab

6.3.1. General

The test was conducted on the 25th June 2002 at the BRANZ Fire Laboratory. Dr. Andy Buchanan and Dr. Peter Moss from the University of Canterbury were present to witness the test. The fire test started at 10.00am and lasted for 3 hours.

6.3.2. Observations

When the test started, the strain gauge data logger registered an error, indicating that it had a hardware problem. Despite repeated attempts to restart the software and solve the problem, the data logger would not respond. The problem was eventually solved; but the data from the strain gauges during the first 42 minutes were not recorded. However, the rotary potentiometers were not affected and were able to record the deflections throughout the entire duration of the test.

This problem appeared during the start of every subsequent test, when the furnace was switched on. Although the cause of the problem was not identified, the problem was rectified every time it appeared during the start of each test.

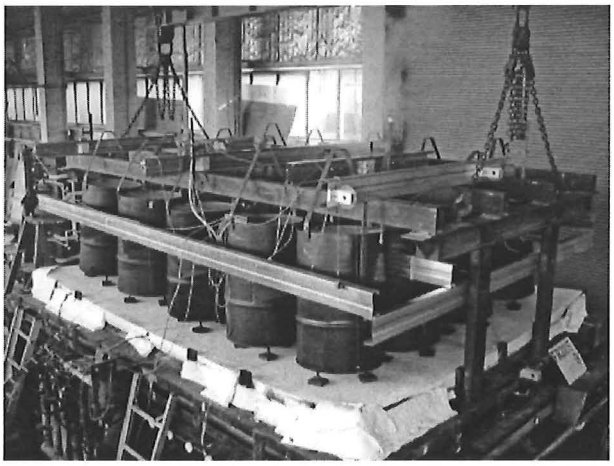

Figure 6-12: Fire test for the HD12 lat slab underway.

Similar to the first test, the corners of the slab curled upwards very significantly, allowing the hot gases to escape through the openings. The first cracks appeared at the top surface of the slab, propagating from the middle of the slab in the transverse direction, towards the supports. When the surface cracks reached the edges of the slab, they form a full-depth crack at the sides of the slabs. Fine diagonal cracks could be seen at the corners of the top surface.

Similar to the previous test, a large amount of steam and water was driven off resulting in a puddle of water forming in the middle of the slab. At 1 hour and 40 minutes, the puddle of water in the middle of the slab dried up and the cracks in the middle of the slab could be seen more clearly. Through the viewing ports, there were no cracks visible on the heated surface of the slab and there were also no signs of spalling. At 163 minutes, some of the hot gases that escaped through one of the corners and burnt the string of the rotary potentiometer which measured the corner deflections (V10).

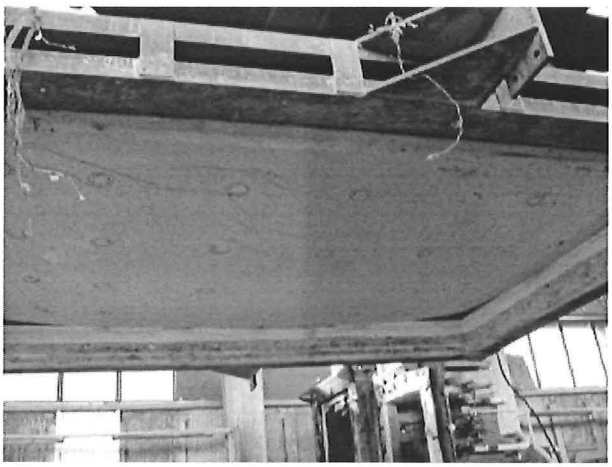

Figure 6-13: Underside of the slab after the fire test.

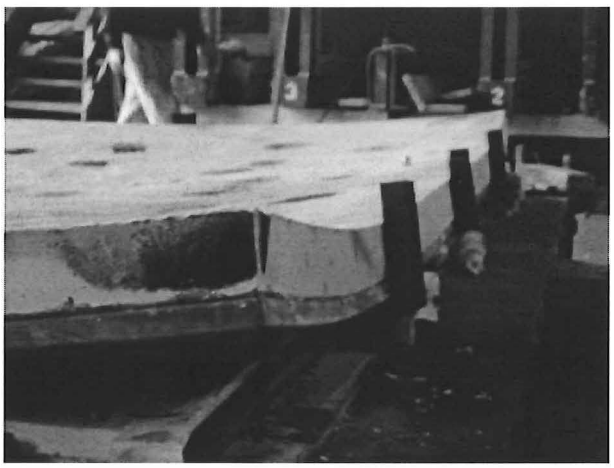

Figure 6-14: Deflection of the edges of the slab.

The test was stopped at 3 hours. The instruments were disconnected and the water drums were lifted off the slab with the crane. Figure 6-13 shows the bottom surface of the slab when it was lifted off the furnace. It showed no visible cracks or signs of spalling. The lines

underneath the slab were due to the creases of the polyethylene sheets during the construction of the slab. The corners of the slab had curled upwards very significantly, while the central region of the slab edges remained relatively flat. The surface cracks of this slab were less than those seen in the first test due to the higher reinforcing steel content.

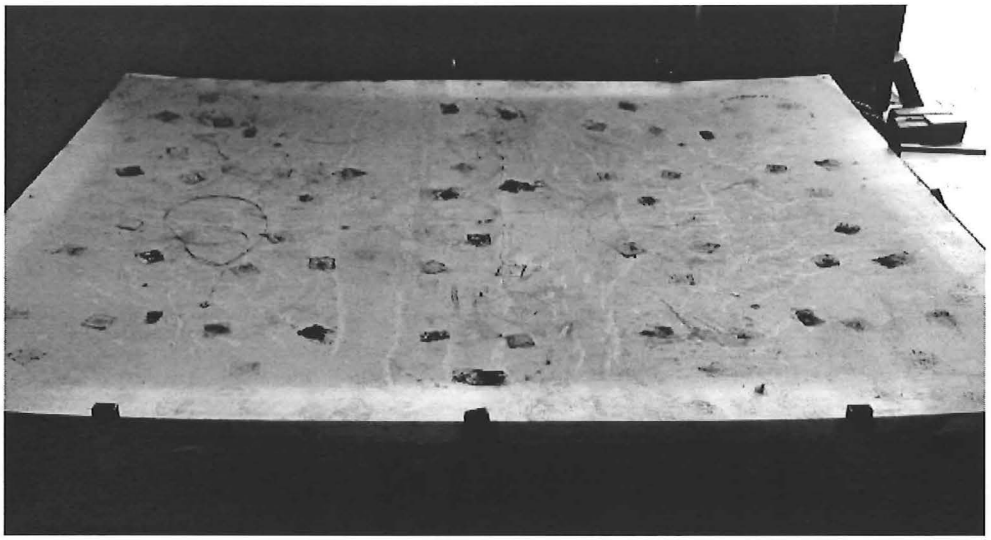

Figure 6-15: Top view of the slab after the test.

6.3.3. Deflections

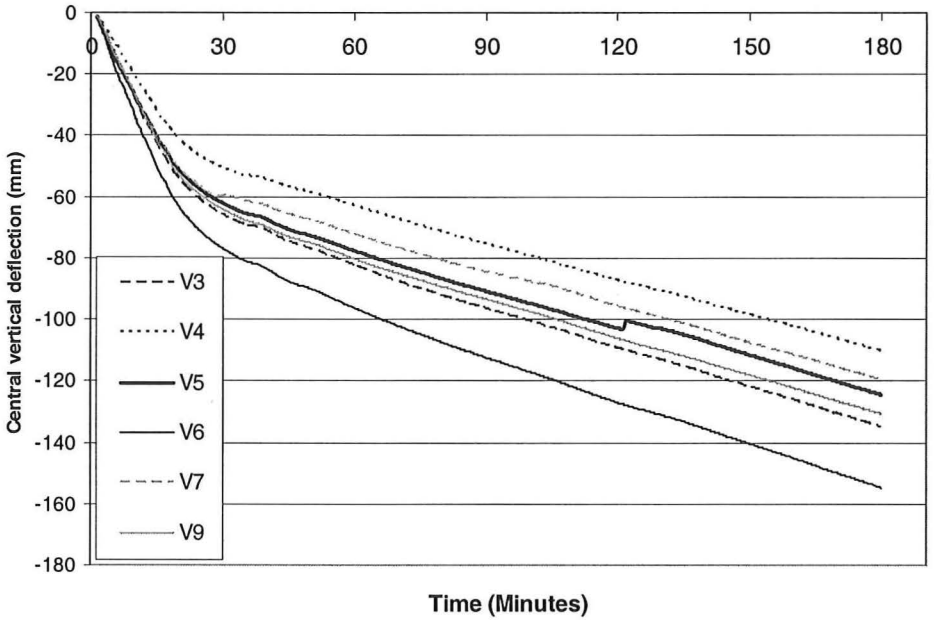

Figure 6-16: Central vertical deflections of the HD12 flat slab.

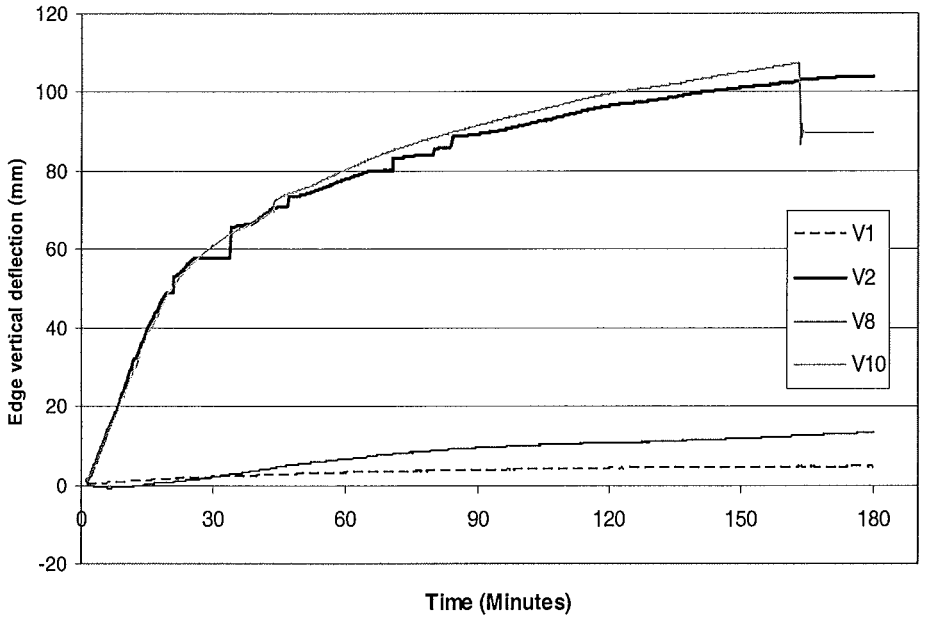

Figure 6-17: Edge vertical deflections of the HD12 flat slab.

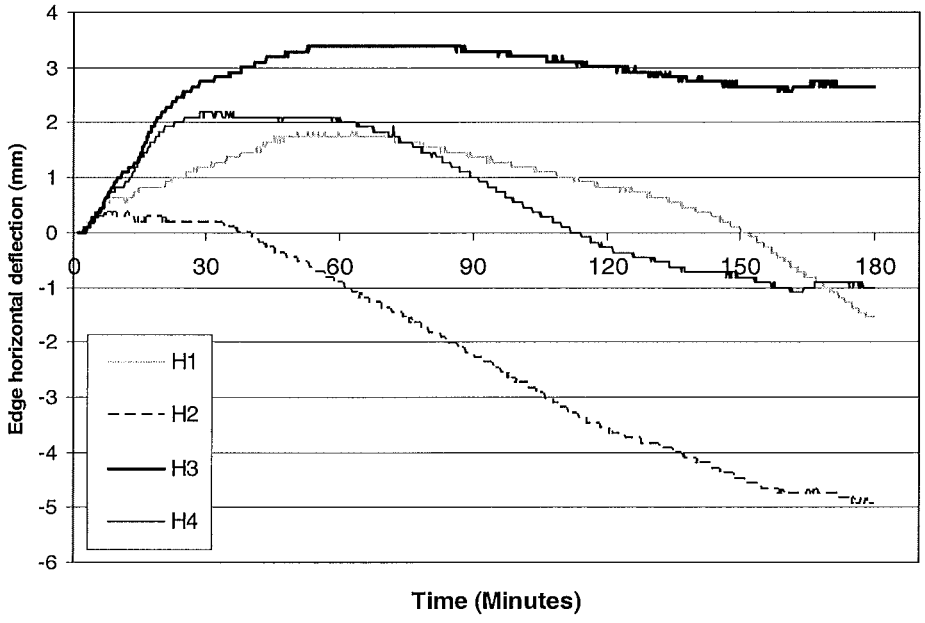

Figure 6-18: Edge horizontal deflections of the HD12 flat slab.

Figure 6-16 shows the central vertical deflections of the slab. The deflection trend of the slab is similar to that seen in the first test. The slab deflects downwards rapidly during the first 20 minutes, with its midspan deflection reaching -63mm by 20 minutes. After this, the deflection rate decreases, maintaining a linear rate of -0.52mm per minute until the end of the test, reaching -155mm.

Figure 6-17 shows the vertical deflections at the edges of the slab. V1 and V8 measured the vertical deflections at the middle of the short and long spans of the slabs, respectively (refer to Figure 4-13). V2 and V10 measured the vertical deflections of the south-west and south-east corners of the slab, respectively. The corners deflected upwards in a similar trend as the central deflections of the slab, but in the opposite direction; increasing rapidly during the initial stage, followed by a lower, non-linear rate of rise. At 163 minutes, the deflection measurements at position V10 drops suddenly from 107mm to 90mm. The string attached to the potentiometer was burnt and was severed by the flames which escaped through the corner of the slab.

Figure 6-18 shows the horizontal deflections of the slab. The graph shows that the amount of horizontal movement in any of the four directions is small, ranging from +3.4mm to -5mm. The horizontal deflections of the slab show a similar trend, starting with outward expansion during the initial stage, followed by contraction at the later stage of the fire.

6.3.4. Slab temperatures

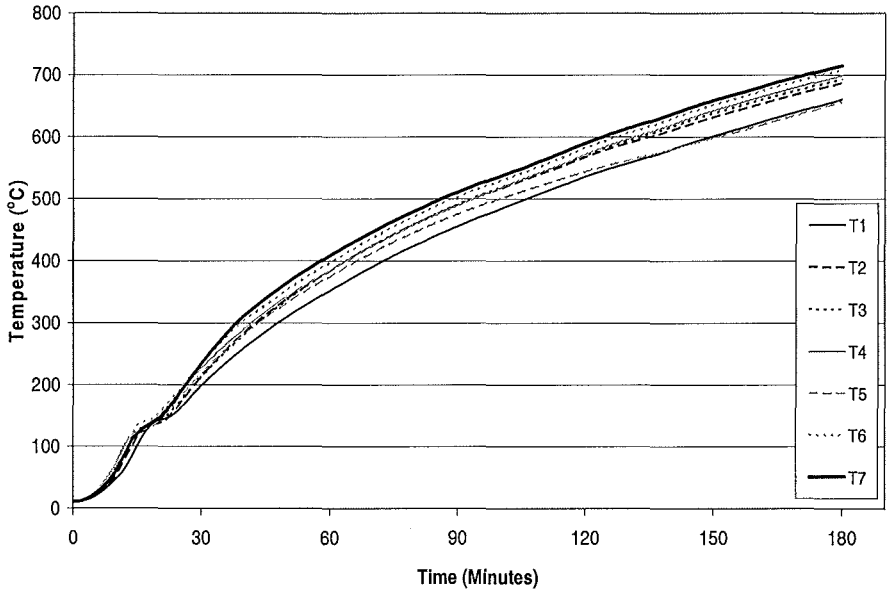

Figure 6-19: Temperatures of the reinforcing bars of the HD12 flat slab.

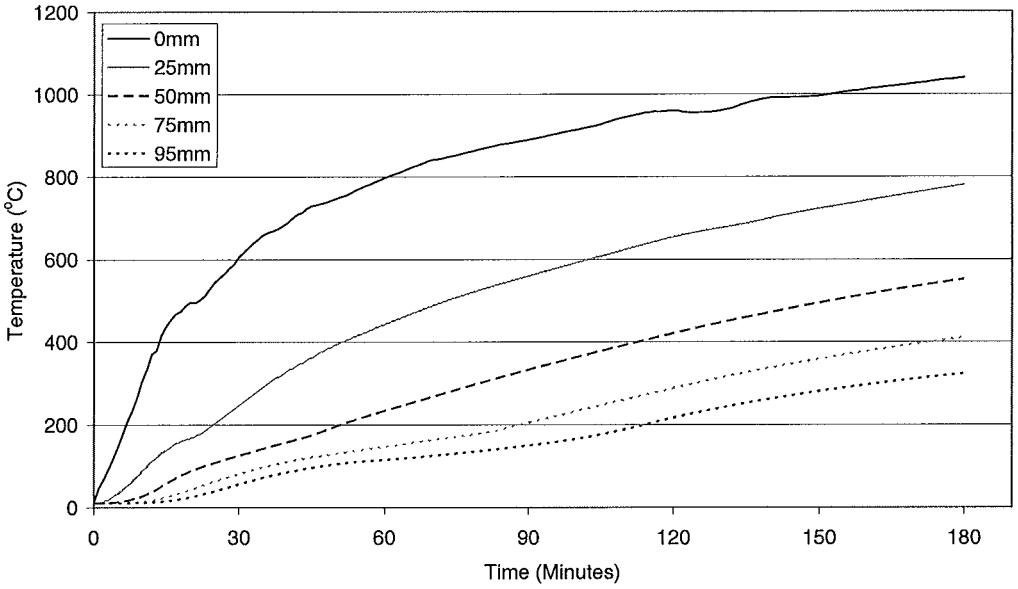

Figure 6-20: Temperatures in thermocouple tree 1 in the HD12 flat slab.

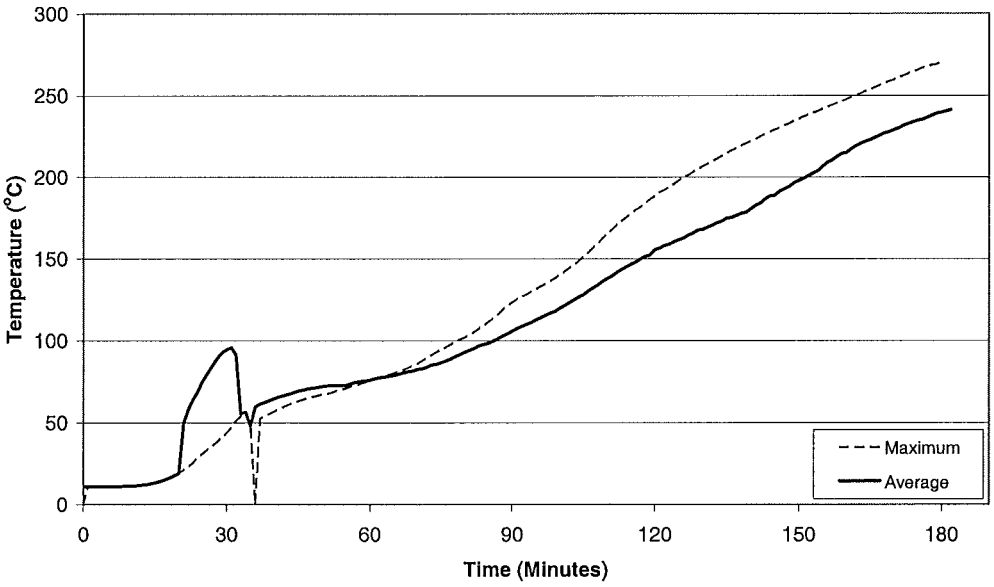

Figure 6-21: Temperatures at the unheated side of the HD12 flat slab.

Figure 6-19 shows the temperature rise of the reinforcing bars. It shows a consistent trend between all the thermocouples, rising from 11°C during the start of the fire test, up to a maximum of 715°C at the end of three hours. Figure 6-20 shows the temperatures of one of the thermocouple trees in the slab. The thermocouples measured the temperatures at various positions from the heated slab surface, ranging from 0mm (exposed face) to 95mm. The graph shows that the maximum temperature measured at the exposed face of the slab reached 1040°C at the end of the fire test.

Figure 6-21 shows the temperatures of the unexposed face of the slab. The initial temperature on the unexposed side was 11°C. The average temperature rise measured by the five thermocouples exceeded the failure criterion of the 140°C temperature rise at 118 minutes (151°C). The maximum temperature rise measured by one of the five key thermocouples exceeded the 180°C criteria at 146 minutes (191°C). The curve of the average temperatures shows a sudden increase between 21 minutes to 32 minutes. This is due to a sudden increase in one of the key thermocouples, therefore increasing the average temperatures. The reason for the sudden temperature increase is possibly due to a short circuit in the connections.

6.3.5. Strain gauge measurements

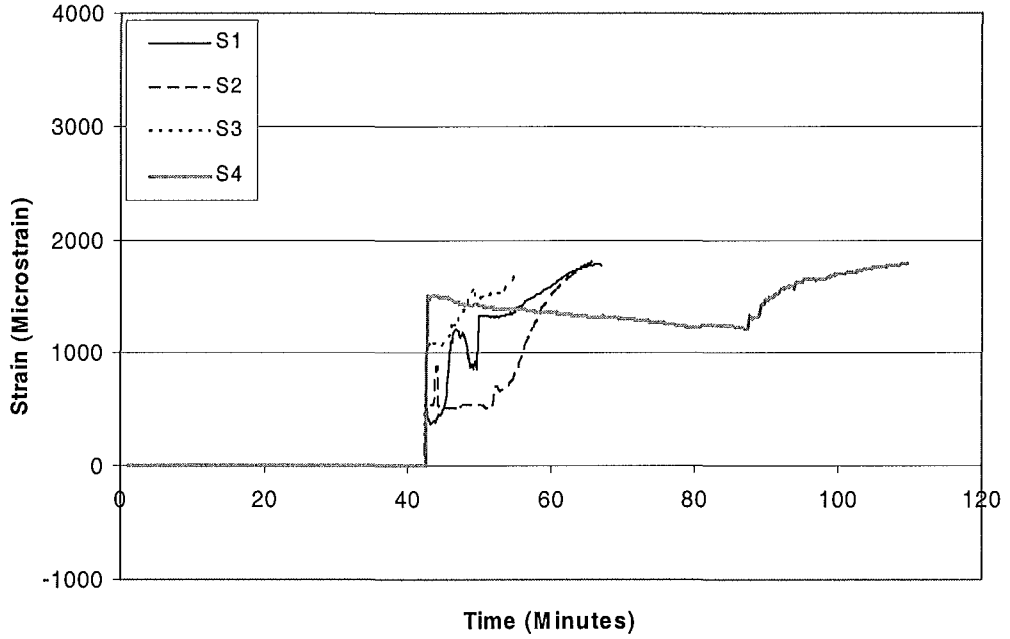

Figure 6-22: Strain gauge measurements in the HD12 flat slab.

Figure 6-22 shows the measurements of the strain gauges S1 to S4. The plots for strain gauges S5 to S8 are in the appendices. The data during the first 42 minutes of the fire test was not recorded due to the electronic problem with the data logger. When the data recording commenced at 43 minutes, the strain gauges were already measuring tensile strains in the range of 400 to 1500 microstrains. The strain gauge data was recorded for only a short period before they started to burn out progressively, shown by the sudden increase in strains which went out of the scale of the plot.

6.4. Test 3: D147 flat slab

6.4.1. General

The test was conducted on the 27th June 2002 at the BRANZ Fire Laboratory. The fire test started at 10.56am and lasted for 3 hours. The corners of this slab in this test (and subsequent slabs) were clamped down to prevent them from curling upwards.

6.4.2. Furnace temperature

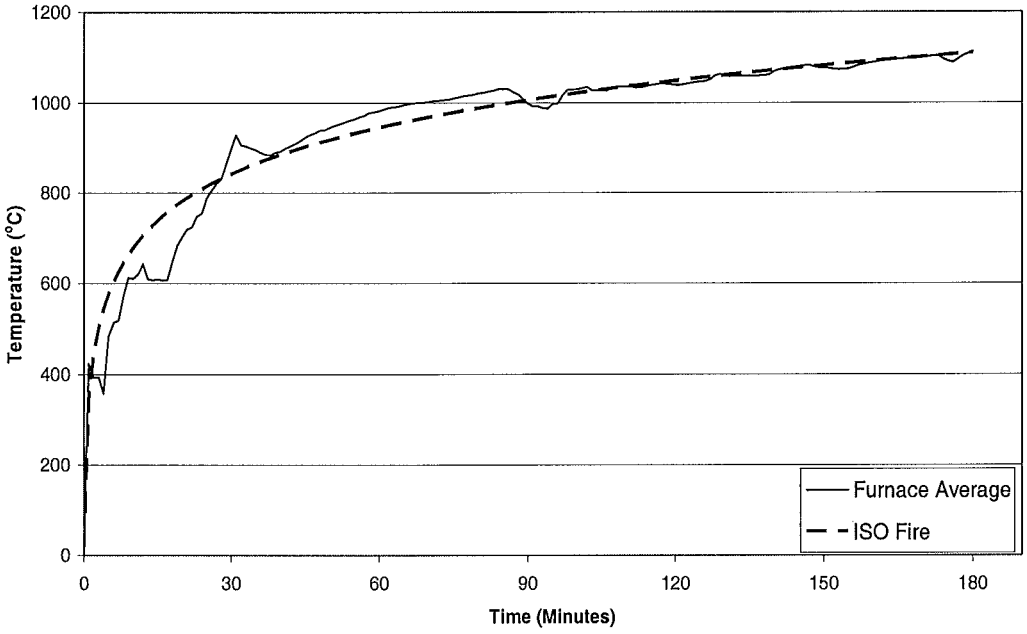

Figure 6-23: Furnace temperatures during the D147 flat slab fire test

Figure 6-23 shows the temperature in the furnace during the third fire test. During the first thirty minutes of the fire, the temperatures in the furnace showed significant deviation from the expected temperatures of the ISO standard fire. This was due to insufficient air ventilation into the furnace which caused incomplete combustion and resulted in a lot of black smoke pouring out of the furnace. After 30 minutes, the problem was fixed and the furnace temperature started to follow the predicted fire curve more closely.

6.4.3. Observations

During the early stages of the fire, diagonal cracks rapidly formed at the corners of the top surface. These cracks were due to restraint of the corners against curling. Three cracks also formed at an early stage of the fire in the middle of the slab, propagating in the transverse direction. The first crack formed 150mm off-centre in the transverse direction, with two more cracks running on each side, 600mm (2 bar spaces) parallel to the centre crack.

A large amount of water and steam seeped through the cracks, forming a puddle of water in the middle of the slab. After 35 minutes, the diagonal cracks on the top surface had widened noticeably. Cracks had also appeared at the sides of the slabs. These cracks formed a 45 degree angle across the full depth to the top surface where it meets the surface diagonal cracks (Figure 6-24).The centre edges of the slab progressively deflected upwards, eventually reaching double curvature by two hours. The cracks on top of the slab continued to widen as the test progressed; particularly the transverse cracks in the middle of the slab and the diagonal cracks at the corners.

At about 2 hours, hairline cracks started to form (through the viewing ports of the furnace) at the bottom surface of the slab. A crack was clearly seen propagating in the transverse direction on the east side of the furnace (closest to the viewing port). Another crack could also have formed on the west side of the slab but could not been seen as there were no viewing ports on that side. Some of the drums on the slab had tilted significantly due to the large vertical deflections. After 2 hours 25 minutes, the midspan deflection readings reached the maximum limit of the potentiometer (V6). The test was stopped at 3 hours and before the loads were removed, the final midspan deflection was measured manually.

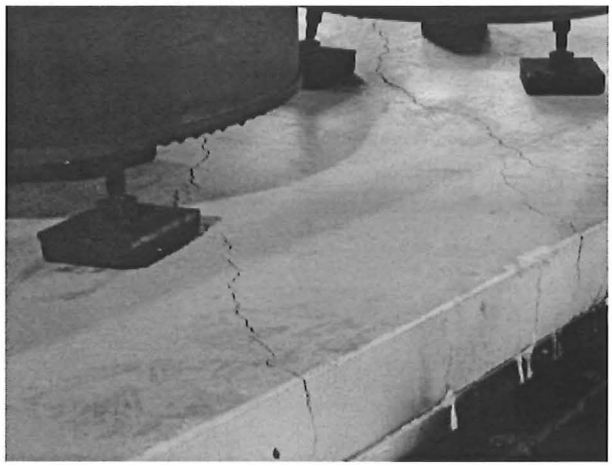

Figure 6-24: Diagonal cracks at the corners extending to full depth cracks at the sides of the slab.

Figure 6-25: Underside of the slab after the fire test, showing the yield line cracks.

Figure 6-25 shows the bottom of the slab and the deformed shape immediately after the fire test, respectively. Figure 6-26 shows the deformed slab after the test. On the top surface, the white paint had discoloured and became brown. Figure 6-27 and Figure 6-28 show that three large cracks formed across the transverse direction of the slab. These cracks were spaced at 600mm apart, equivalent to two grid spacings of the mesh. One full depth crack formed in the longitudinal direction at the centre of the slab. This full-depth crack is approximately 1200mm long. Surface cracks formed in a circular pattern around these large central cracks. Large cracks also formed in the longitudinal direction, located approximately 200mm from the edges of the slabs. In spite of cracks as wide as 10mm on the top surface, flames did not pass through the cracks, which would have caused integrity failure.

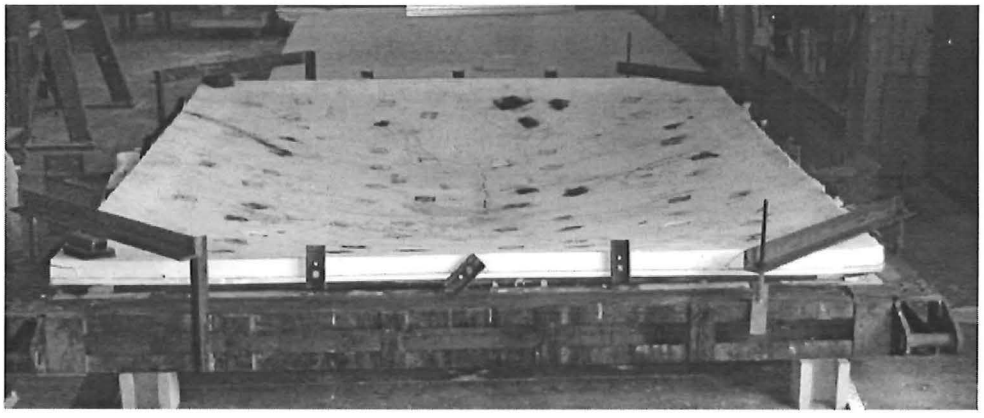

Figure 6-26: Deformed slab after the test.

Unlike the first two tests which showed a smooth and uncracked bottom surface, large cracks were clearly visible underneath this slab (Figure 6-25). There were no signs of spalling on the

underside of the slab. Figure 6-28 shows that a small portion of the bottom surface cover near the centreline had fallen off. This occurred after the slab had cooled down and was not due to spalling. The large surface crack in the longitudinal direction had extended to its full depth and was clearly seen on the bottom surface of the slab. Two large full depth cracks which propagated in the short span could also be clearly seen at the bottom of the slab. A finer crack also formed in the middle of the slab, between the larger full depth cracks. This crack had closed up when it was examined the following day and corresponds to the large crack on the top surface. In addition to the transverse, fine diagonal cracks running at 45 degrees from the corners towards the centre region of the slab could also be seen. After the slab was broken, examination of the reinforcing bars showed that the bars in the slab had not ruptured across the full depth cracks during the fire.

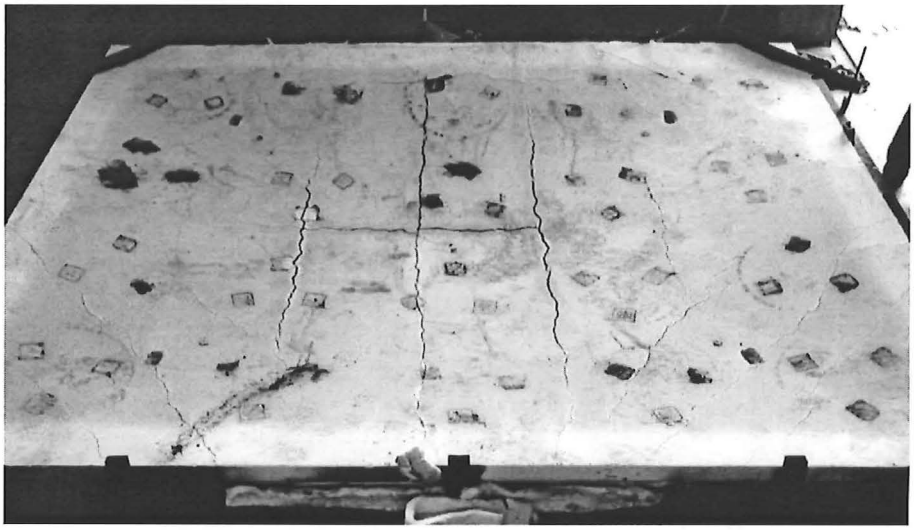

Figure 6-27: Crack pattern at the top surface of the slab.

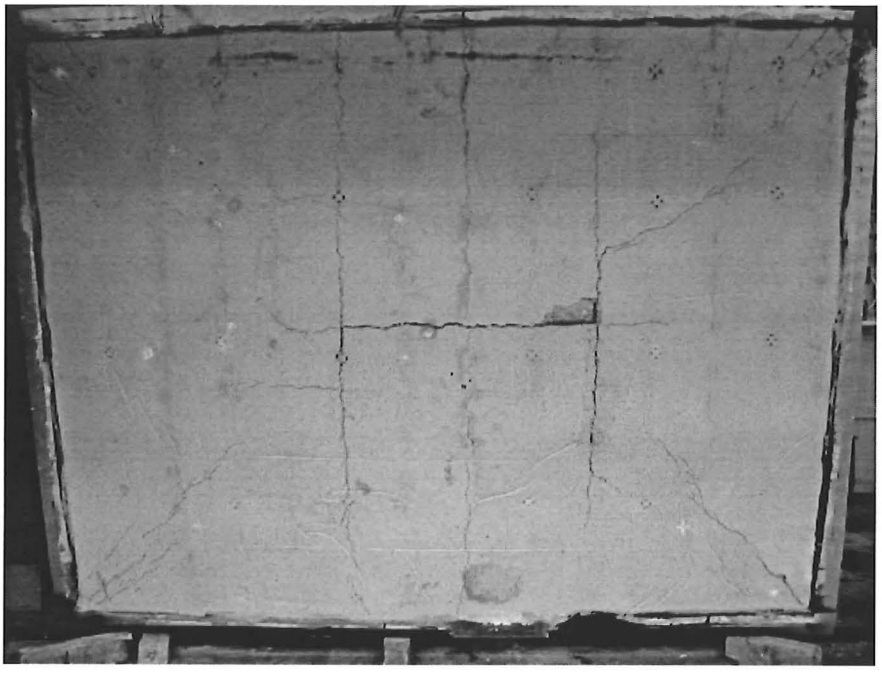

Figure 6-28: Crack pattern at the bottom surface of the slab.

6.4.4. Deflections

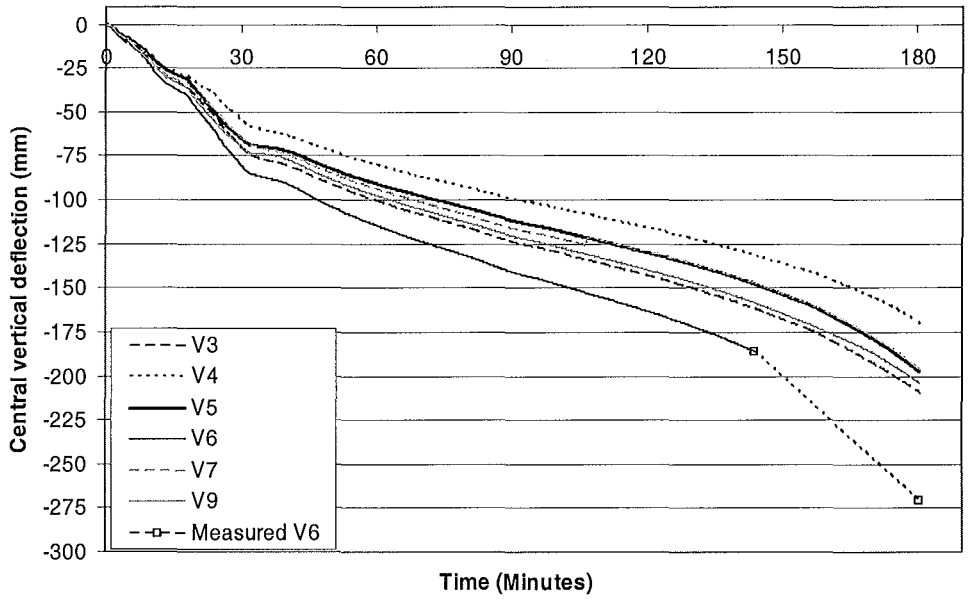

Figure 6-29: Central vertical deflections of the D147 flat slab.

Figure 6-57 shows the central vertical deflections of the slab. Unlike the first two tests, the vertical deflections did not show a smooth deflection trend during the first 45 minutes, due to the erratic furnace temperature (section 6.4.2). When the midspan vertical deflection reached -186mm, the central rotary potentiometer (V6) had reached its limit of travel and could not measure further deflections. A physical measurement made at the end of the test showed that the slab had deflected to -271mm at midspan.

6.4.5. Slab temperatures

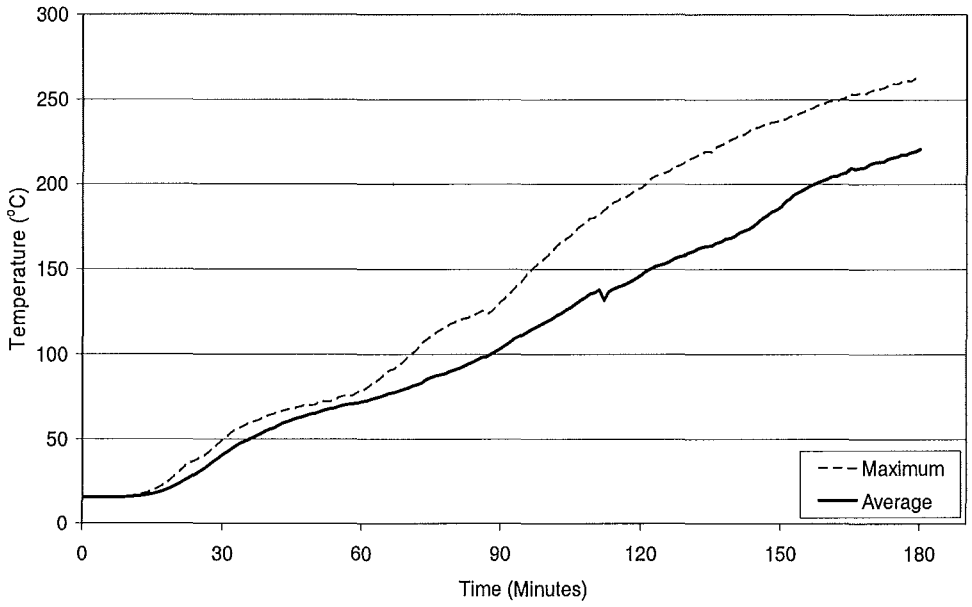

Figure 6-30: Temperatures at the unheated side of the D147 flat slab.

Figure 6-30 shows the temperatures of the unexposed face of the slab. The initial temperature on the unexposed side was 13°C. The average temperature rise measured by the five thermocouples exceeded the failure criterion of 140°C temperature rise (153°C) at 125 minutes. The maximum temperature rise measured by one of the five key thermocouples exceeded the 180°C criteria (193°C) at 153 minutes.

6.4.6. Strain gauge measurements

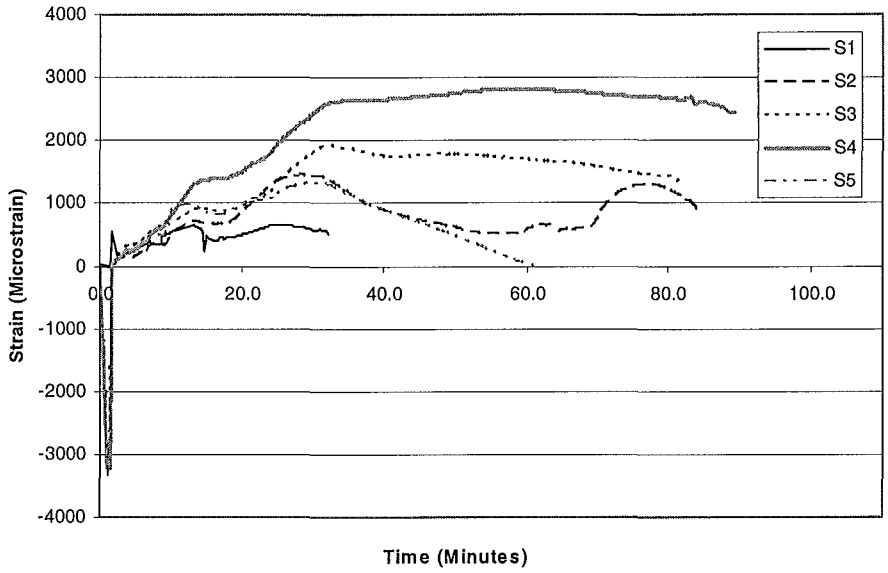

Figure 6-31: Strain gauge measurements of the D147 flat slab.

Figure 6-31 shows the measurements from the strain gauges S1 to S5 in the third test. The plots for the remaining strain gauges, S6 to S26 are in the Appendices. The graph shows that as the fire started, tensile strains in the steel increased and levelled off at strains between 640 to 2600 microstrain. Most of the strain gauges shown managed to record data in excess of 60 minutes before they started to fail.

6.5. Test 4: Dimond Hibond slab

6.5.1. General

The test was conducted on the 1st July 2002 at the BRANZ Fire Laboratory. The fire test started at 11.07am and lasted for 3 hours.

6.5.2. Observations

Before the test started, the slab had already cracked on the top surface due to mishandling when it was shipped from Christchurch to BRANZ. The crack formed across the middle of the short span of the slab. Strain gauges S1 and S3 did not function as it was damaged during the casting of the concrete.

Approximately 5 minutes after the start of the test, the steel decking at the bottom surface started to buckle and debond from the concrete. Figure 6-33 shows the steel decking debonding from the slab, creating a gap between the decking and the concrete. After 20 minutes, diagonal cracks started to form at the east and west sides of the slab, where the corners were held down (Figure 6-33). The cracks propagated upwards from the intersection between the top of the rib and the concrete flat slab at a 45 degree angle. Popping noises were heard during the early stages of the fire test, due to the concrete which was mechanically

anchored to the decking, being ripped from the slab when the decking debonded. Small pieces of concrete also spalled off the sides of the slab.

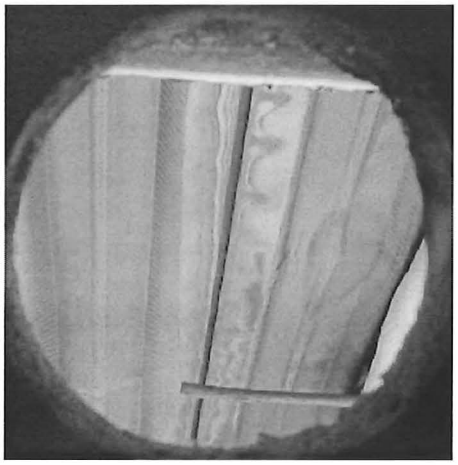

Figure 6-32: Buckling of the steel decking during the fire, seen through the east viewing port.

Figure 6-33: Debonding of the steel decking and diagonal cracks forming at the rib-slab intersection.

Cracks appeared at an early stage at the top of the slab at midspan, running in the transverse direction of the slab and diagonally, where the corners of the slab were clamped down (Figure 6-34). Similarly with the other tests, there was a lot of steam and water seeping out of the cracks. After 1 hour 20 minutes, the diagonal and horizontal cracks at the top surface had widened significantly but had not allowed the flames to pass through the openings. After 2 hours and 30 minutes, blisters started to appear beneath the steel decking (Figure 6-35). The blisters formed when the galvanizing of the steel oxidised.

Figure 6-34: Steam seeping through the diagonal cracks at one of the corners of the Hibond slab. The crack had extended the full depth of the slab.

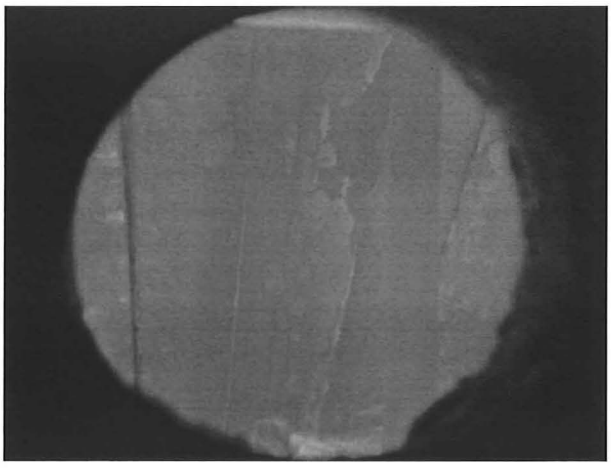

Figure 6-35: Severe blistering of the steel decking due to oxidisation.

As 3 hours approached, large longitudinal cracks had formed at the top surface, 200mm from the edges, running parallel to the long sides of the slab. The initial crack (due to mishandling) had widened significantly and at 3 hours, flames started to penetrate this crack. When the slab was lifted off the furnace, the steel decking was glowing pink, with severe blistering on the decking surface (Figure 6-36).

Figure 6-36: Hibond slab being lifted off the furnace.

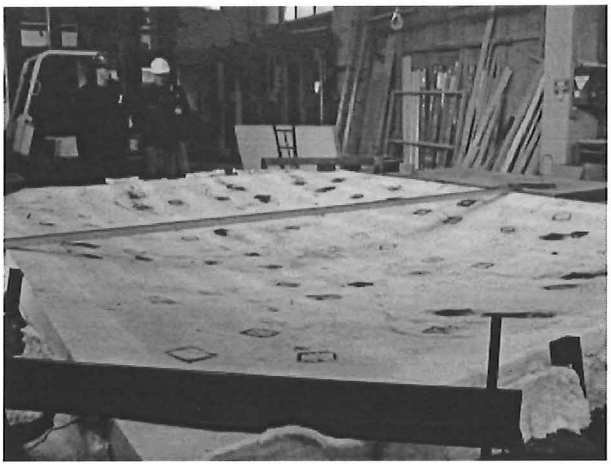

Figure 6-37: Deflected slab after the fire test.

Figure 6-37 shows the large deflections in the Hibond slab after the fire test. Figure 6-38 shows a large crack (up to 9mm wide) had formed across the middle of the slab in the longitudinal direction. The slab also had a series of horizontal cracks running across the short span at regular parallel spaces. The cracks were spaced at 300mm apart which corresponded to the position of the bars of the reinforcing mesh. The diagonal cracks which formed at the corners were also spaced at regular intervals.

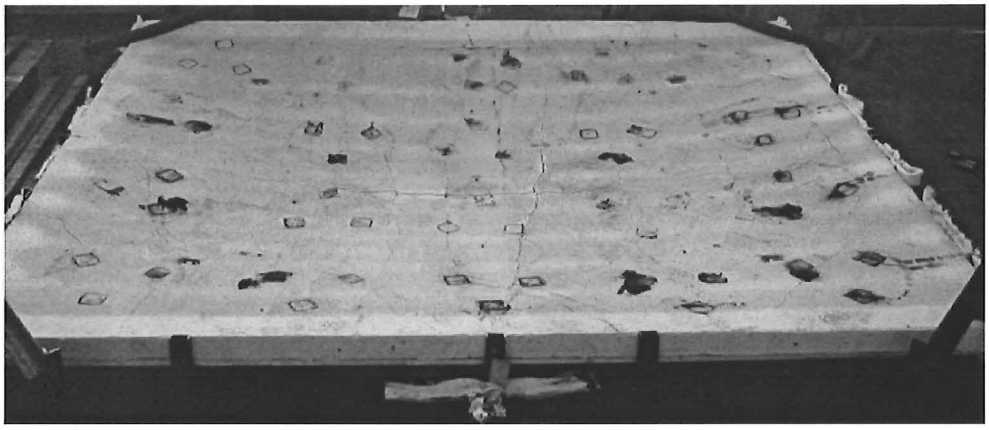

Figure 6-38: Deformed Hibond slab after the fire test.

Figure 6-39 shows that the centre region of the sides of the slab had deflected inwards, relative to the corners of the slabs. The large midspan deflections had caused the centre regions of the sides to contract and deflect inwards. Figure 6-40 shows a large amount of concrete had spalled off the ribs of the slab when the steel decking was pried from the slab. The steel decking held the concrete in place, preventing it from falling off the slab and exposing the reinforcing steel.

Figure 6-39: Inward deflection of the centre regions of the sides of the slab.

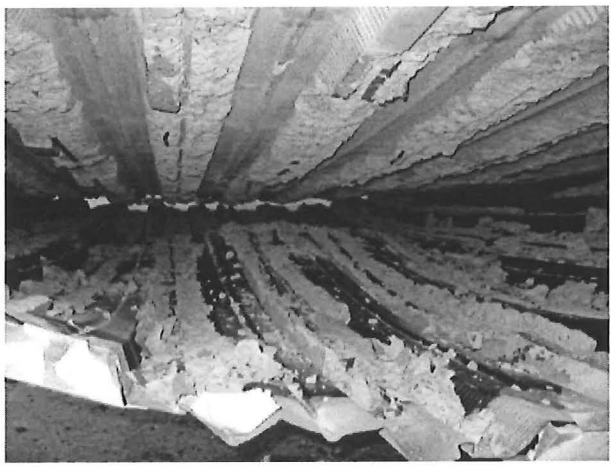

Figure 6-40: Bottom of the Hibond slab after the steel decking was pried from the slab.

6.5.3. Deflections

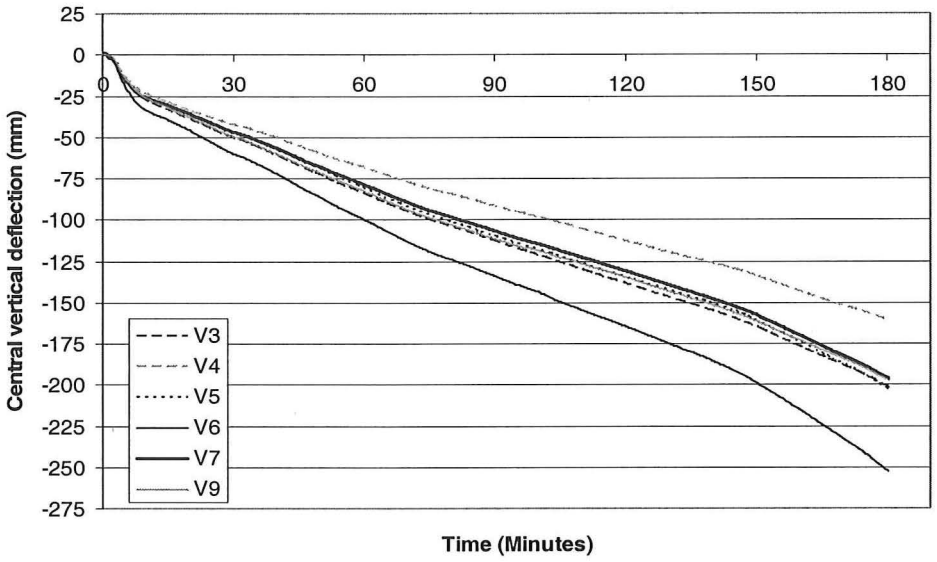

Figure 6-41: Central vertical deflections of the Hibond slab

Figure 6-41 shows the central vertical deflections of the HiBond slab, showing a distinct bilinear trend. The slab deflected downwards very rapidly at a rate of approximately -3.7mm per minute during the first 8 minutes of the fire. During the remaining 140 minutes, the slab deflected at a lower rate of -1.2mm per minute. The deflection rate increased slightly during the last 30 minutes, resulting in a final midspan deflection of -253mm at the end of the test.

6.5.4. Slab temperatures

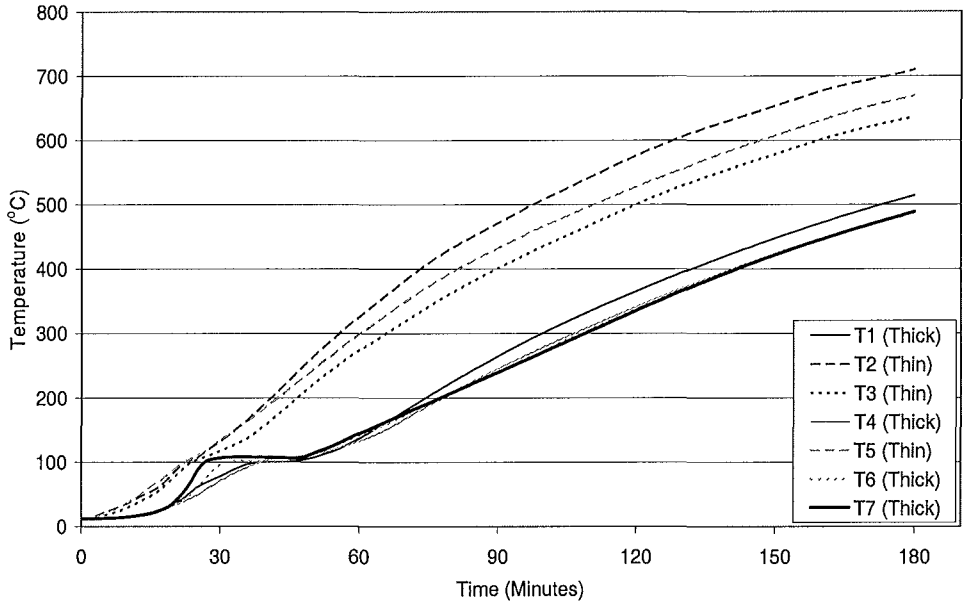

Figure 6-42: Temperatures of the reinforcing mesh of the Hibond slab.

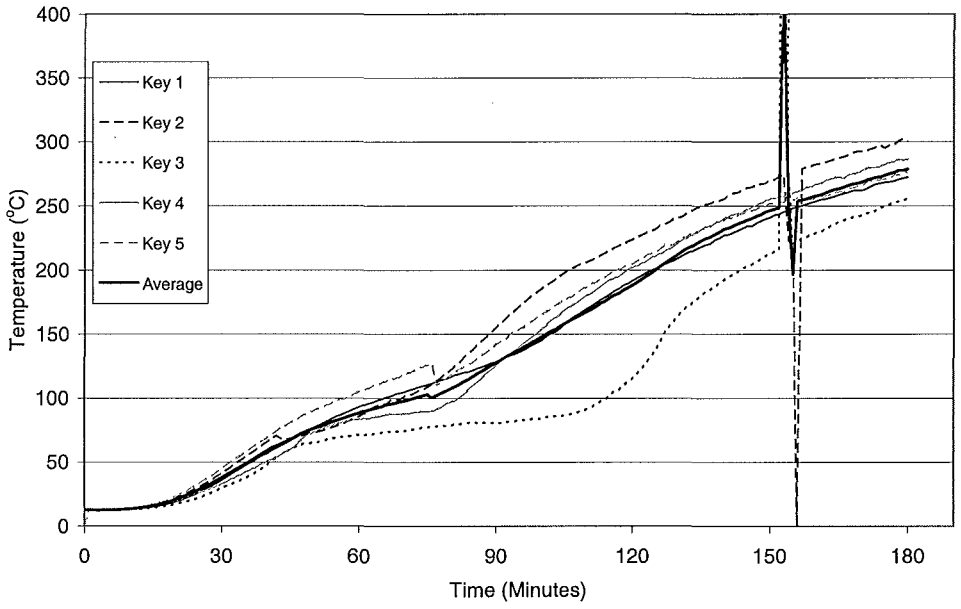

Figure 6-43: Temperatures at the unheated side of the Hibond slab.

Figure 6-42 shows the temperatures of the unexposed face of the slab. The initial temperature on the unexposed side was 13°C. Three of the thermocouples (T2, T3 and T5) show higher temperatures than the other thermocouples. This is because they were mounted on the thin section of the slab while the other thermocouples were mounted on the thicker part of the slab which had the ribs as extra concrete cover. The thermocouples mounted over the ribs show a distinct temperature plateau of 100°C between 26 and 48 minutes. This temperature plateau is due to the moisture accumulation at that level as it was progressively driven off from the heated side towards the cooler side. Figure 6-43 shows the temperatures measured by the key thermocouples. The temperatures on the unheated side exceeded the failure criterion of the 140°C temperature rise (153°C) at 103 minutes. The maximum temperature rise measured by

any one of the five key thermocouples exceeded the 180°C criteria temperature rise (193°C) at 103 minutes.

6.5.5. Strain gauge measurements

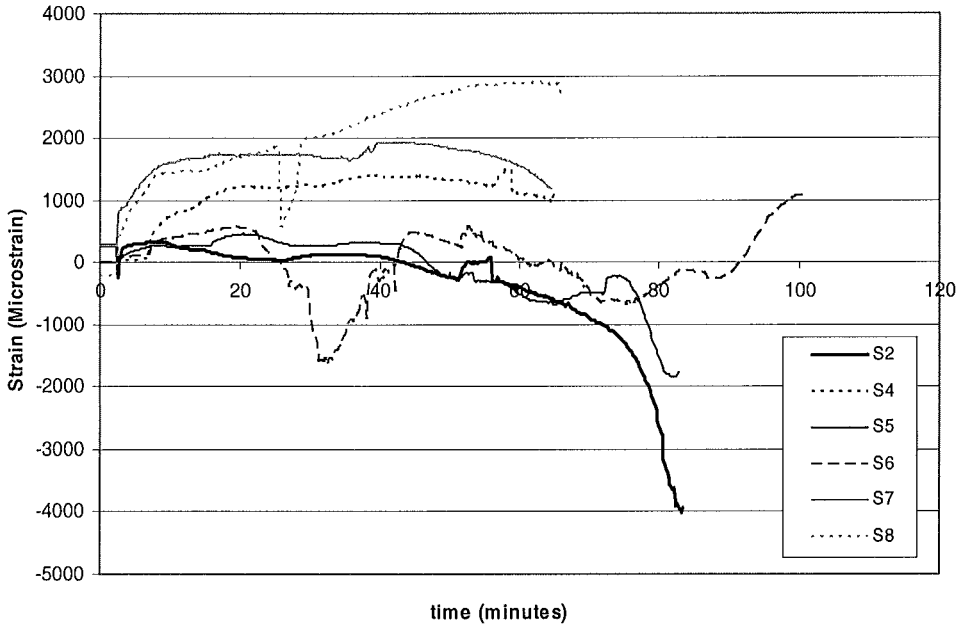

Figure 6-44: Strain gauge measurements of the Hibond slab.

Figure 6-44 shows the strain gauge measurements in the functioning strain gauges in the Hibond slab. Strain gauges S1 and S3 are not plotted because they had been damaged during the casting of the slab. The graph shows that some of the strain gauges lasted up to 65 minutes while some of them failed as early as 22 minutes. The strain gauges which lasted the shorter period were positioned at locations with thinner cover, resulting in earlier failures.

6.6. Test 5: Traydec slab

6.6.1. General

The test was conducted on the 3rd July 2002 at the BRANZ Fire Laboratory. The fire test started at 10.30am and lasted for 3 hours.

6.6.2. Observations

Several minutes after the test started, popping noises similar to those during the Hibond test, were heard. After 20 minutes, cracks started to appear at the east and west sides of the slab. The cracks formed at the side of the slab and propagated upwards at a 45 degree angle from the top of the steel ribs. After 30 minutes, cracks started to appear at the top of the slab, running in the transverse direction in the middle of the slab. The cracks were spaced at 300mm centres, corresponding to the positions of the reinforcing bars of the mesh. The diagonal cracks at the top surface appeared soon after the horizontal cracks formed. The diagonal surface cracks were due to the restraint of the corners against curling. As with the other slabs, a lot of steam and water was generated at the sides and top surface of the slab.

The Traydec slab did not deflect and deform as much as the slabs of the previous tests. When the test was stopped at 3 hours, the mid-span deflection had reached -126mm. Figure 6-45 shows the deflected shape of the slab after the fire test. The diagonal cracks which extended from the top of the ribs had widened up to 3mm (Figure 6-46). There were a series of parallel

cracks running in the transverse direction at the top of the slab, spaced at 300mm centres (Figure 6-47). Compared to that seen in the third and fourth tests, this slab had fewer diagonal cracks and the widths of its surface cracks were generally much smaller.

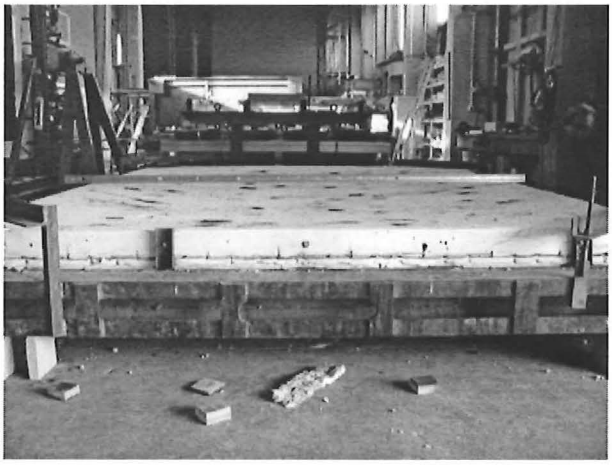

Figure 6-45: Deformed shape of the slab after the test.

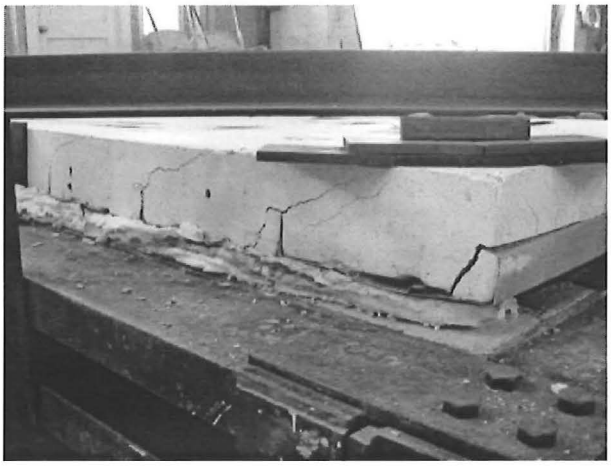

Figure 6-46: Diagonal cracks at the edges of the slab.

The bottom surface of the steel decking did not oxidise as much as the Hibond slab (Figure 6-48). The flat surface of the decking had de-bonded from the concrete, but each individual sheet was locked into the concrete by the steel ribs, which prevented the whole sheet from separating from the concrete (Figure 6-49).

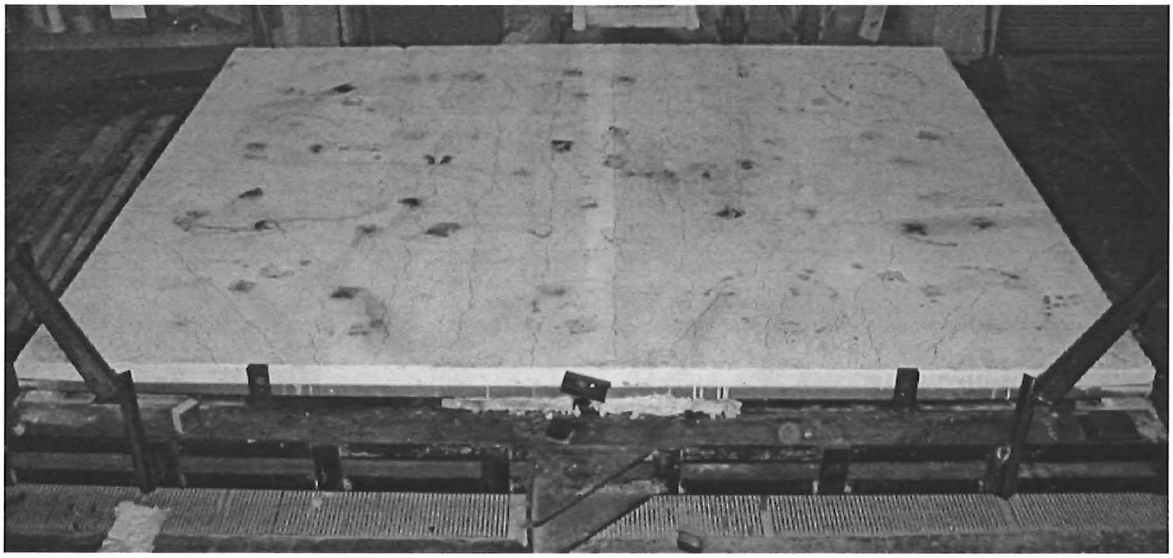

Figure 6-47: Top view of the Traydec slab.

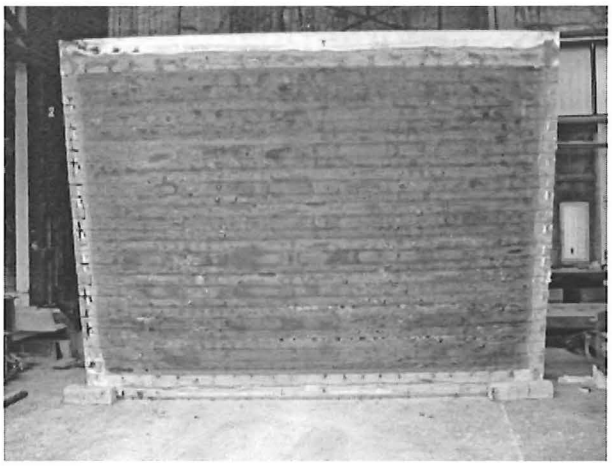

Figure 6-48: Underside of the Traydec slab after the test.

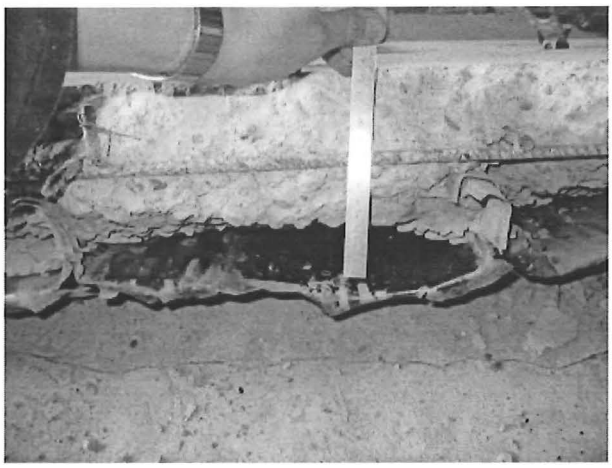

Figure 6-49: Slab cut in half, showing the steel decking locked into the concrete by the ribs.

6.6.3. Deflections

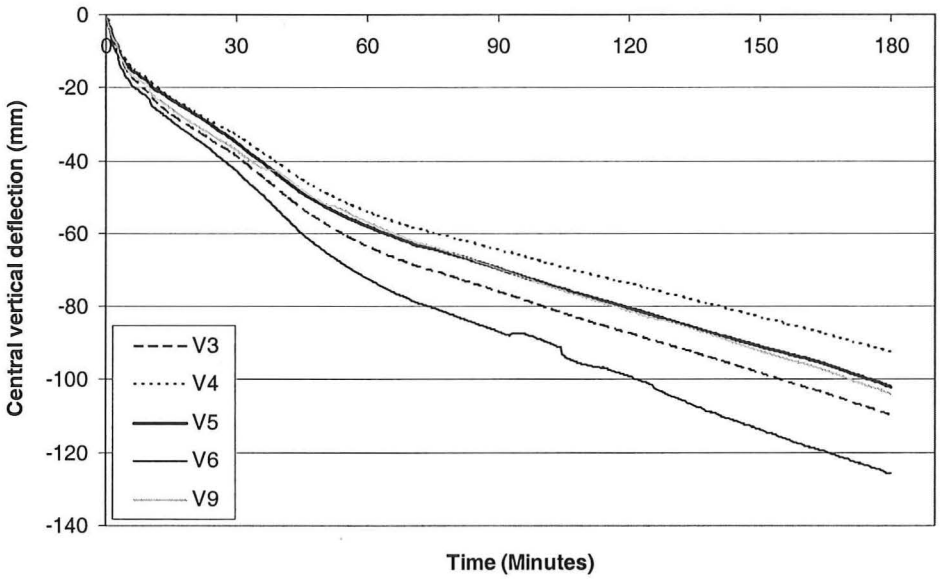

Figure 6-50: Central vertical deflections of the Traydec slab.

Figure 6-50 shows the central deflections of the slab. The graph shows that the slab deflected much quicker during the initial stages (6 minutes), followed by a slower deflection rate during the remainder of the test, which is a consistent trend with the results seen in the other tests. Compared to the previous slabs, the deflection rate of this slab is significantly lower, resulting in a final midspan deflection -126mm at the end of the test. The smaller deflections of the slab were attributed to the thicker section of the slab. The greater cover to the reinforcing steel and embedded ribs of the steel decking in the concrete (Figure 6-49) kept the steel cool, preventing significant loss of stiffness and subsequently large deflections forming in the slab.

6.6.4. Slab temperatures

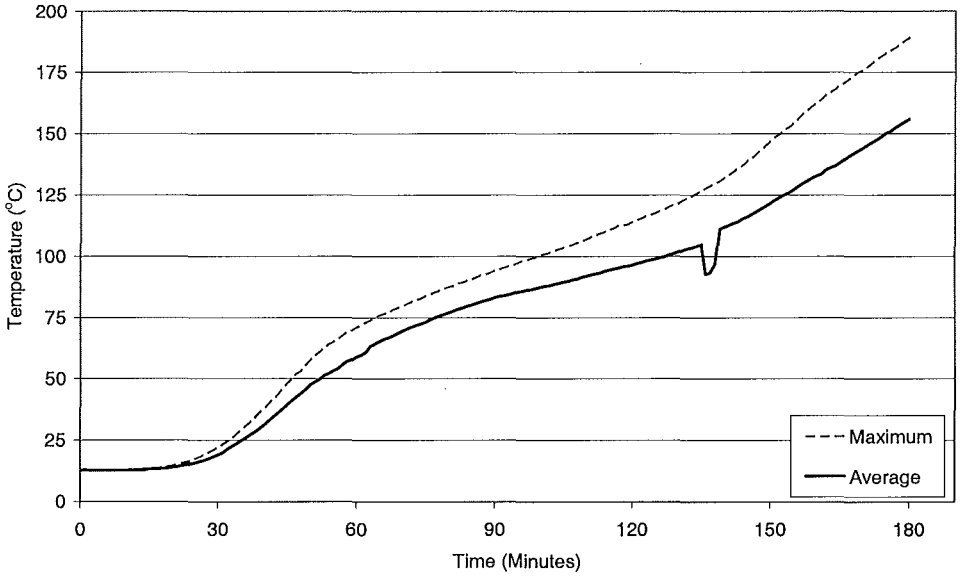

Figure 6-51: Temperatures at unheated side of the Traydec slab.

Figure 6-51 shows the temperatures of the unexposed face of the slab. The average temperature rise measured by the five thermocouples exceeded the failure criterion of the 140°C temperature rise (151°C) at 176 minutes. However, none of the five key thermocouples exceeded the 180°C maximum temperature rise criteria.

6.6.5. Strain gauge measurements

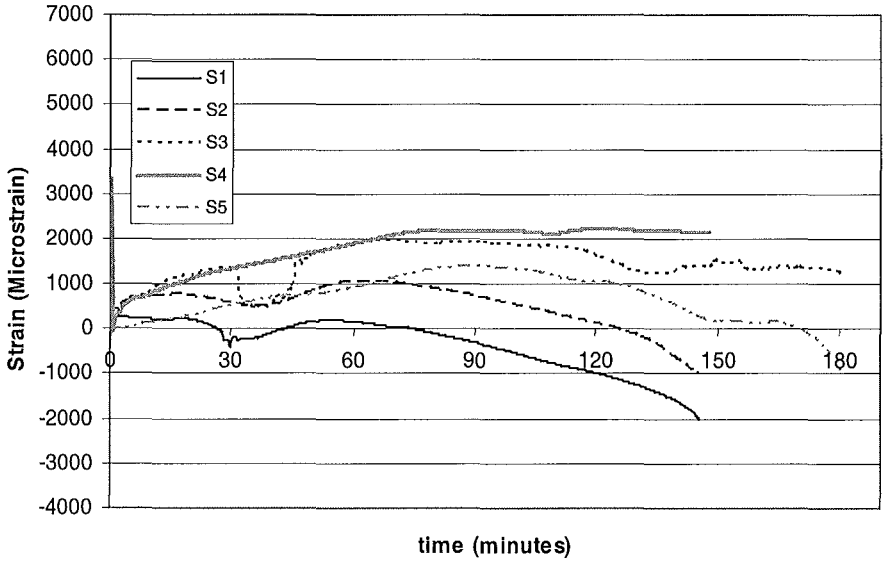

Figure 6-52: Strain gauge measurements of the Traydec slab.

Figure 6-52 shows the measurements from the strain gauges S1 to S5 in the Traydec test. The plots for the remaining strain gauges, S6 to S20, are in the Appendices. Unlike the previous tests, the strain gauges in this slab managed to function and record data in excess of 145 minutes, before they started to fail. The greater concrete cover (75mm) to the reinforcing steel kept the temperatures of the reinforcing steel and strain gauges cooler and allowed the strain gauges to operate for a longer time before failure.

6.7. Test 6: Speedfloor slab

6.7.1. General

The test was conducted on the 7th July 2002 at the BRANZ Fire Laboratory. The fire test started at 10.29am and lasted for 3 hours.

6.7.2. Observations

Figure 6-53 shows the Speedfloor slab before the fire test. Before the test started, a short circuit was detected in strain gauges S7 and S12 and did not function during the test. Five minutes after the test started, fine cracks appeared at the top surface of the slab, running in the transverse direction of the slab. Diagonal cracks formed at the corners soon after the transverse cracks formed. After 25 minutes, the side steel joists were glowing red and had buckled (Figure 6-54). Only the joists closer to the side of the slab could be seen through the viewing ports.

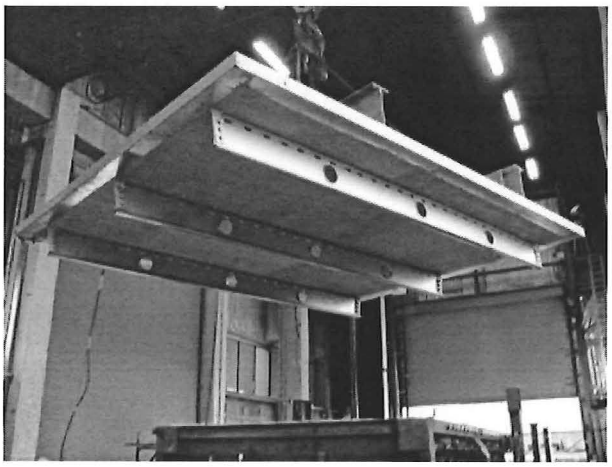

Figure 6-53: Speedfloor slab, before the test.

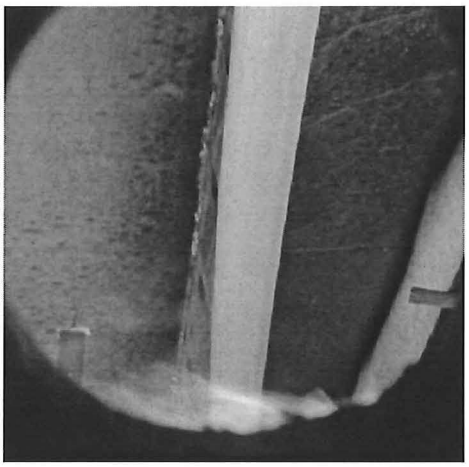

Figure 6-54: Buckling of the joist during the fire test.

After approximately 1 hour, the rotary potentiometer measuring the midspan deflection (V6) malfunctioned, resulting in erratic measurements. To continue measuring the midspan deflections, a wooden block marked with measurements was placed in the middle of the slab. A steel channel was placed across the slab, in front of the wooden block and the level of the midspan deflection was measured by sight using the wooden block and the steel purlin (Figure 6-55 and Figure 6-56).

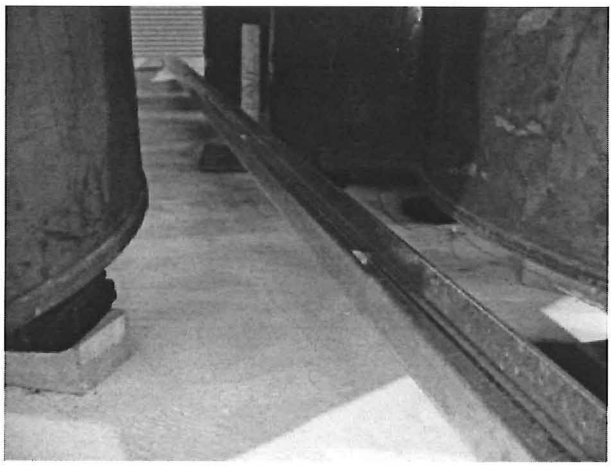

Figure 6-55: Steel channel suspended across the slab to measure the midspan deflections.

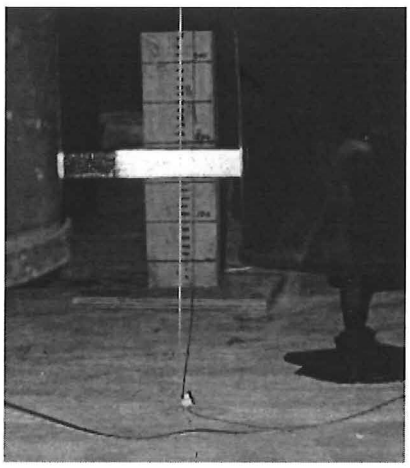

Figure 6-56: Wooden block with notched measurements to measure the midspan deflections.

After 2 hours and 15 minutes, a longitudinal crack had formed at the top surface, propagating across the middle of the slab. The position of the crack corresponded to the location of the centre joist. The water in the middle of the slab had also evaporated by this stage and a crack running in the transverse direction in the middle of the slab could be clearly seen.

At the end of the test (3 hours), the slab had deflected to -180mm at midspan. When the slab was lifted from the furnace, the steel joists were glowing pink (Figure 6-57) and the surface of the joists suffered extensive oxidisation. The centre joist had buckled very severely while the joists closer to sides showed less deformation. Figure 6-58 shows the ends of the joists near the face of the concrete beam. The bottom flanges of the joists did not butt up against the concrete beam, shown by a 10mm gap between the bottom flange of the joist and the vertical face of the concrete beam. The web of one of the side joists had expanded and butted up against one of the steel plates which supported the rollers. This formed a notch at the top of the web.

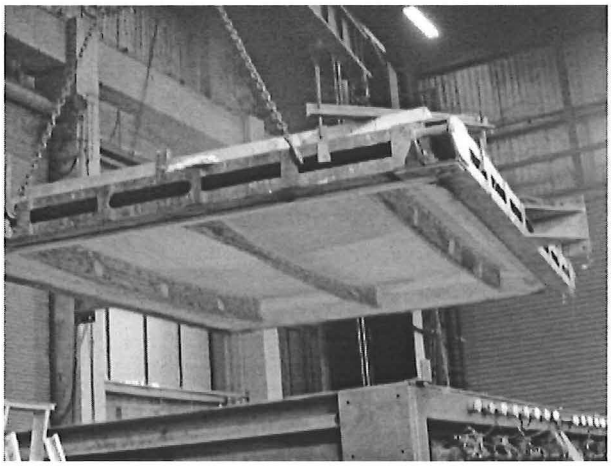

Figure 6-57: The Speedfloor slab being lifted off the furnace after the fire test.

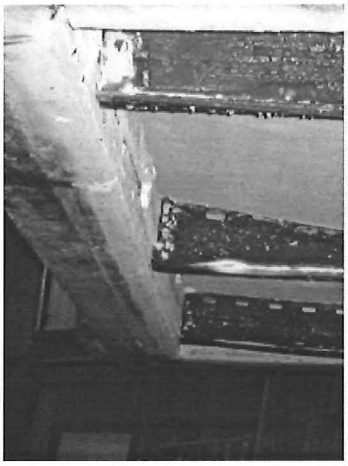

Figure 6-58: Extensive oxidization and buckling of the steel joists.

The top surface of the slab showed extensive cracking in the transverse direction and diagonally at the corners of the slab (Figure 6-59). The widths of the cracks were narrow (maximum of 3mm) and did not crack the full depth of the slab. The transverse cracks in the middle of the slab were spaced at 150mm apart, equal to the spacing of the bars of the mesh. The largest crack on the top surface formed across the longitudinal direction, in the middle of the slab. This crack position corresponded to the location of the centre joist. The bottom surface of the slab showed a few hairline cracks propagating diagonally from the corners of the slab towards the centre region but there was no sign of full depth cracks. The hairline cracks were possibly due to yield lines forming.

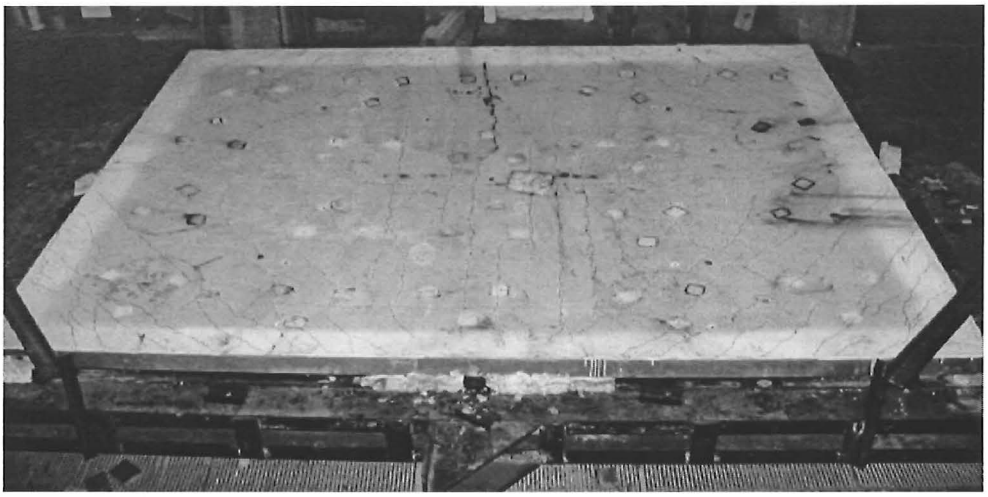

Figure 6-59: Top view of the Speedfloor slab.

6.7.3. Deflections

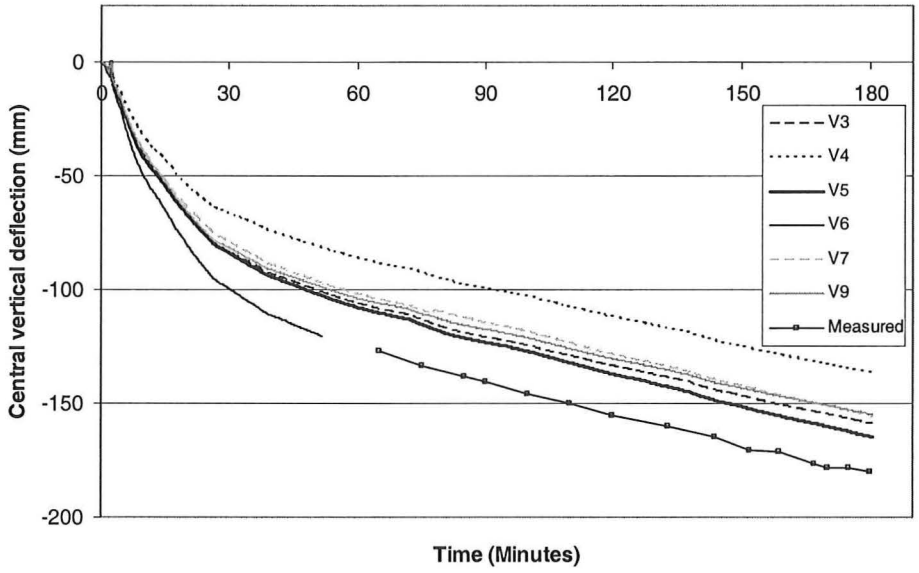

Figure 6-60: Central vertical deflections of the Speedfloor slab.

Figure 6-60 shows the central vertical deflections of the Speedfloor slab. The graph shows that the slab deflects downwards very rapidly during the initial stages, reaching 100mm by 30 minutes. The rate of deflection of the slab decreased after the initial stage into a linear rate. At 55 minutes, potentiometer V6 started to malfunction as it measured very erratic deflection readings. The malfunction was a result of the repeated cycles of heating from the first five tests. The potentiometer could not be replaced and the midspan deflections were measured with a block of wood with notched measurements placed in the middle of the slab. The deflections were measured by sighting the level from the notches and a steel purlin placed across the middle of the slab.

6.7.4. Slab temperatures

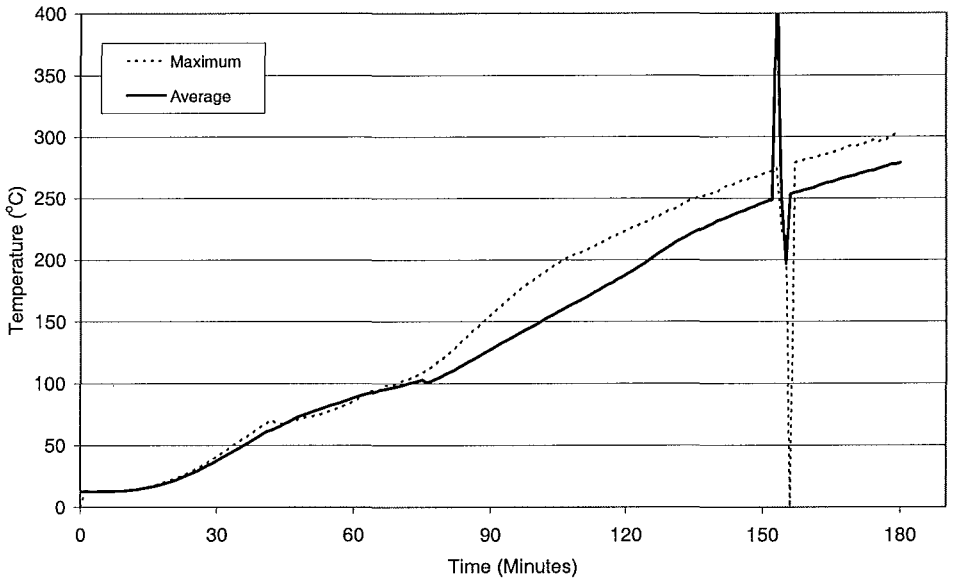

Figure 6-61: Temperatures at unheated side of Speedfloor slab

Figure 6-61 shows the temperatures of the unexposed face of the Speedfloor slab. The initial temperature on the unexposed side was 13°C. The average temperature rise measured by the five thermocouples exceeded the failure criterion of the 140°C temperature rise (153°C) at 103 minutes. The maximum temperature rise measured by one of the five key thermocouples exceeded the 180°C temperature rise criteria (193°C) at 103 minutes.

6.7.5. Strain gauge measurements

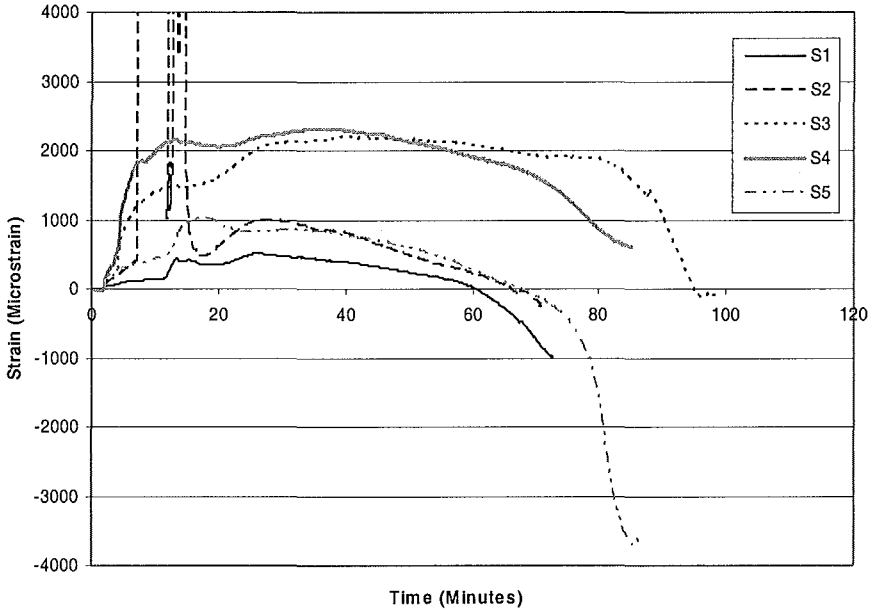

Figure 6-62: Strain gauge measurements of S1-S5 in Speedfloor slab

Figure 6-62 shows the measurements of strain gauges S1 to S5 in the Speedfloor test. The plots for the remaining strain gauges, S6 to S14, are located in the Appendices. The graph shows that as the fire started, the tensile strains in the strain gauges increased very rapidly.

The tensile strains then levelled off and at approximately 30 minutes, the strains in some of the gauges (S1, S2 and S5) started to decrease. After 72 minutes, the average steel temperatures had reached 330°C and the strain gauges progressively started to fail, shown by the sudden strain fluctuations.

6.8. Material properties after the test

6.8.1. Reinforcing steel properties

Slab	Reinforcing steel	Max steel temperature*	Yield stress	Young's Modulus	Rupture strain
Hibond	**D147 mesh**	672 °C	372 MPa	185 GPa	26.7%
Traydec	**D147 mesh**	351 °C	592 MPa	180 GPa	8.72%

* Average of three thermocouples

Table 8: D147 mesh properties after the fire test

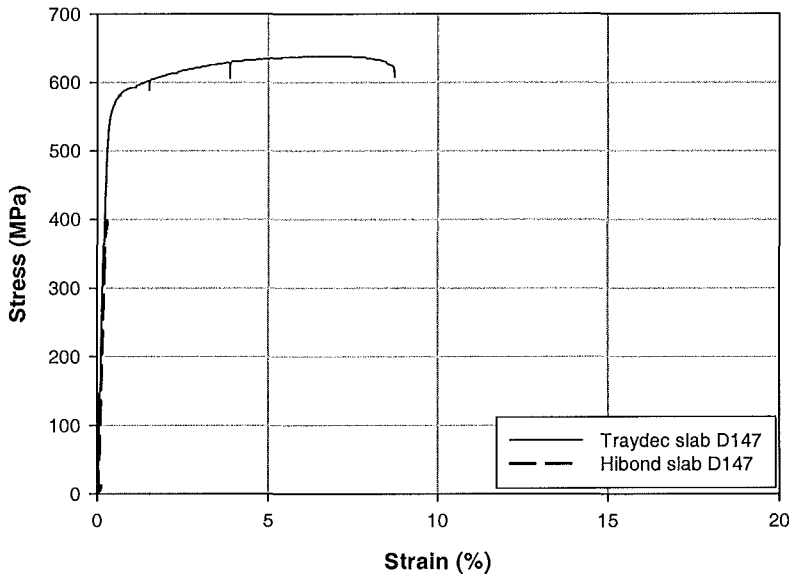

Figure 6-63: Stress-strain curves of D147 mesh after the tests

A week after the fire tests were completed, tensile tests were conducted on the D147 mesh to measure its ductility after the steel was exposed to elevated temperatures. Only the mesh from the Traydec and Hibond slab were available for testing because the steel samples from the other slabs did not fit the test machine as they were too short. Table 8 shows the properties of the steel after they were exposed to varying levels of maximum temperatures. The maximum temperatures of the reinforcing steel of the Hibond and Traydec slabs measured at the end of the tests were 672°C and 351°C, respectively. The yield strength of the Hibond mesh had dropped from 565MPa to 372MPa, but had slightly increased to 592MPa in the Traydec mesh.

Figure 6-63 shows the stress-strain curves of the 147 mesh in the Hibond and Traydec slab after they were exposed to various levels of heating. The rupture strain in the Traydec mesh had increased to 8.72%. Despite being heated up to only 351°C, the steel shows a substantial increase in ductility from its initial value of 2.25%. The stress-strain curve of the Hibond mesh in Figure 6-63 does not show a yield plateau because the steel ruptured outside the measured gauge length and was not detected by the gauge. The rupture strain of the Hibond mesh was determined by manually measuring the steel sample with a ruler. The 26.7%

rupture strain indicated that the ductility of the cold-drawn mesh had increased significantly after being exposed to high temperatures. This prevented fracture of the steel in the slab which would have occurred if the steel was not heated.

6.8.2. Concrete moisture content

	Slab	Slab weight		Water content	
		Before (kN)	After (kN)	Volume (litres)	Percent
1	661 flat slab	33.4*	31.2	225	6.5%
2	HD12 flat slab	35.7	33.8	188	5.2%
3	D147 flat slab	32.9	31.4	147	4.4%
4	Hibond slab	34.5	32.6	196	5.6%
5	Traydec slab	42.8	40.7	221	5.1%
6	Speedfloor	32.9	31.0	192	5.7%

*Estimated weight based on concrete density of 2400kg/m^3

Table 9: Moisture content of slabs

Table 9 shows the moisture content of the slabs, measured by weighing the slabs before and after the tests. The difference of the weight is due to the moisture driven from the slabs during the heating of the slabs. The measured moisture content of the slabs ranged from 4.4% to 6.5%, and the average of moisture content is 5.4% for the six slabs. The low moisture content of the slabs and the absence of spalling of the concrete during the tests gave a good indication that the slabs had been well cured and dried before the tests.

6.9. Summary of results

6.9.1. Midspan deflections

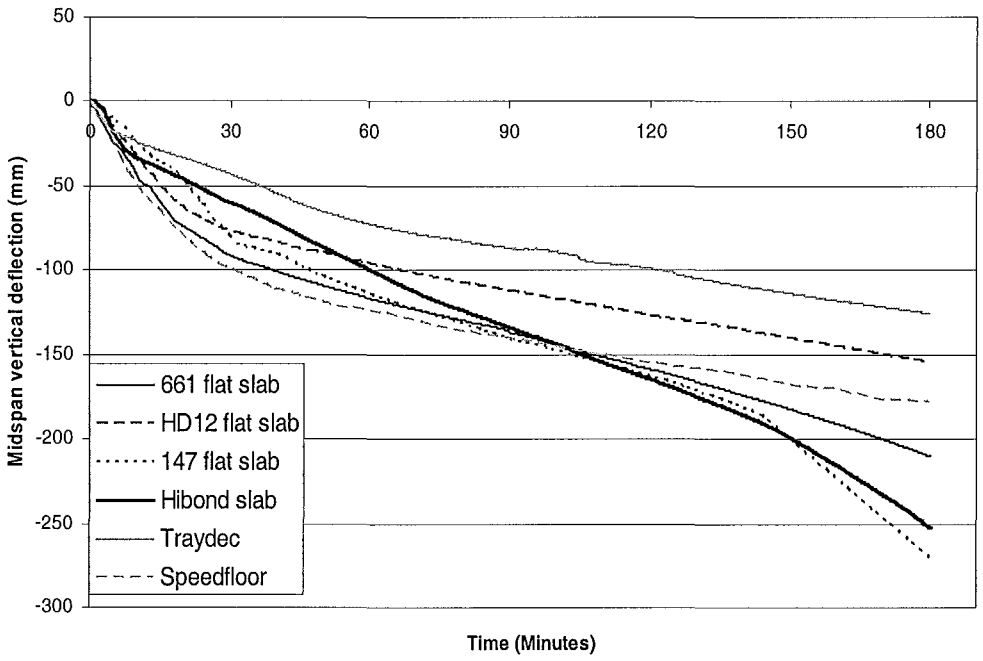

Figure 6-64: Comparison of the midspan vertical deflections in the six slabs tested at BRANZ

Figure 6-64 compares the midspan deflections of the six different slabs during the fire tests. The graph shows that all the slabs had similar deflection rates during the initial stage of the fire. This deflection is due to thermal bowing of the slabs. The slabs with the steel decking show a distinct bilinear deflection trend, with a rapid deflection rate during the initial stages,

followed by a lower deflection rate for the remainder of the fire test. The transition to the lower deflection rate was possibly due to the steel deck buckling and debonding from the concrete, creating an insulating layer of air between the decking and the bottom surface of the concrete. The deflection rates of the other slabs showed a gradual reduction, after 20 minutes, into a steady rate for the remaining duration of the fire. The maximum deflections of the plain slabs with 198mm^2/m, 295mm^2/m and 565mm^2/m were -271mm, -210mm and -154mm, respectively. The similar deflection trends of the plain slabs during the initial stages were due to thermal bowing of the slab while the steel content had negligible effect. The final deflections of the slab were governed by the steel content of the slab, and were not due to thermal bowing.

6.9.2. Test results versus code recommendations

Stability criteria

	Expected fire resistance rating	Test result
100mm flat slab	120 minutes[1] (Two-way, simply supported)	180 minutes
Hibond slab	30 minutes[2] (One way, simply supported)	180 minutes
Traydec slab	240 minutes[1]	180 minutes
Speedfloor slab	120 minutes[1] (Two-way simply supported)	180 minutes

1 = NZS 3101: Part 1 (SNZ, 1995)
2 = Manual No. 7, Hibond Design Manual (Dimond Industries, 1997)

Table 10: Comparison of test results with existing design recommendations for stability criteria

Table 10 compares the expected fire resistance stability rating with the test result. The fire resistances recommended by NZS 3101 (SNZ, 1995) are based on the concrete cover to the reinforcement. Apart from the Traydec slab, the other slabs had higher stability ratings than those recommended by codes and design manuals. The stability ratings recommended by the codes are based only on the concrete cover to the reinforcing steel. The recommended fire resistance rating of the Hibond slab is significantly lower than that achieved in the test because its recommended rating is based on a one way slab.

Insulation criteria

	Expected fire resistance rating	Test result
100mm flat slab	100 minutes[1]	114 minutes
Hibond slab	105 minutes[2]	103 minutes
Traydec slab	160 minutes[3]	176 minutes
Speedfloor slab	83 minutes[1]	103 minutes

1 = NZS 3101: Part 1 (SNZ, 1995), Type A aggregate
2 = Manual No. 7, Hibond Design Manual (Dimond Industries, 1997)
3 = Traydec 300 Specification and Design Manual (Forgan Jones Structural Ltd, 1996)

Table 11: Comparison of test results with existing design recommendations for insulation criteria

Table 11 compares the insulation ratings recommended by the codes with the test results. The fire resistance ratings from the tests were similar to the test results and in most cases, the times to insulation failure in the tests were greater than the recommended ratings.

Integrity criteria

The only slab that had an integrity failure was the Hibond slab. The integrity failure was minor and occurred when small flames passed through one of the full depth cracks in the middle of the slab. It occurred just before the furnace was turned off at 180 minutes. The other slabs did not have integrity failures.

6.9.3. Comparison of test results with yield line theory

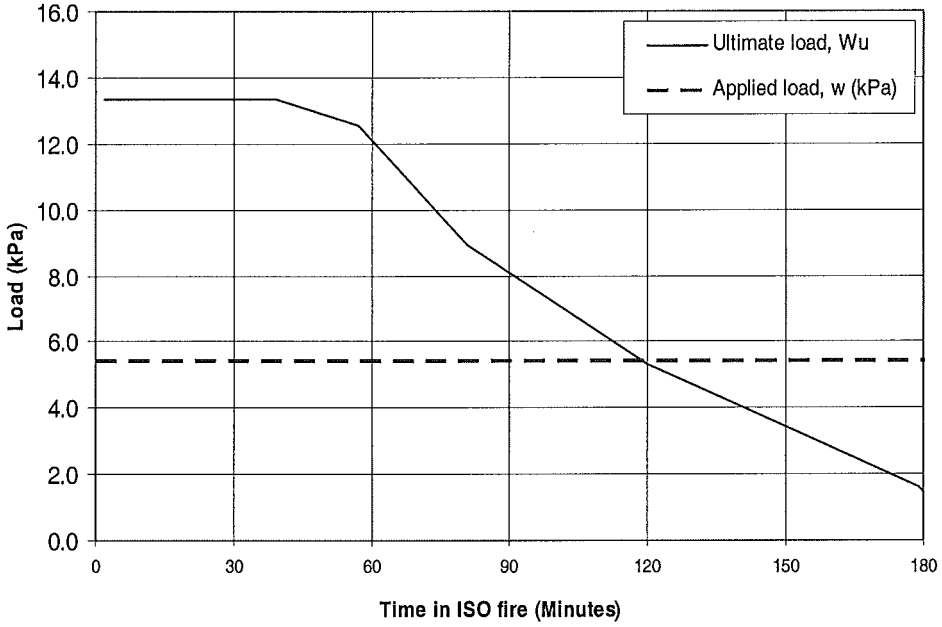

Figure 6-65: Variation of the ultimate load carrying capacity, W_u, with time (D147 mesh flat slab)

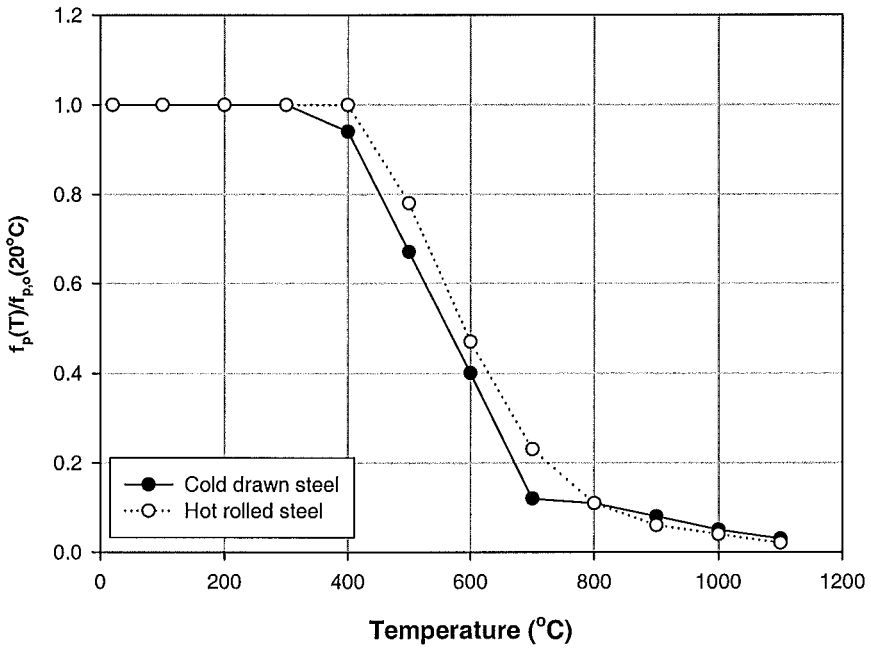

Figure 6-66: Yield strength reduction factors for cold drawn and hot-rolled steel (EC2, 1995)

Figure 6-65 shows the variation of the calculated ultimate load capacity for one of the flat slabs (D147 flat slab) during the ISO fire. The theoretical ultimate load carrying capacities, $W_{u,f}$, were calculated using yield line theory (Park et al, 2000). The calculated ultimate load capacity of the slab reduces with increasing time of exposure in the standard fire. The reduction of the load carrying capacities were calculated using the reduced strengths of the reinforcing steel at elevated temperatures. The temperatures of the reinforcing steel were obtained from the measured temperatures of the reinforcing during the fire tests and the reduced strengths of the hot-rolled and cold-drawn reinforcing steel were determined from the strength reduction factors from the Eurocode (EC2, 1995), as shown in Figure 6-66.

Figure 6-65 shows that the predicted load carrying capacity, $W_{u,o}$, of the D147 flat slab at the start of the fire, was 13.3kPa. The applied load on the slab is 5.40kPa; hence the corresponding load ratio, r_{load}, is:

$$r_{load,\ o} = \frac{w}{W_{u,\ o}} = \frac{5.4\ \ kPa}{13.3kPa} = 0.41$$

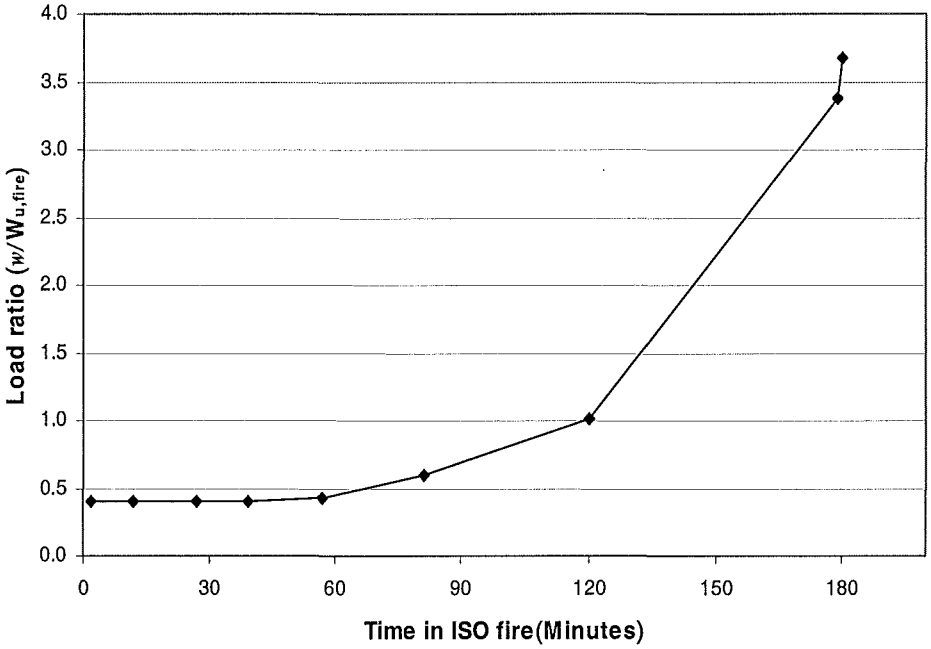

Figure 6-67: Variation of the load ratio during the fire.

Figure 6-67 shows the variation of the load ratio of the D147 flat slab during the ISO fire. During the first 39 minutes, the load ratio of the slab remains constant, at 0.41. As the temperatures of the reinforcing steel increased, the flexural strength and the load carrying capacity of the slab decreased. At 120 minutes, the load carrying capacity of the slab had decreased to the point where it equalled the applied loads. However, the tests showed that the slab could still carry the applied loads for the full duration of 3 hours in the fire without collapse despite its calculated load capacity dropping below the applied loads.

By 3 hours, the predicted load carrying capacity of the slab ($W_{u,f}$) had dropped significantly, below the level of the applied loads, to 1.47kPa and the load ratio had increased up to 3.67.

$$r_{load,\ f} = \frac{w}{W_{u,\ fire}} = \frac{5.4\ \text{kPa}}{1.47\text{kPa}} = 3.67$$

This indicates that after being exposed for 3 hours to the ISO fire, the slab was able to carry a load 3.67 times greater than predicted by conventional yield line theory. Although the flexural strength of the slab had decreased below the level of the applied loads, the slab did not collapse and resisted the loads by tensile membrane action.

Slab		Applied load, w (kPa)	Ambient temperature	After 3 hours exposure to ISO fire		
			$W_{u,o}$ (kPa)	Max. Steel Temp. (°C)	$W_{u,f}$(kPa)	Load ratio, $r_{load,f}$ ($w/W_{u,f}$)
1	**661 Flat slab**	5.40	20.0	683	***2.40***	***2.25***
2	**HD12 Flat slab**	5.40	28.2	688	6.49	0.83
3	**D147 Flat slab**	5.40	13.3	703	***1.47***	***3.67***
4	**Hibond slab**	5.52	70.2	672	***1.09***	***5.06***
5	**Traydec slab**	6.12	75.0	339	8.57	0.71
6	**Speedfloor**	5.16	55.1	623	***2.02***	***2.55***

Table 12: Load carrying capacities of the slabs, before and after the fire tests.

Table 12 shows the predicted load carrying capacity of the slabs, before and after the fire tests. The table shows that by 3 hours in the ISO fire, the ultimate load carrying capacities ($W_{u,f}$) of the slabs had decreased significantly. The slabs whose load carrying capacities had dropped below the level of the applied loads are shown in the bold italics numbers. The load ratios of these slabs had exceeded unity, ranging from 2.25 in the 661 flat slab up to 5.06 in the Hibond slab.

The ultimate loads of the HD12 flat slab and the Traydec slab had also decreased, but their load ratios had not exceeded unity at 3 hours. The ultimate load of the HD12 flat slab did not drop below the level of the applied load despite its reinforcing steel reaching temperatures similar to those in the other flat slabs. This is due to the high steel content in the slab, which results in the higher flexural strength of the slab. The ultimate load of the Traydec slab did not drop below the level of the applied loads because of the thicker concrete cover to the reinforcing mesh. This prevented the mesh from reaching excessively high temperatures which would have caused significant loss of strength. The ribs of the steel deck were also embedded in the concrete and remained relatively cool. It acted as fire emergency reinforcement and allowed the slab to retain its stiffness.

7. CONCLUSIONS

Six fire tests of two-way concrete and composite slabs were conducted at the BRANZ furnace. The slabs were simply supported and horizontally unrestrained and loaded with a live load of 3.0kPa. The slabs were exposed to the ISO standard fire for three hours.

The slabs supported the full design loads for the entire duration of the fire. The temperatures of the reinforcing steel in some of the slabs exceeded 700°C after 3 hours and very high temperatures were measured in the slabs. The slabs suffered extensive surface cracking on the unheated surface and full depth cracks formed in some of the slabs. None of the slabs collapsed in spite of the large deflections (up to 270mm) sustained by some of the slabs. The fire tests showed that the closer bar spacing and higher steel content of the 661 mesh and the HD12 mesh prevented large, full-depth cracks from forming and enabled the slabs to maintain their integrity rating. The cold-drawn mesh used in the tests performed well and did not rupture due to the significant increase of the ductility of the steel at elevated temperatures.

The tests illustrated the significant influence of tensile membrane action on maintaining the structural stability of the floor slabs under fire conditions, by supporting loads significantly in excess of their predicted yield line capacities.

The data from these tests will be very useful for verification of computer models for predicting structural behaviour of reinforced concrete slabs in fire conditions.

8. REFERENCES

Bailey, C.G. (2001) Membrane action of unrestrained lightly reinforced concrete slabs at large displacements. *Engineering Structures.* Vol. 23. No. 5. Pp. 470-483.

Bailey, C.G., Lennon, T. and Moore D.B. (1999) The behaviour of full-scale steel-framed buildings subjected to compartment fires. The Structural Engineer. Vol. 77 No. 8., pp. 15-21.

Bailey, C.G., White, D.S. and Moore, D.B. (2000) The tensile membrane action of unrestrained composite slabs simulated under fire conditions. *Engineering Structures.* Vol. 22 No. 11. pp 1583-1595.

Bailey, C.G. and Moore, D.B. (2000a) The structural behaviour of steel frames with composite floorslabs subject to fire: Part 1: Theory. *The Structural Engineer.* Vol. 78 No. 11. pp. 19-27.

Bailey, C.G. and Moore, D.B. (2000b) The structural behaviour of steel frames with composite floorslabs subject to fire: Part 2: Design. *The Structural Engineer.* Vol. 78 No. 11. pp. 28-33.

Clifton, G.C., Hinderhofer, M.D., and Schmid, R. (2001) Design of Multi-Storey Steel Framed Buildings with Unprotected Secondary beams or joists for Dependable Inelastic Response in Severe Fires. *HERA Steel Design and Construction Bulletin No. 60,* HERA, Manukau City, New Zealand.

Dimond Industries (1997) Manual No. 7, Hibond Design Manual, *Diamond Industries.*

EC2, (1995). Eurocode 2: *Design of concrete structures. ENV 1992: Part1-2: General rules-Structural fire design,* European Committee for Standardization, Brussels.

Elghazouli, A.Y., Izzuddin, B.A. (200) Analytical assessment of the structural performance of composite floors subject to compartment fires. *Fire Safety Journal.* Vol. 36 No. 8. pp. 769-793.

Forgan Jones Structural Ltd (1996) Traydec 300 Specification and Design Manual, Silverdale, New Zealand.

Franssen, J.-M., Kodur, V.K.R. and Mason J. (2002) *User's manual for SAFIR2001 free: A computer program for analysis of structures at elevated temperature conditions.* University of Liege, Department Structures de Genie Civil, Service Ponts et Charpentes, Belgium.

Hayes B. (1968) Allowing for membrane action in the plastic analysis of rectangular reinforced concrete slabs. *Magazine of Concrete Research.* Vol. 20. No. 65, pp. 205-212.

Huang, Z., Burgess, I.W. and Plank, R.J. (1999a) Nonlinear analysis of reinforced concrete slabs subjected to fire. *ACI Structural Journal.* Vol. 96 No.1 pp. 127-135.

Huang, Z., Burgess, I.W. and Plank, R.J. (1999b) Three-dimensional modelling of two full-scale fire tests on a composite building. *Proceedings of the Institution of Civil Engineers Structures and Buildings.* Vol 134 pp. 243-255.

Huang, Z., Burgess, I.W. and Plank, R.J. (2001) Non-linear structural modelling of a fire test subject to high restraint. *Fire Safety Journal.* Vol. 36 No. 8 pp 795-814.

Lamont, S., Usmani, A.S. and Drysdale, D.D. (2001) Fire protection of steel beams in composite framed structures. *Proc. Interflam Conference 2001 (Edinburgh)* pp. 407-418.

Lim, L. (2003) Membrane action in fire exposed concrete floor systems. Ph.D. Thesis. Department of Civil Engineering, University of Canterbury, New Zealand. (*In Preparation*)

Newman, G.M., Robinson, J.T. and Bailey, C.G. (2000) *Fire Safe Design: A New Approach to Multi-Story Steel-Framed Buildings.* The Steel Construction Institute, Berkshire, U.K.

Park, R. and Gamble, W. (2000) *Reinforced Concrete Slabs.* John Wiley and Sons, Inc.

Sanad, A.M., Rotter, J.M., Usmani, A.S. and O'Connor, M.A. (1999) Finite Element Modelling of Fire Tests on the Cardington Composite Building, *Proc of Interflam '99 Int. Fire Science and Engg Conference, pp. 1045-1056 (Edinburgh, Scotland) 29 June- 1 July.*

Sawczuk, A., Winnicki L. (1965) Plastic behaviour of simply supported reinforced concrete plates at moderately large deflections. *Int. Journal of Solids & Structures.* Vol. 1. pp. 97-111

SNZ (1995) NZS 3101: Part1: 1995. *The Design of Concrete Structures,* Standards New Zealand, Wellington.

Standards Australia (1997) AS1530 Methods of fire tests on building materials, components and structures. Part 4: Fire resistance tests of elements of building construction. Standards Australia, New South Wales.

APPENDICES

This section presents the data collected from the tests. The data that were already presented in the main section of the report are not presented here. The appendix is subdivided into the following sections:

Appendix 1: Deflection measurements
Appendix 2: Temperature measurements
Appendix 3: Strain gauge measurements
Appendix 4: Photographs

Within each appendix, the data are presented separately for each slab, in the following order:

1. 661 flat slab
2. HD12 flat slab
3. D147 flat slab
4. Hibond slab
5. Traydec slab
6. Speedfloor

Appendix 1: Deflection data

The layout of the measurement points is shown in Figure 4-13.

Slab		Vertical deflection points	Horizontal deflection points
1.	100mm flat slab (D147 mesh)	V1 – V9	H1 – H4
2.	100mm flat slab (661 mesh)	V1 – V10	H1 – H4
3.	100mm flat slab (HD12 reinforcing)	V1, V3 – V9	H1 – H4
4.	130mm Hi-bond slab	V1, V3 – V9	H1 – H4
5.	130mm Traydec slab	V1, V3 – V9	H1 – H4
6.	90mm flat slab on Speedfloor joists	V1, V3 – V9	H1 – H4

Table 13: Deflection measurement points in the slabs.

Test 1: 661 flat slab

Refer to section 6.2.4.

Test 2: HD12 flat slab

Refer to section 6.3.3.

Test 3: D147 flat slab

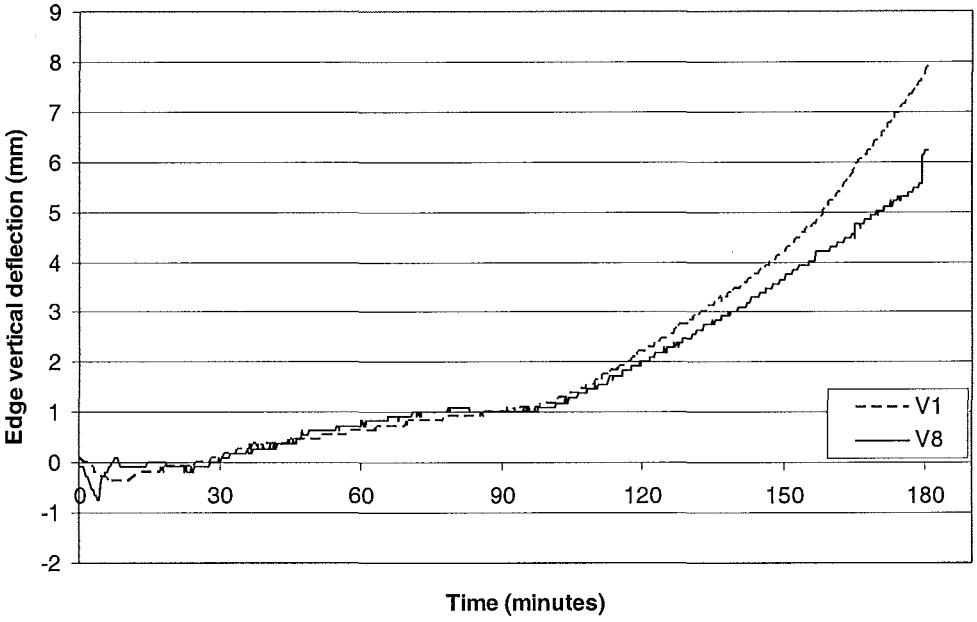

Appendix Fig. 1: Edge vertical deflections of the D147 flat slab.

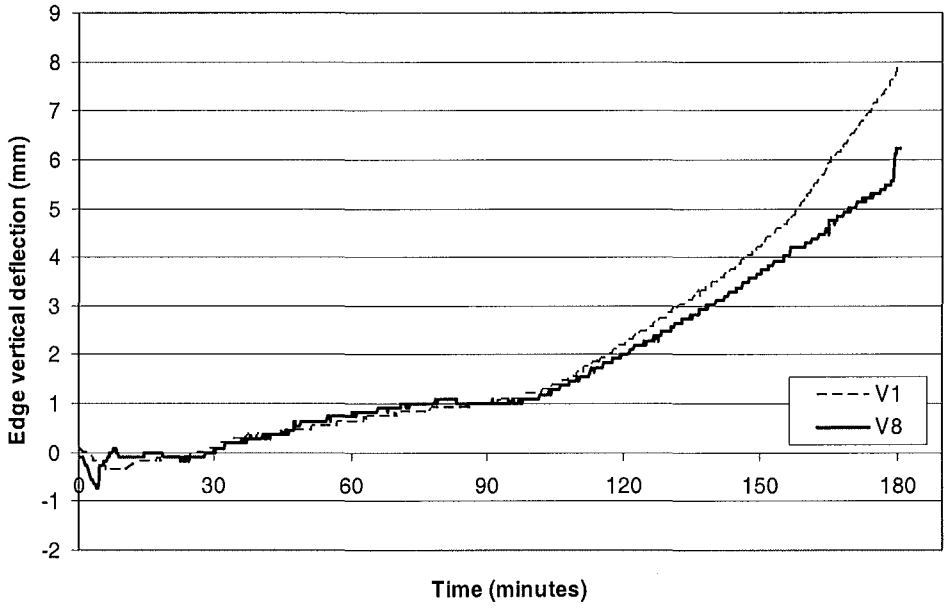

Appendix Fig. 2: Edge horizontal deflections of the D147 flat slab.

Test 4: Hibond slab

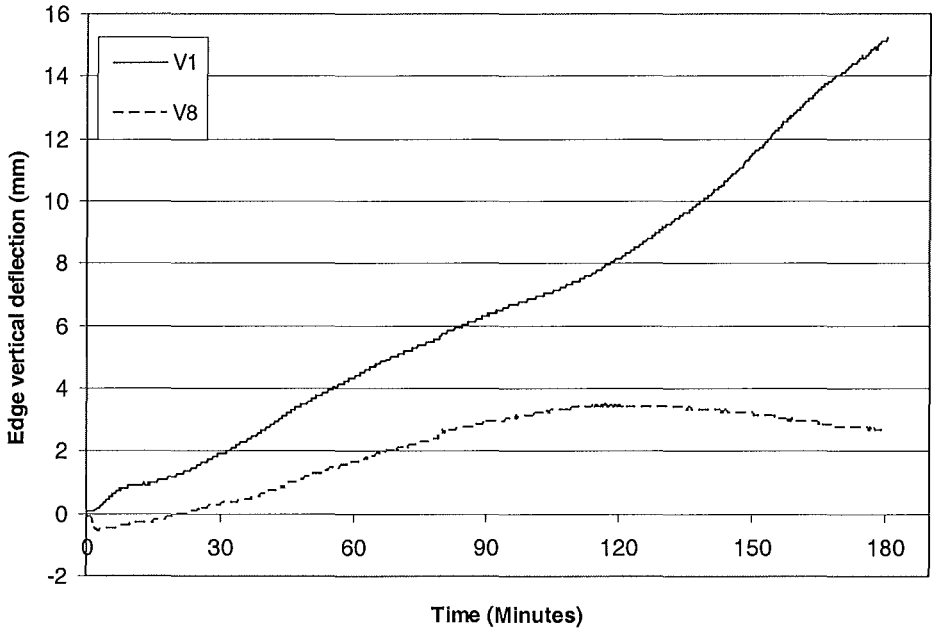

Appendix Fig. 3: Edge vertical deflections of the Hibond slab.

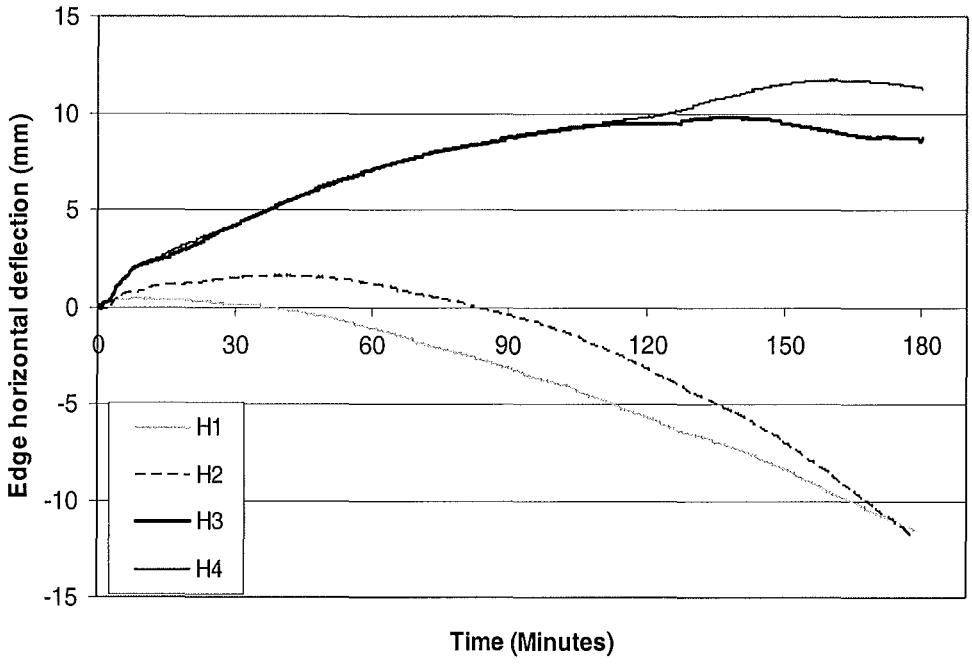

Appendix Fig. 4: Edge horizontal deflections of the Hibond slab.

Test 5: Traydec slab

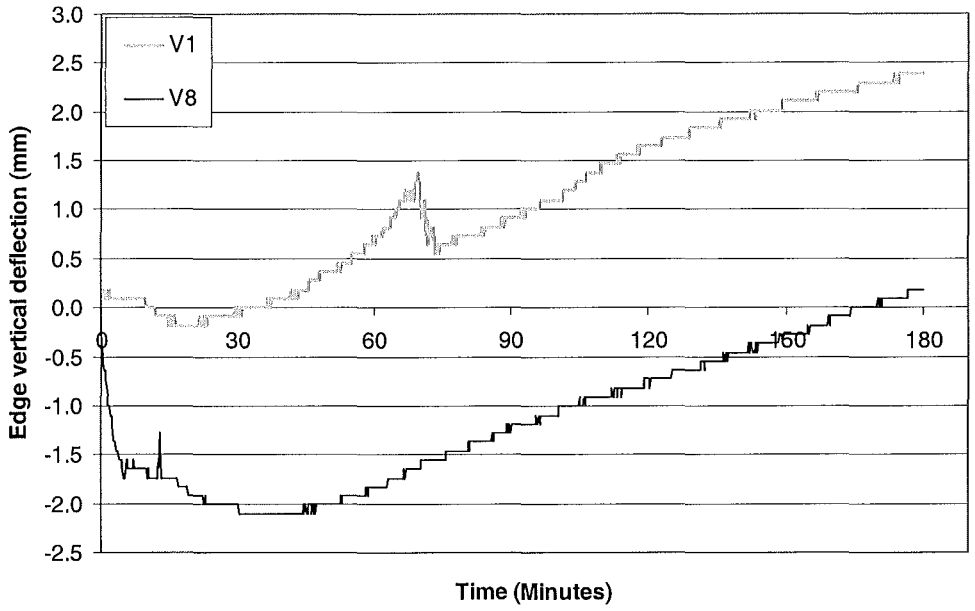

Appendix Fig. 5: Edge vertical deflections of the Traydec slab.

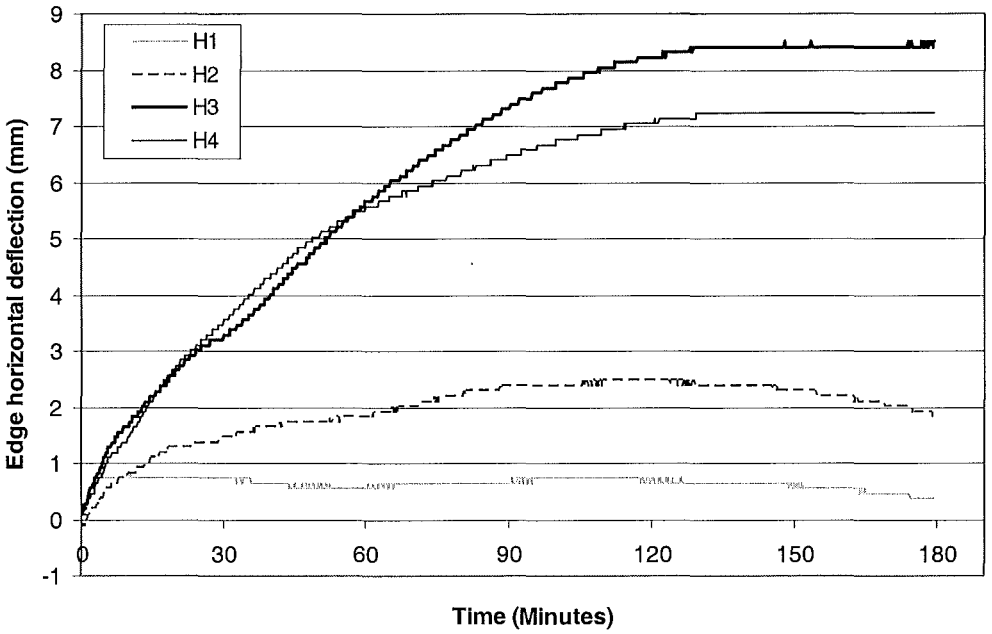

Appendix Fig. 6: Edge horizontal deflections of the Traydec slab.

Test 6: Speedfloor slab

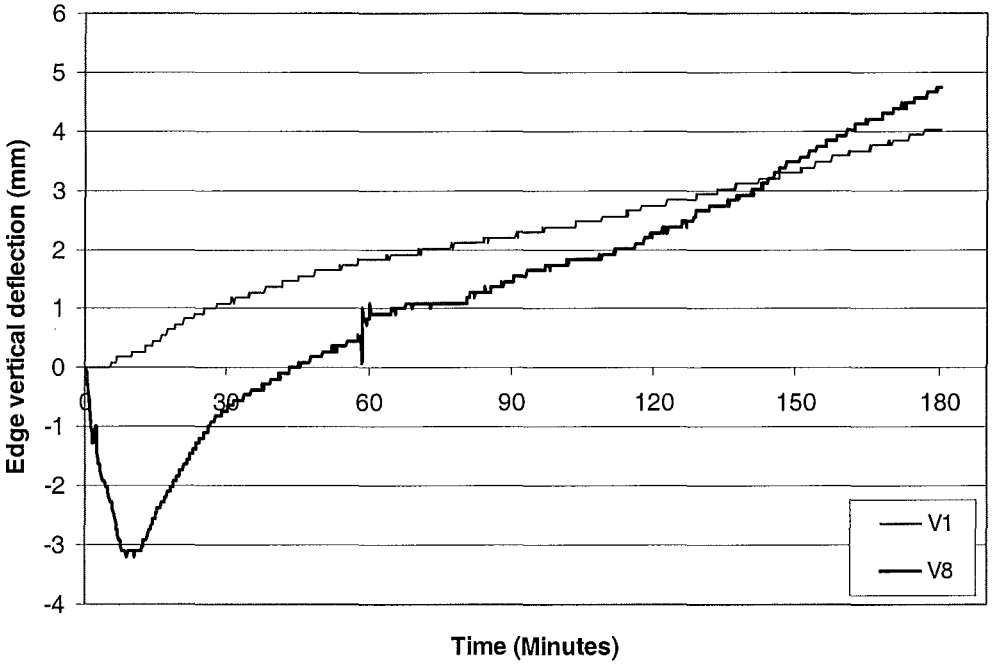

Appendix Fig. 7: Edge vertical deflections of the Speedfloor slab.

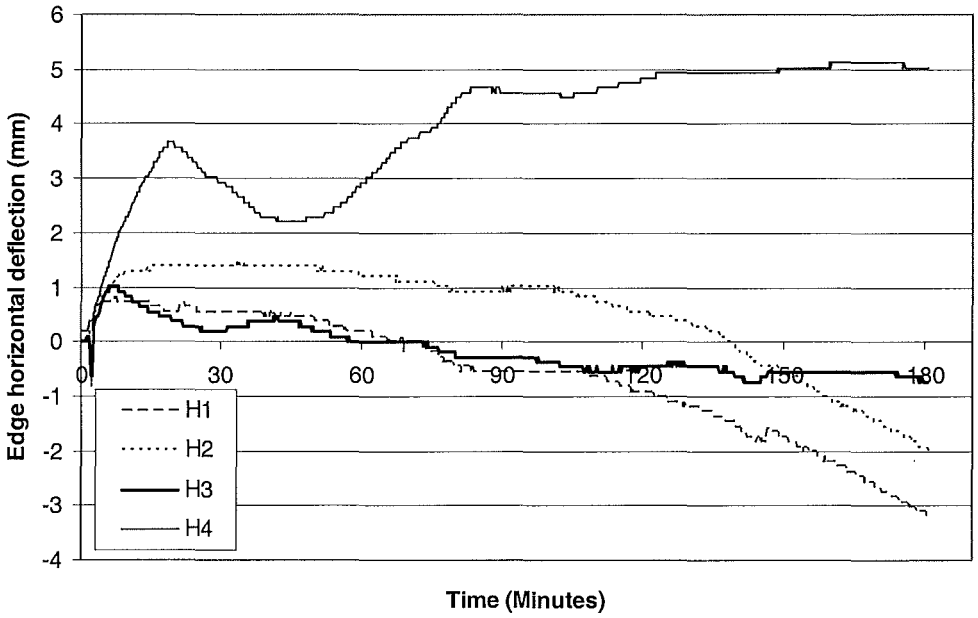

Appendix Fig. 8: Edge horizontal deflections of the Speedfloor slab.

Appendix 2: Temperature data

Test 1: 661 flat slab

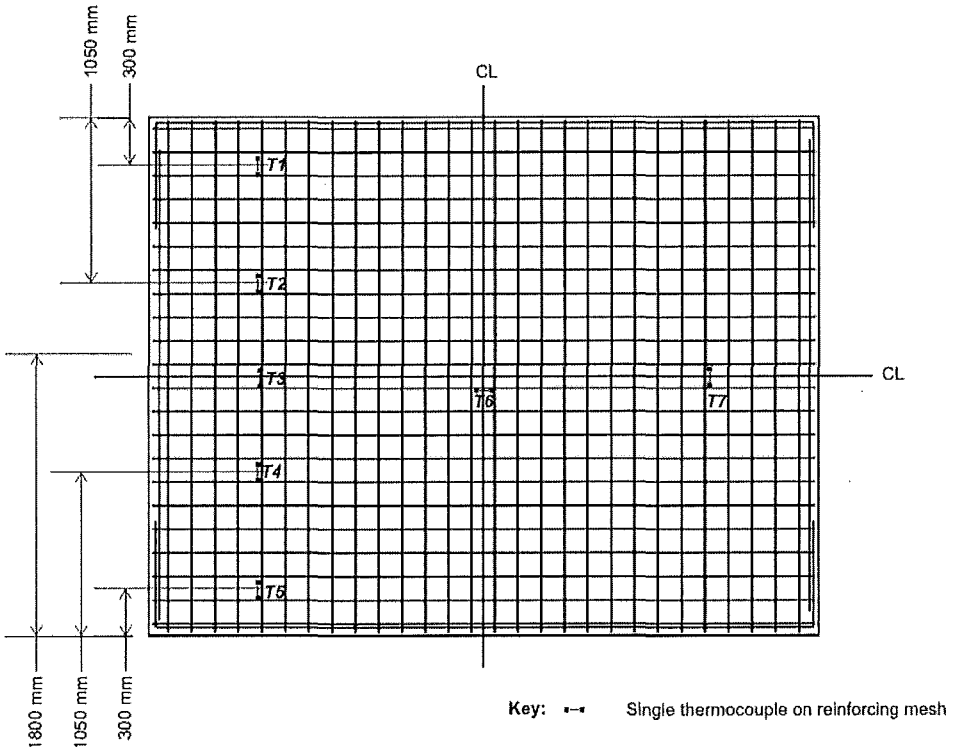

Appendix Fig. 9: Thermocouple layout in the 661 flat slab.

Refer to section 6.2.5 for temperature data.

Test 2: HD12 flat slab

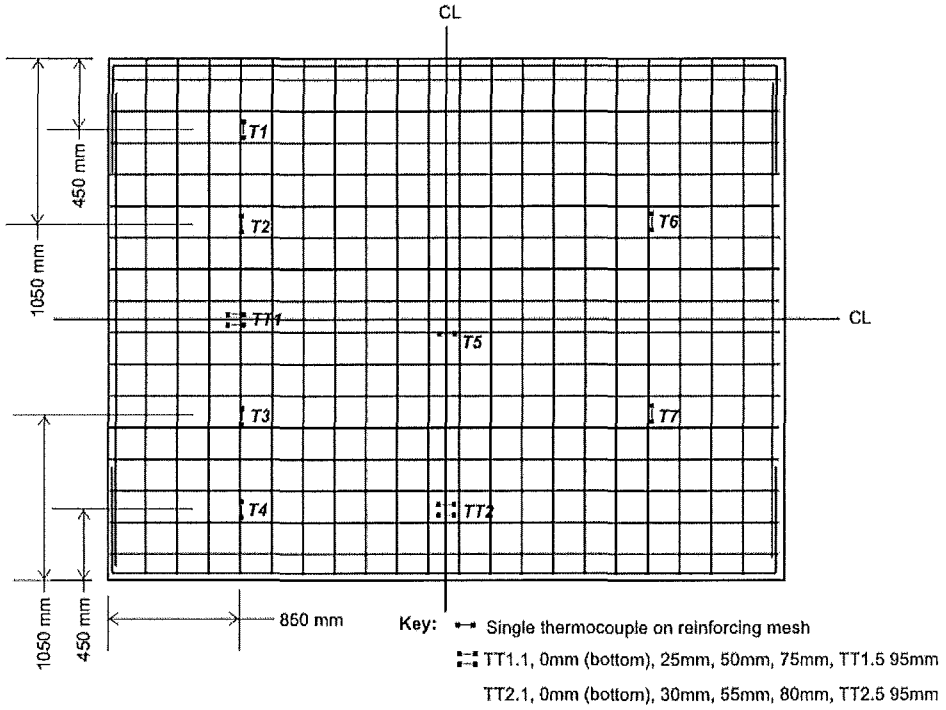

Appendix Fig. 10: Thermocouple layout in the HD12 flat slab.

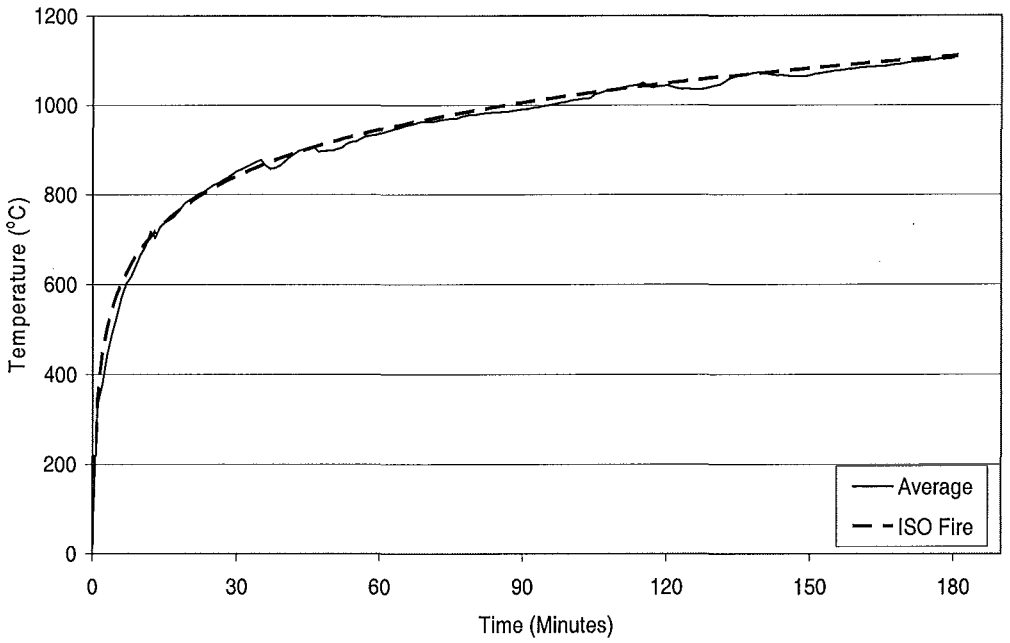

Appendix Fig. 11: Furnace temperatures during the HD12 flat slab test.

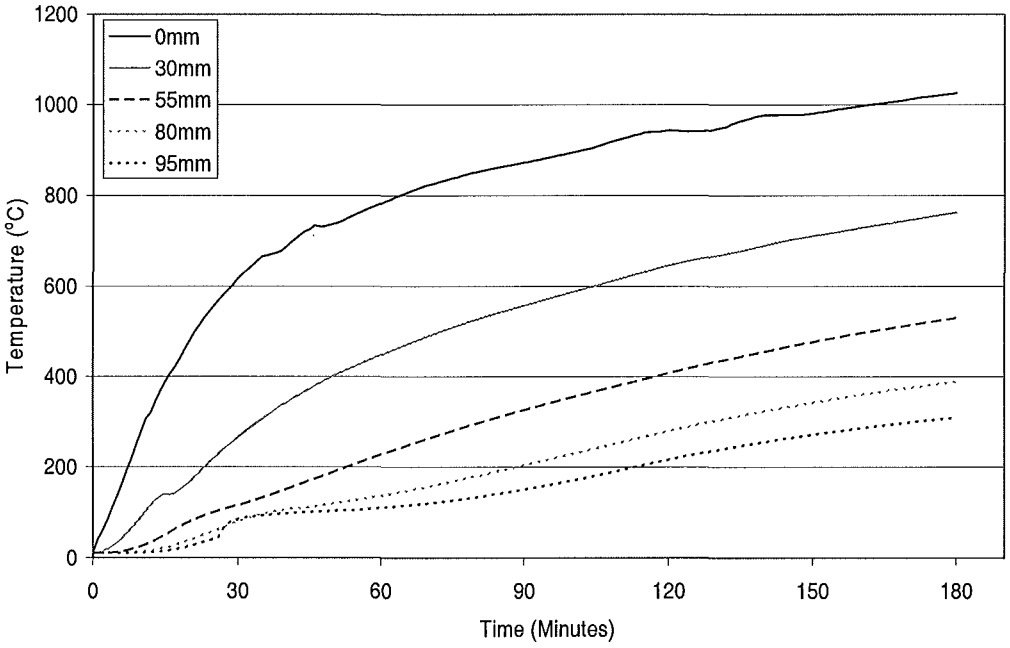

Appendix Fig. 12: Temperatures in thermocouple tree 2 in the HD12 flat slab.

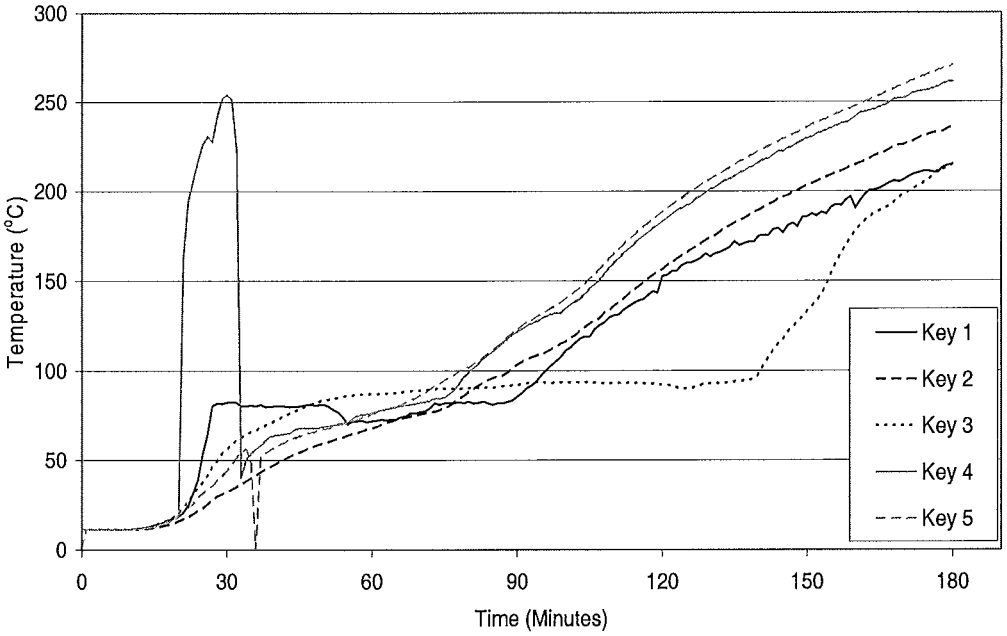

Appendix Fig. 13: Temperatures of the key thermocouples in the HD12 flat slab.

Test 3: D147 flat slab

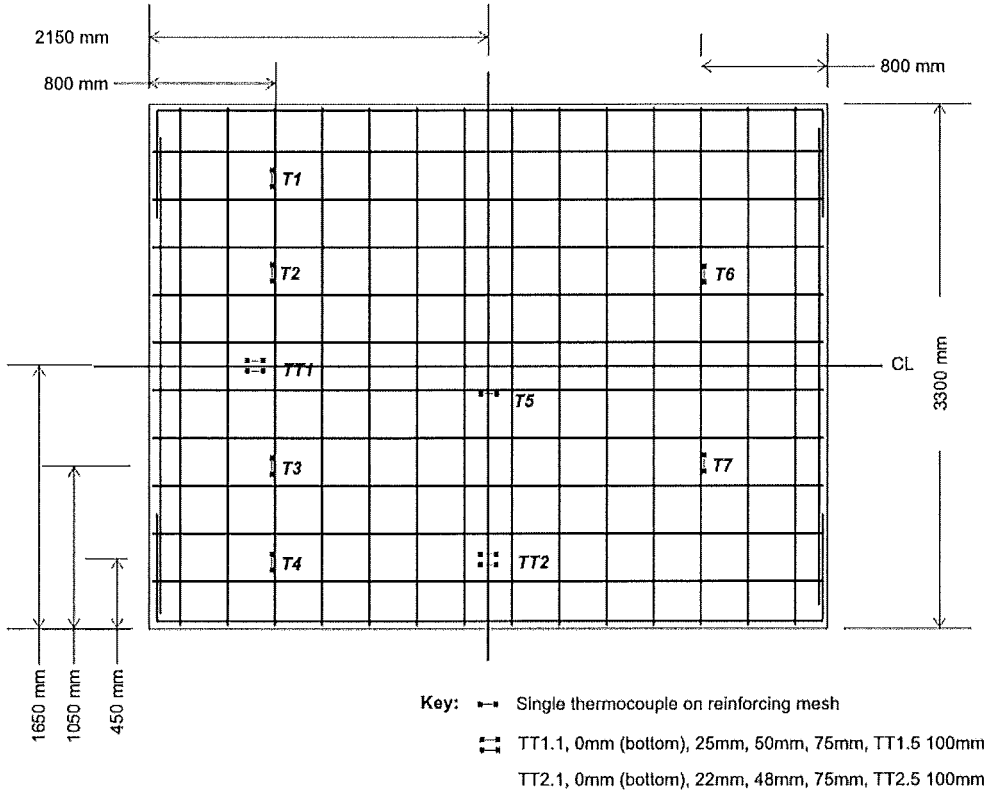

Appendix Fig. 14: Thermocouple layout in the D147 flat slab.

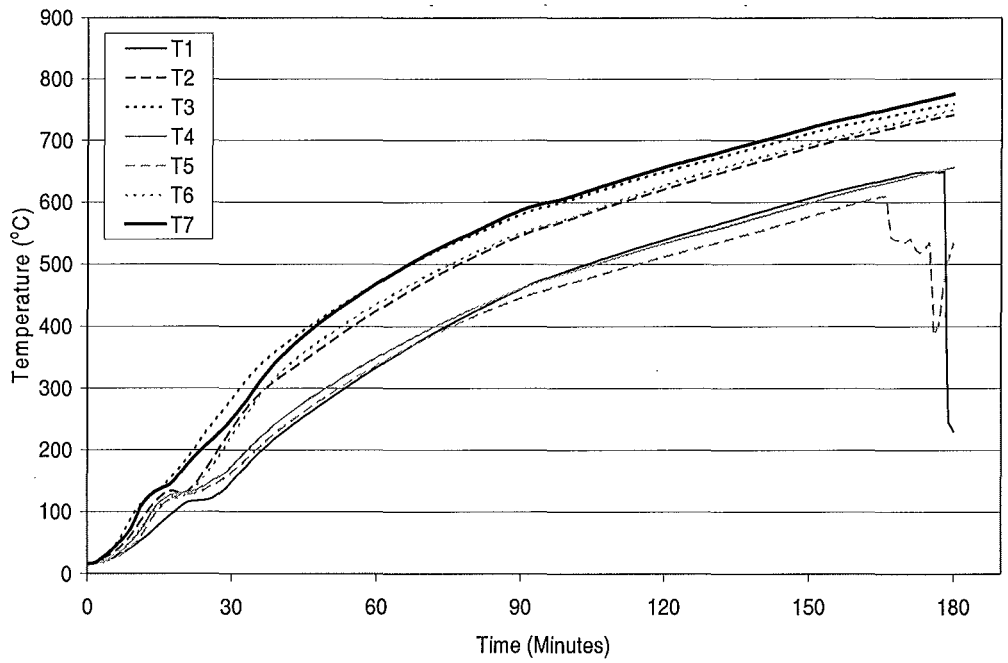

Appendix Fig. 15: Temperatures of the reinforcing mesh in the D147 flat slab.

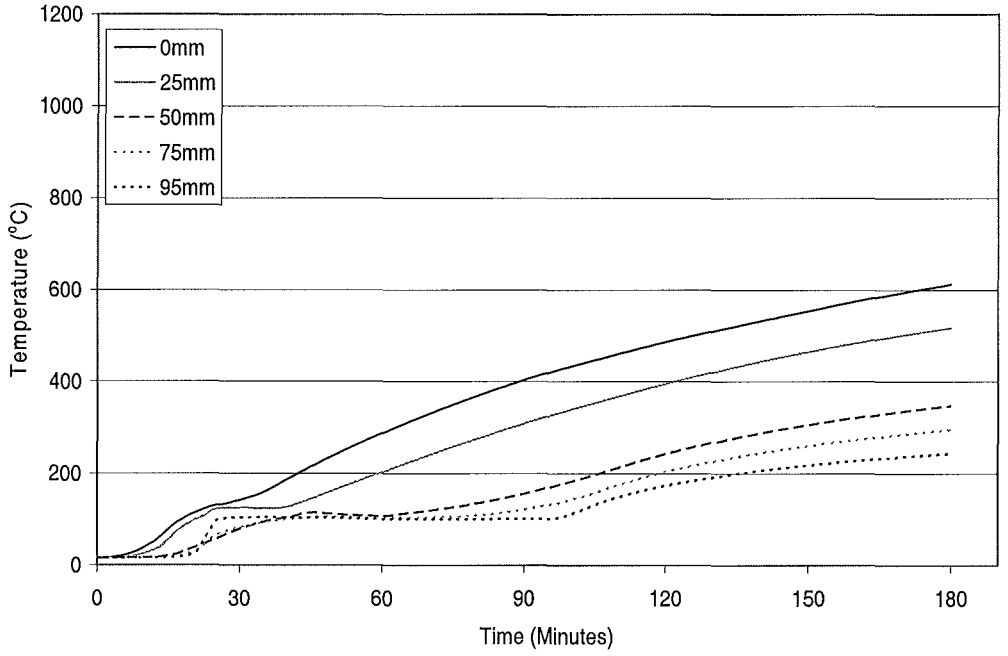

Appendix Fig. 16: Temperatures in thermocouple tree 1 in the HD12 flat slab.

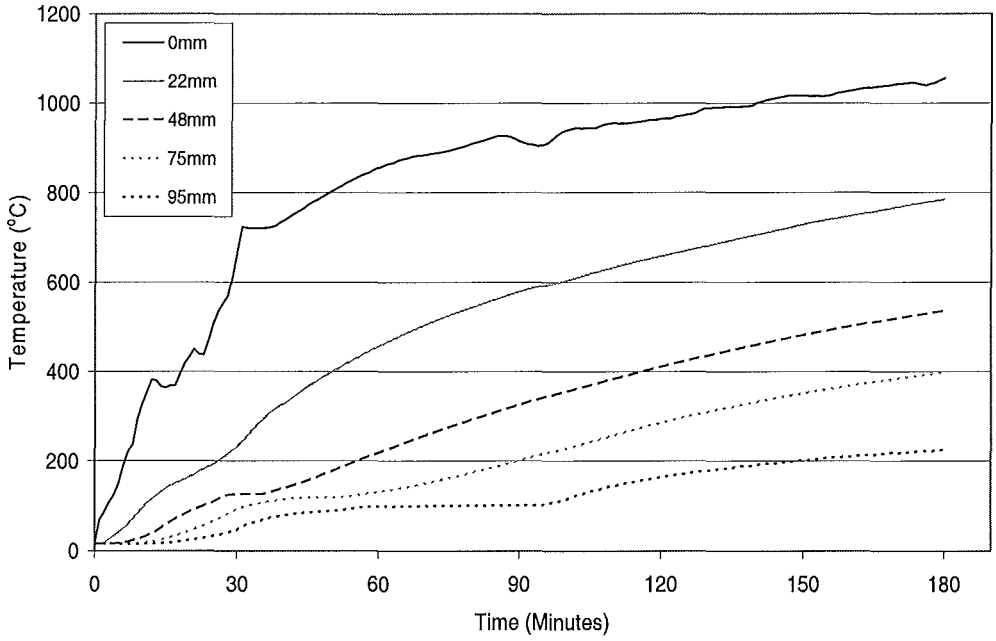

Appendix Fig. 17: Temperatures in thermocouple tree 2 in the D147 flat slab.

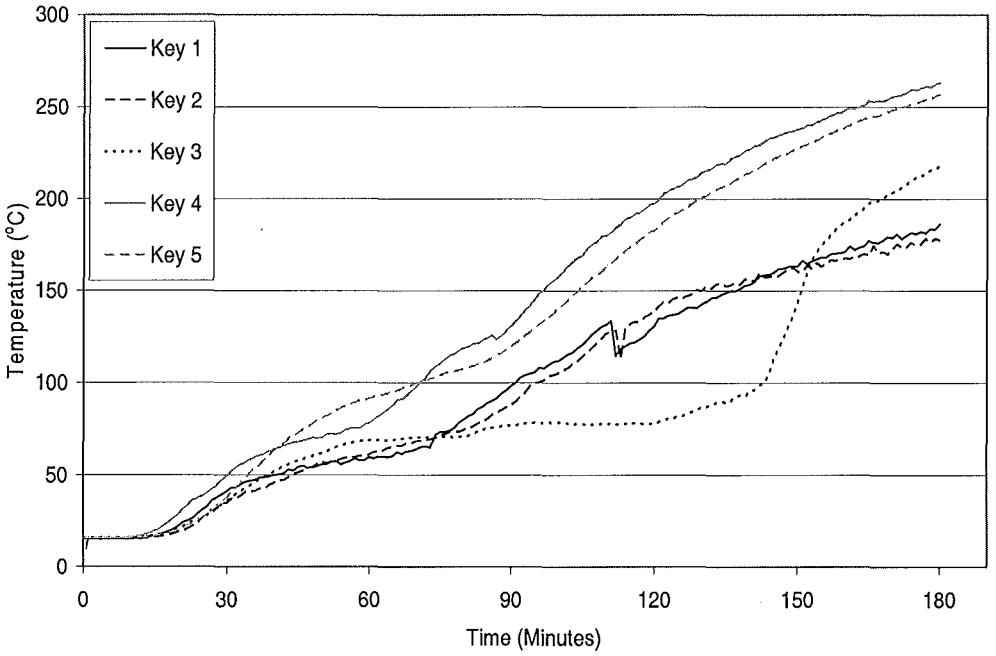

Appendix Fig. 18: Temperatures of the key thermocouples in the D147 flat slab.

Test 4: Hibond slab

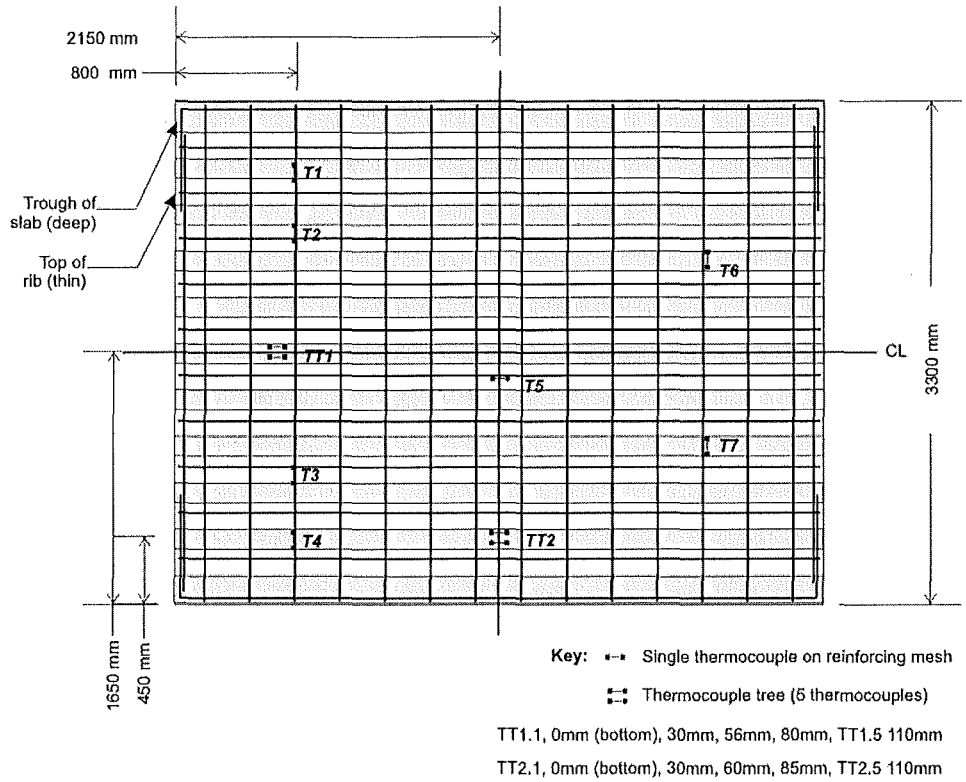

Appendix Fig. 19: Thermocouple layout in the Hibond slab.

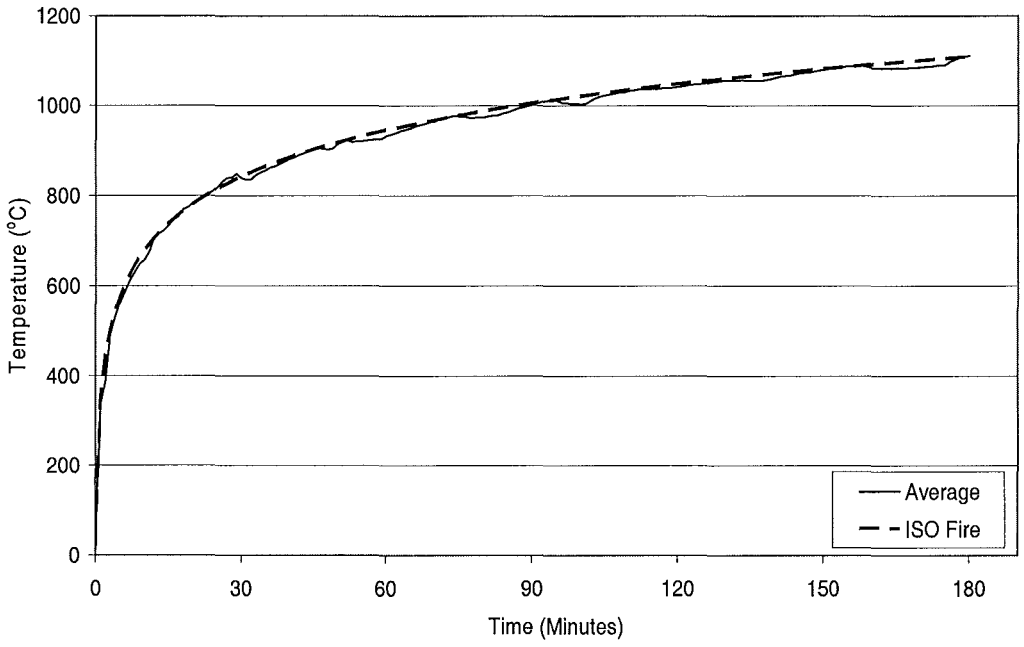

Appendix Fig. 20: Furnace temperatures during the Hibond slab fire test.

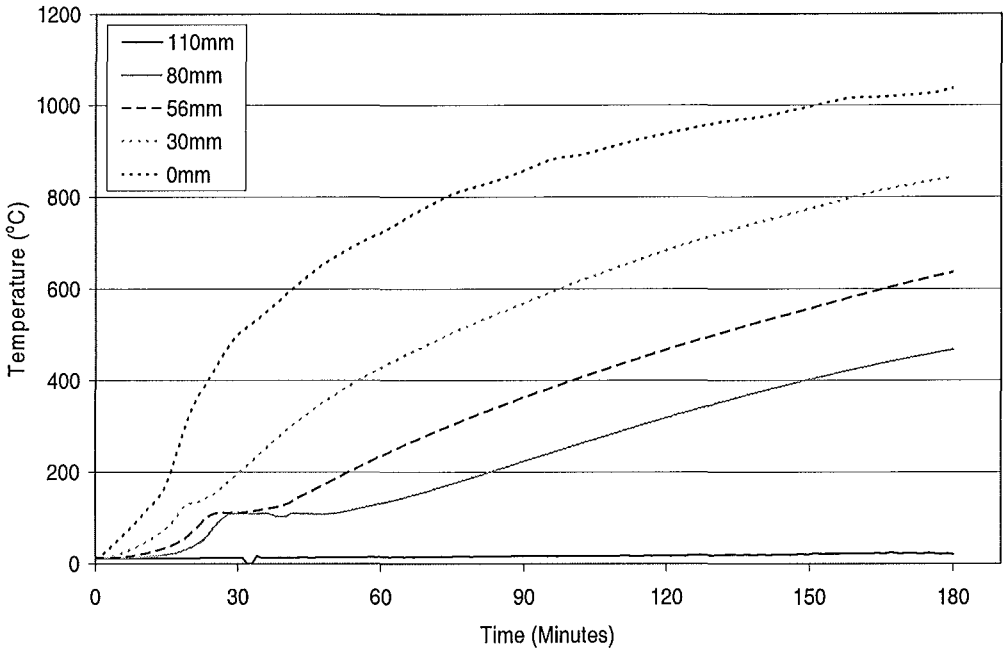

Appendix Fig. 21: Temperatures in thermocouple tree 1 in the Hibond slab.

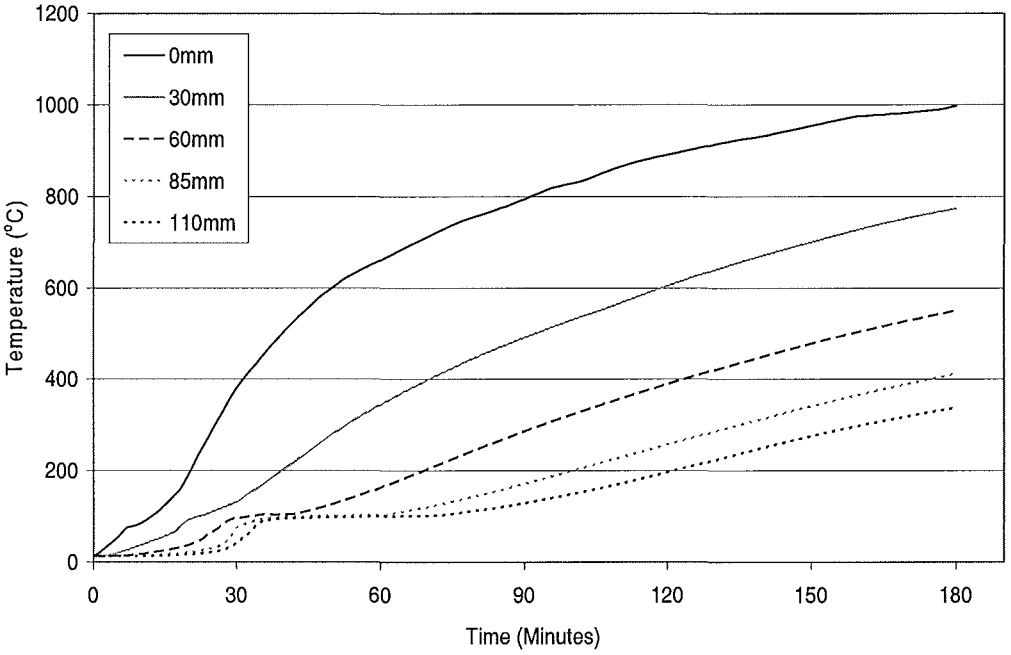

Appendix Fig. 22: Temperatures in thermocouple tree 2 in the Hibond slab.

Test 5: Traydec slab

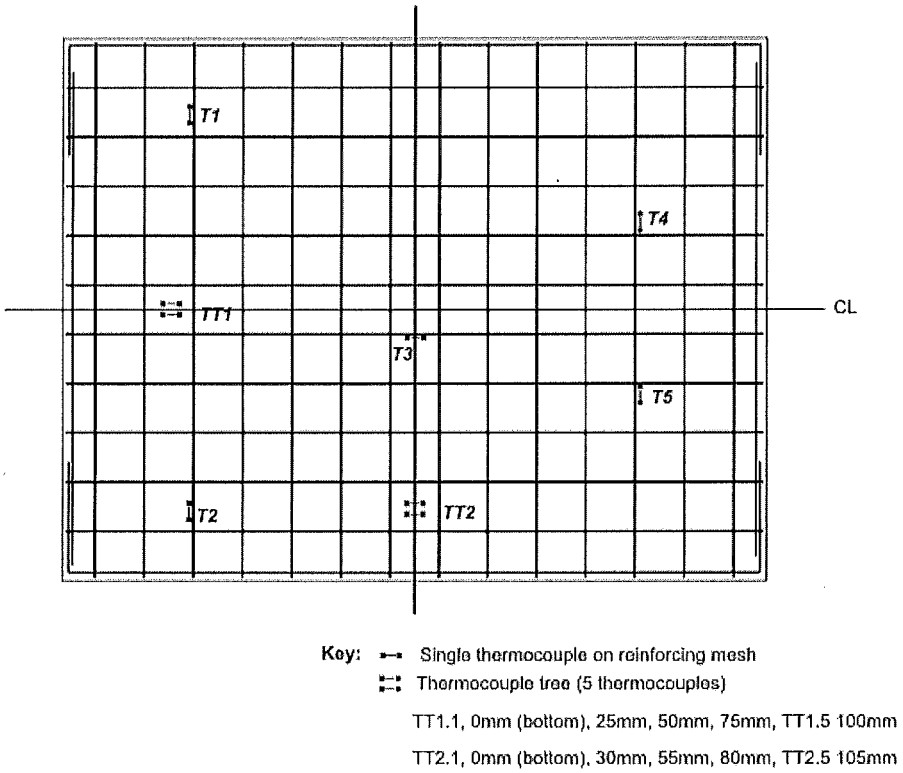

Appendix Fig. 23: Thermocouple layout in the Traydec slab.

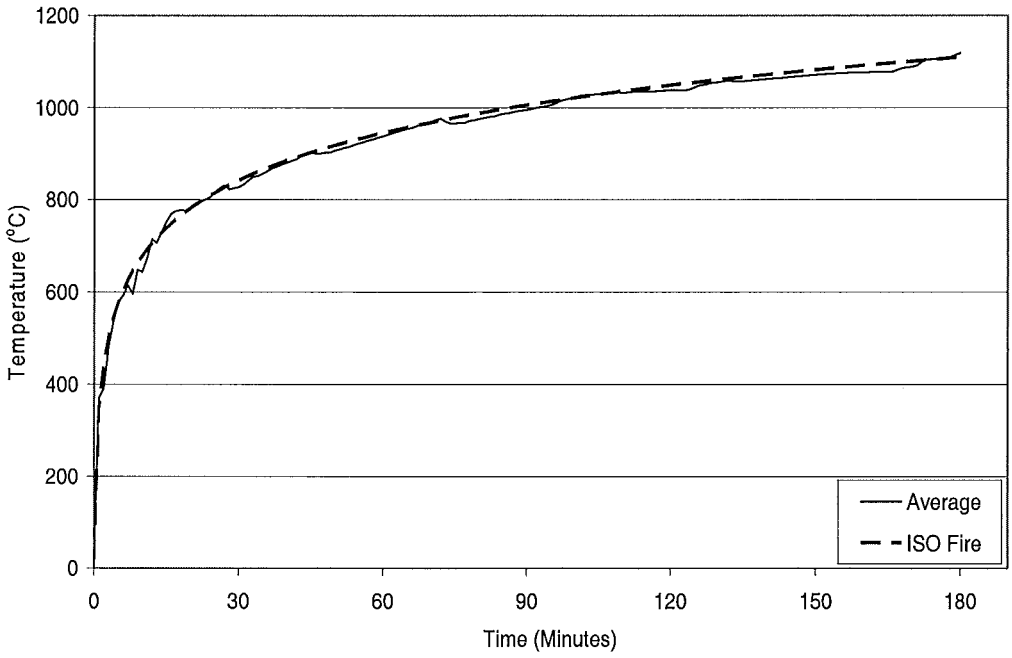

Appendix Fig. 24: Furnace temperatures during the Traydec slab fire test.

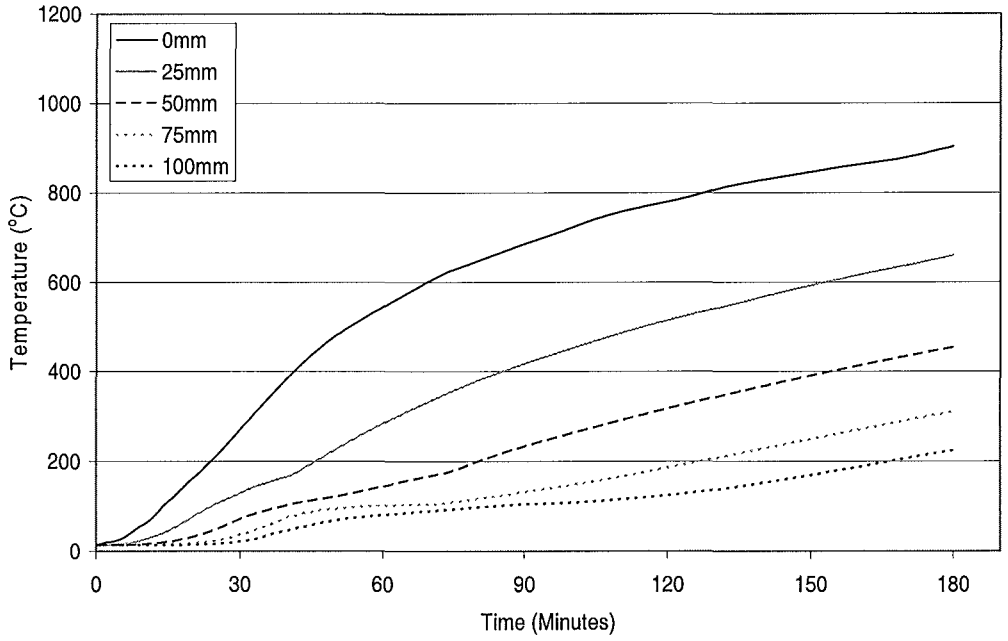

Appendix Fig. 25: Temperatures in thermocouple tree 1 in the Traydec slab.

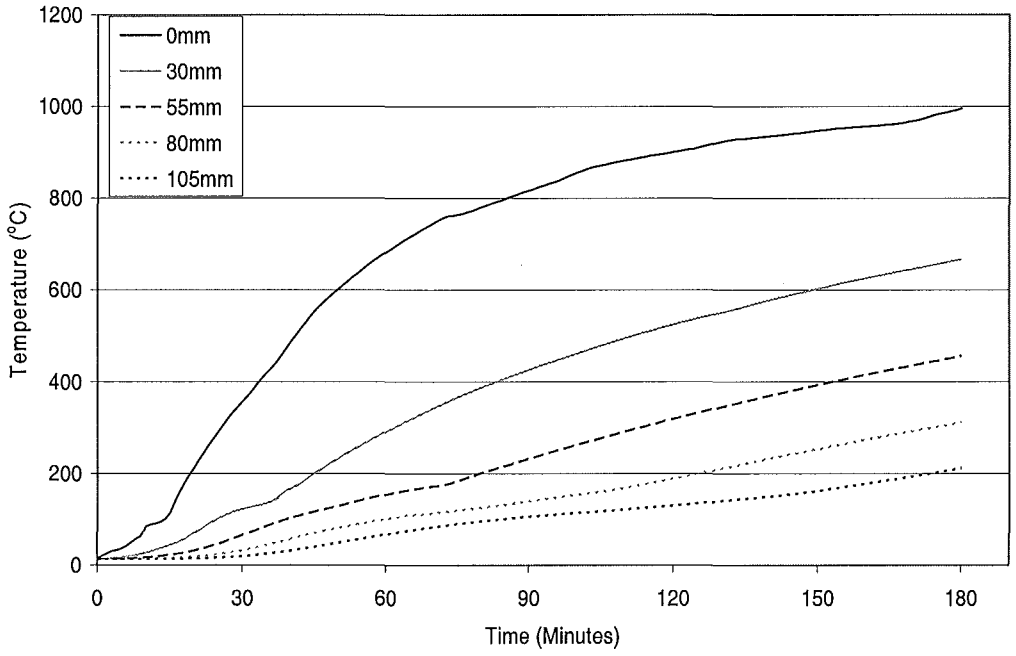

Appendix Fig. 26: Temperatures in thermocouple tree 2 in the Traydec slab.

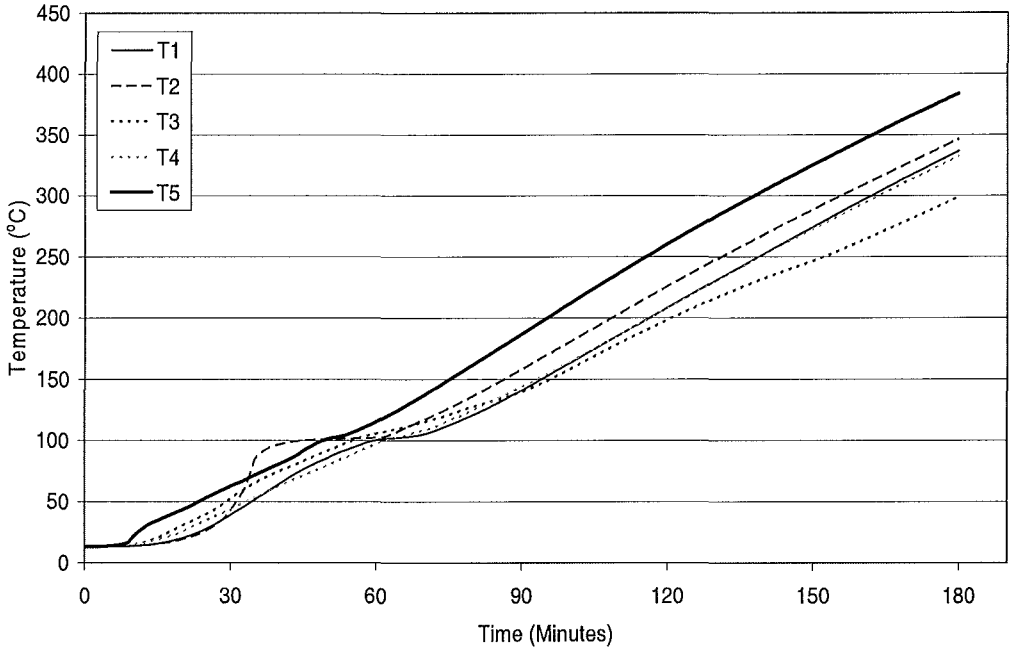

Appendix Fig. 27: Temperatures of the reinforcing in the Traydec slab.

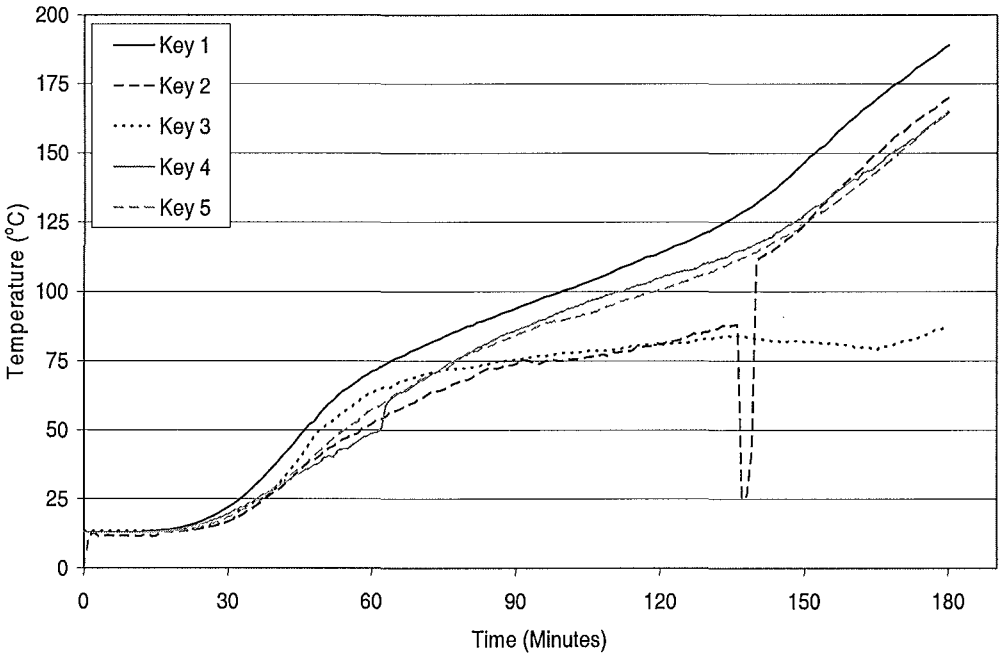

Appendix Fig. 28: Temperatures of the key thermocouples in the Traydec slab.

Test 6: Speedfloor slab

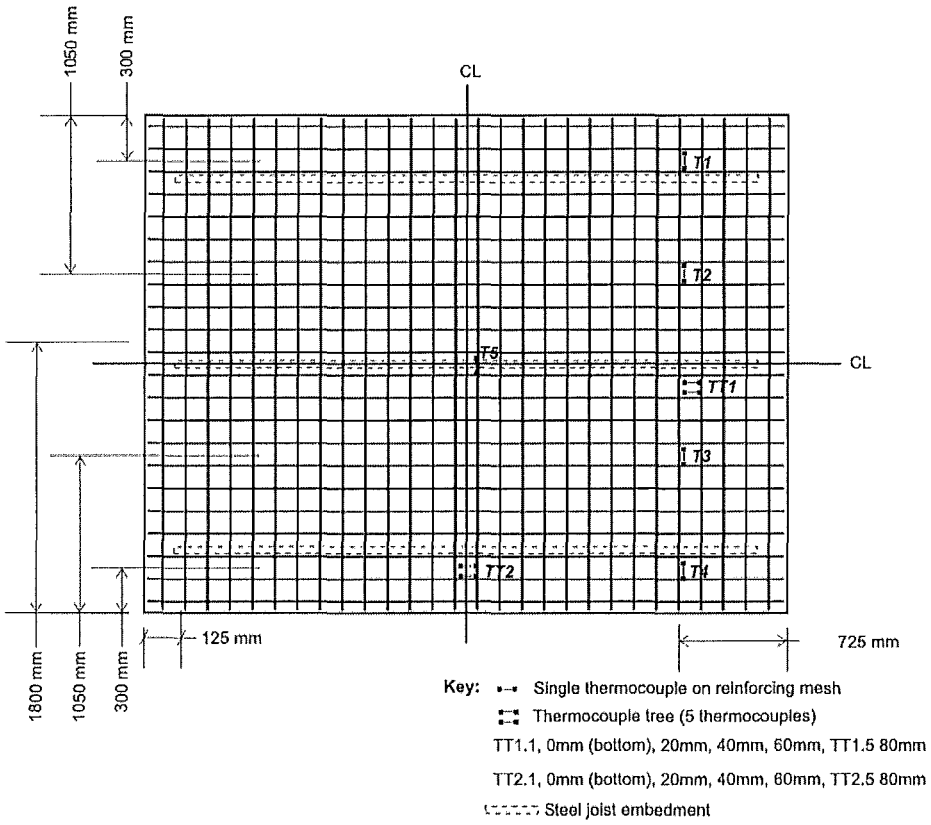

Appendix Fig. 29: Thermocouple layout in the Speedfloor slab.

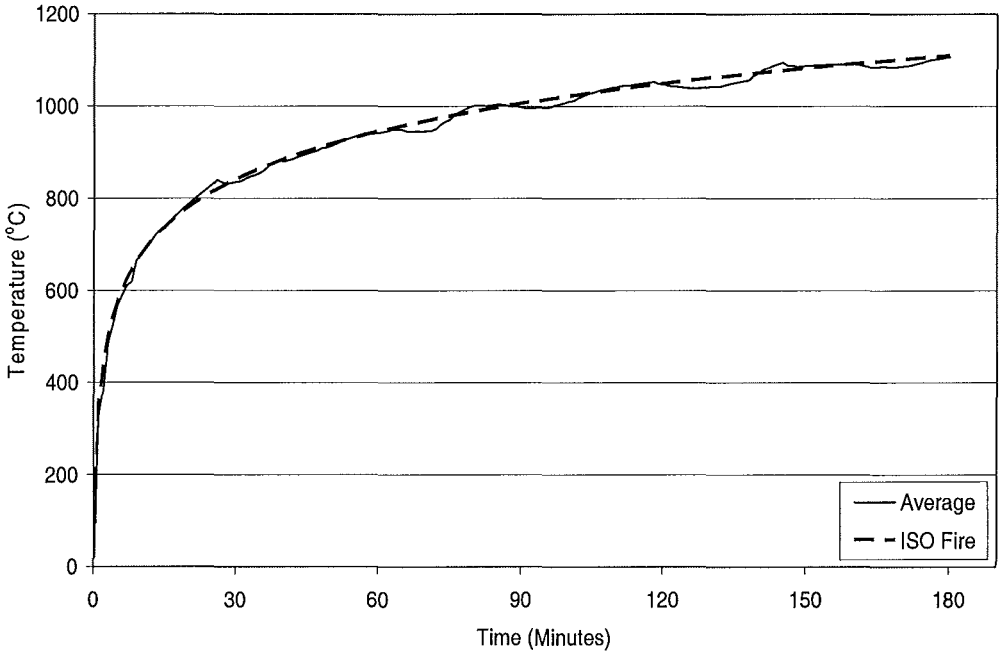

Appendix Fig. 30: Furnace temperatures during the Speedfloor slab fire test.

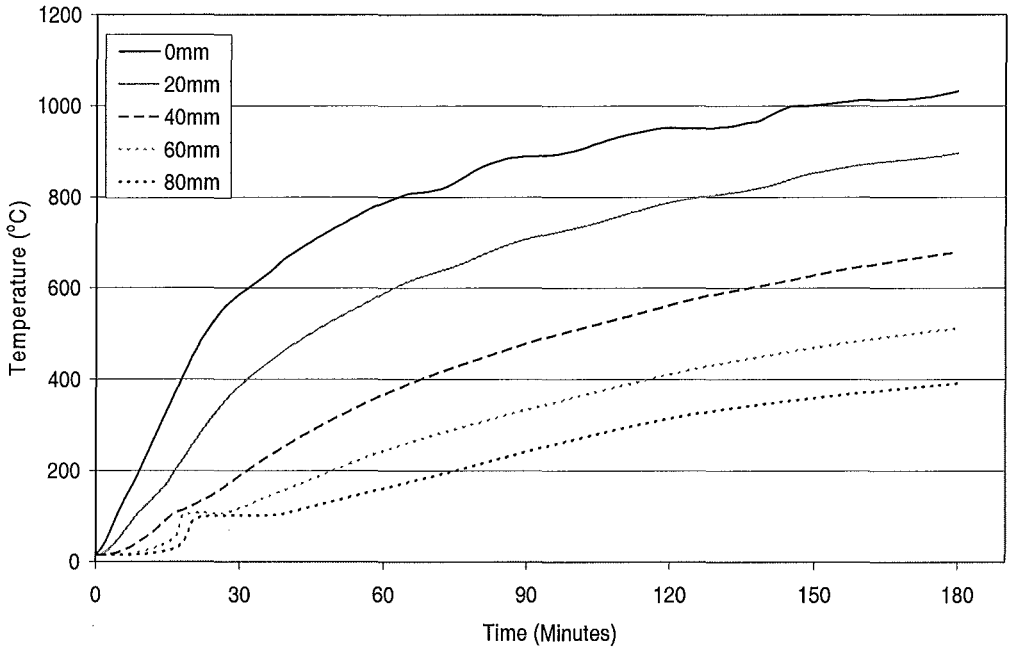

Appendix Fig. 31: Temperatures in thermocouple tree 1 in the Speedfloor slab.

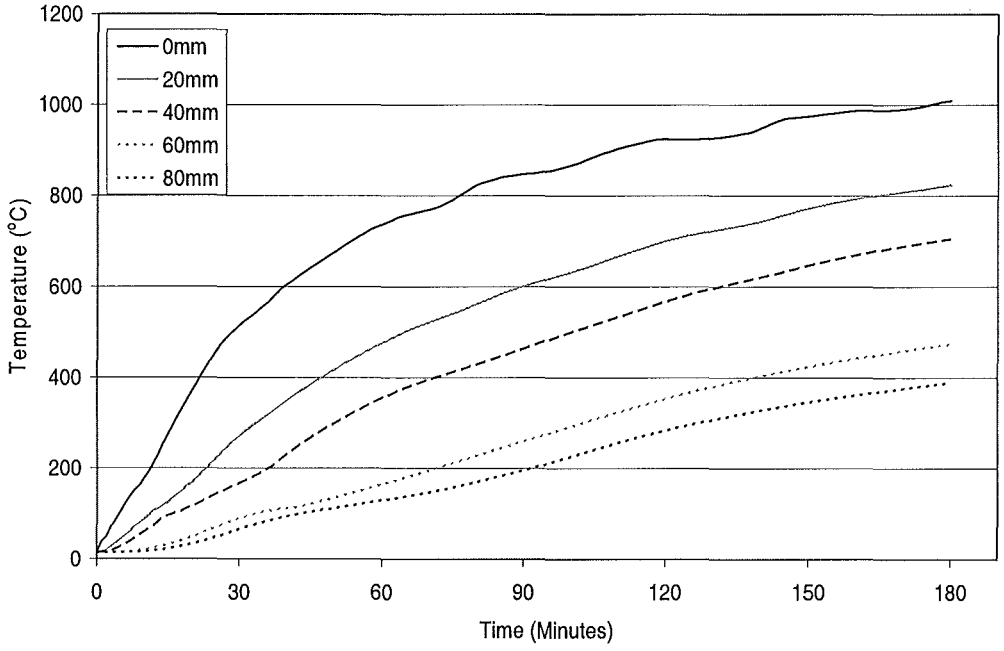

Appendix Fig. 32: Temperatures in thermocouple tree 2 in the Speedfloor slab.

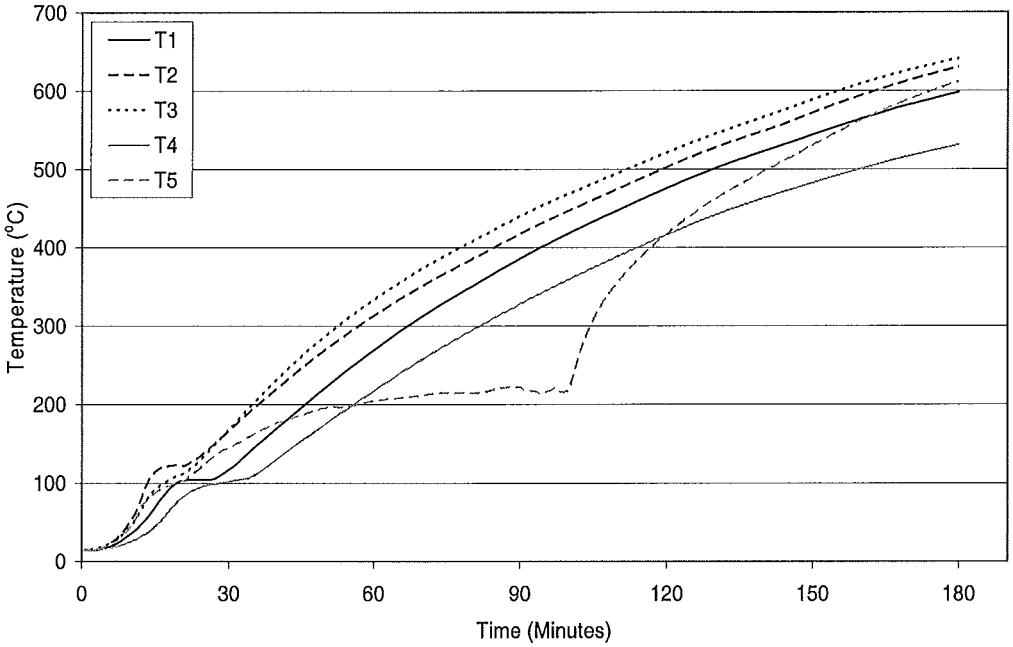

Appendix Fig. 33 Temperatures of the reinforcing bars in the Speedfloor slab.

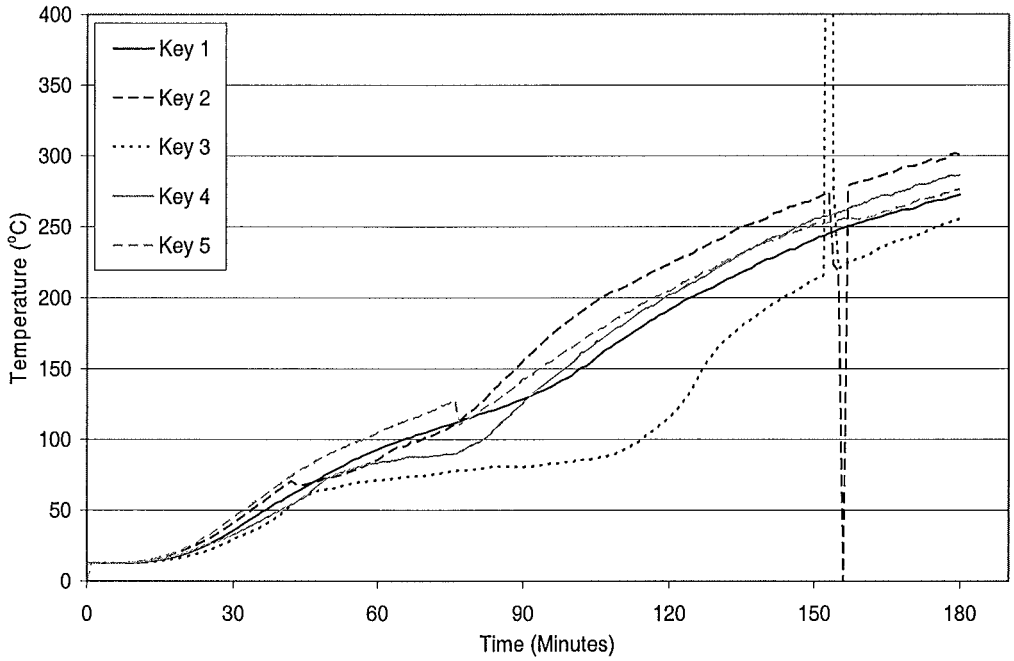

Appendix Fig. 34: Temperatures of the key thermocouples in the Speedfloor slab.

Appendix 3: Strain gauge data

Test 1: 661 flat slab

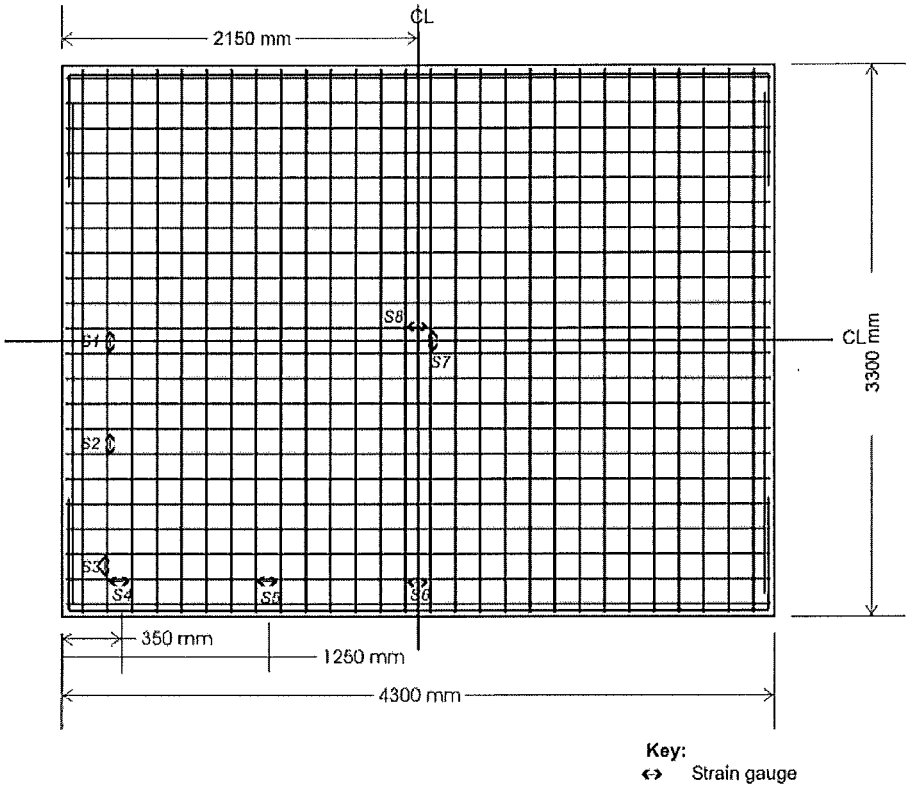

Appendix Fig. 35: Strain gauge layout in the 661 flat slab.

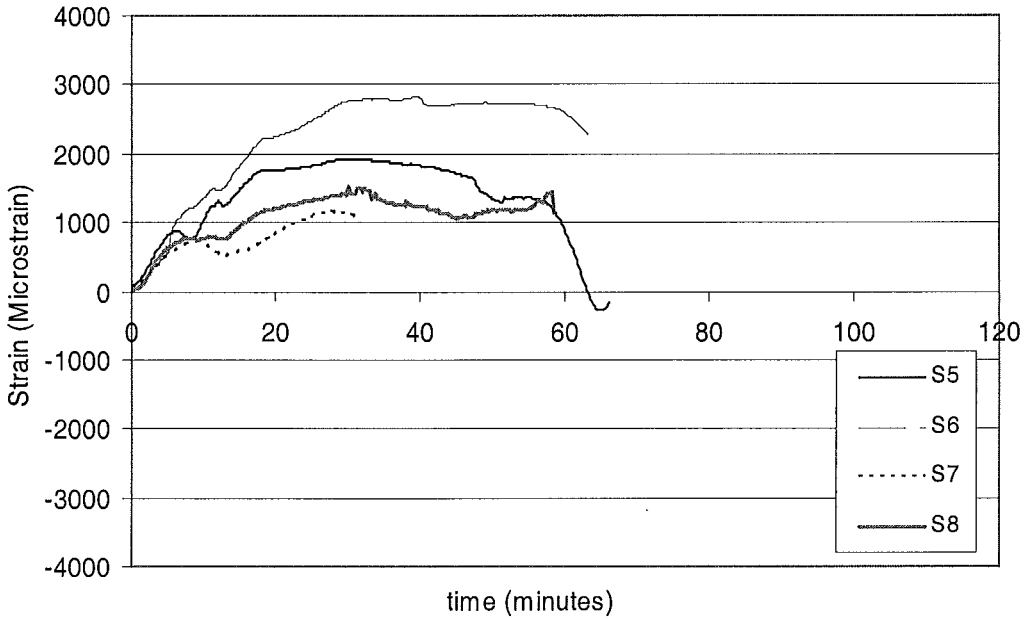

Appendix Fig. 36: Strain gauge measurements of S5-S8 in 661 flat slab.

Test 2: HD12 flat slab

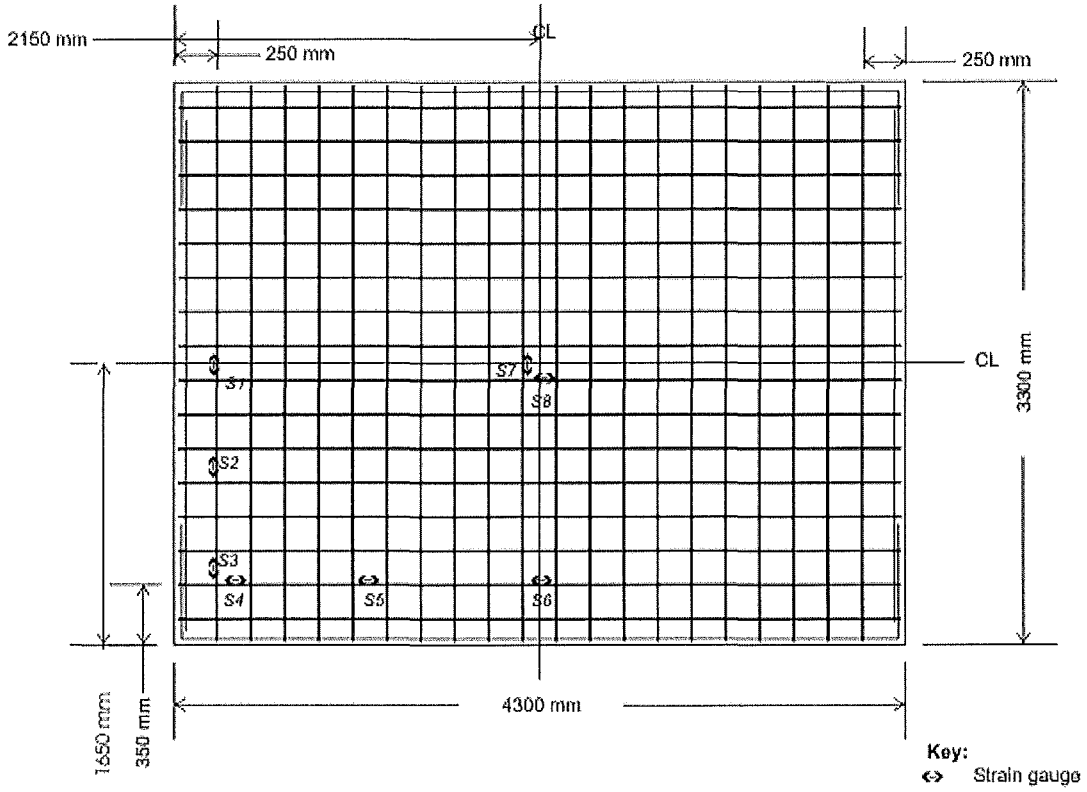

Appendix Fig. 37: Strain gauge layout in the HD12 flat slab.

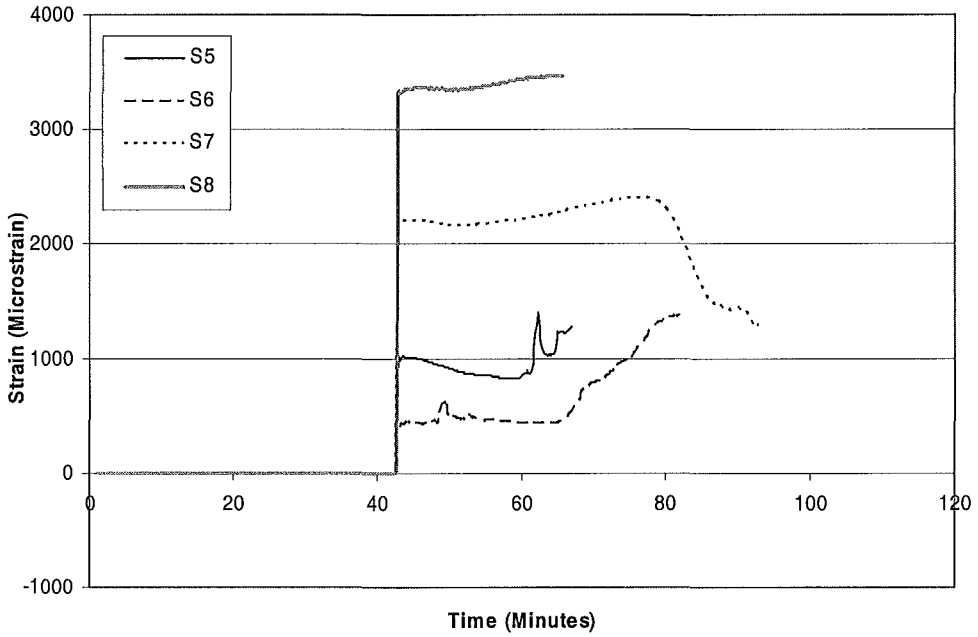

Appendix Fig. 38: Strain gauge measurements of S5-S8 in HD12 flat slab.

Test 3: D147 flat slab

Strain gauges
Debonded - S1,3,4,6,7,8,14,22,23,24,25
Bonded - S2,5,9 - 13,15 - 20,21,26

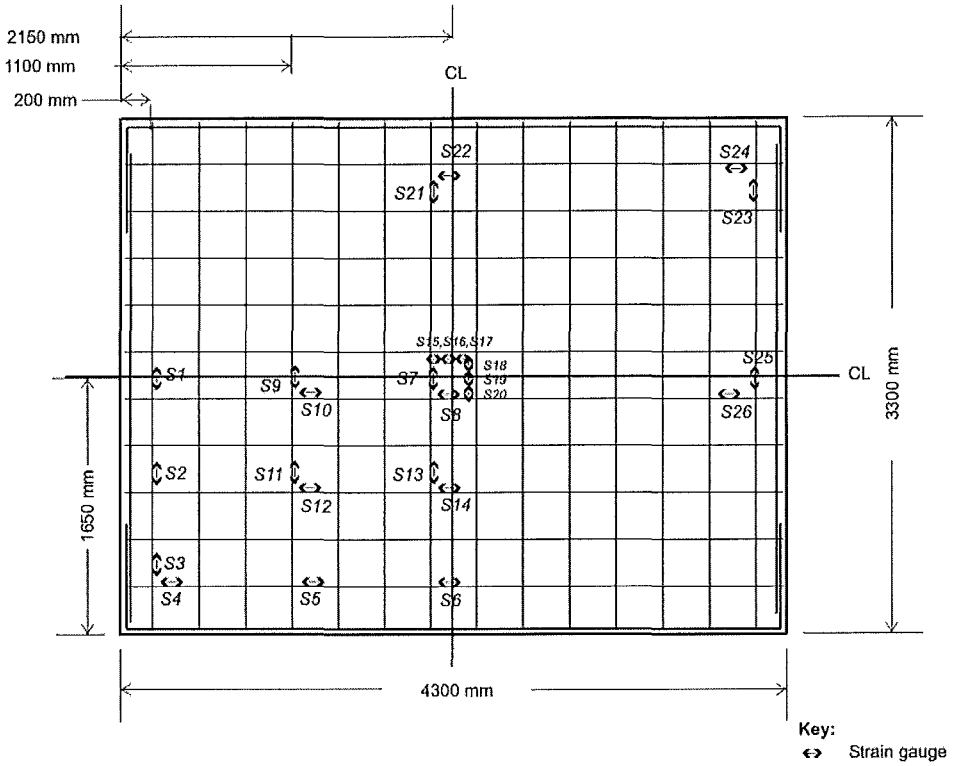

Appendix Fig. 39: Strain gauge layout in the D147 flat slab.

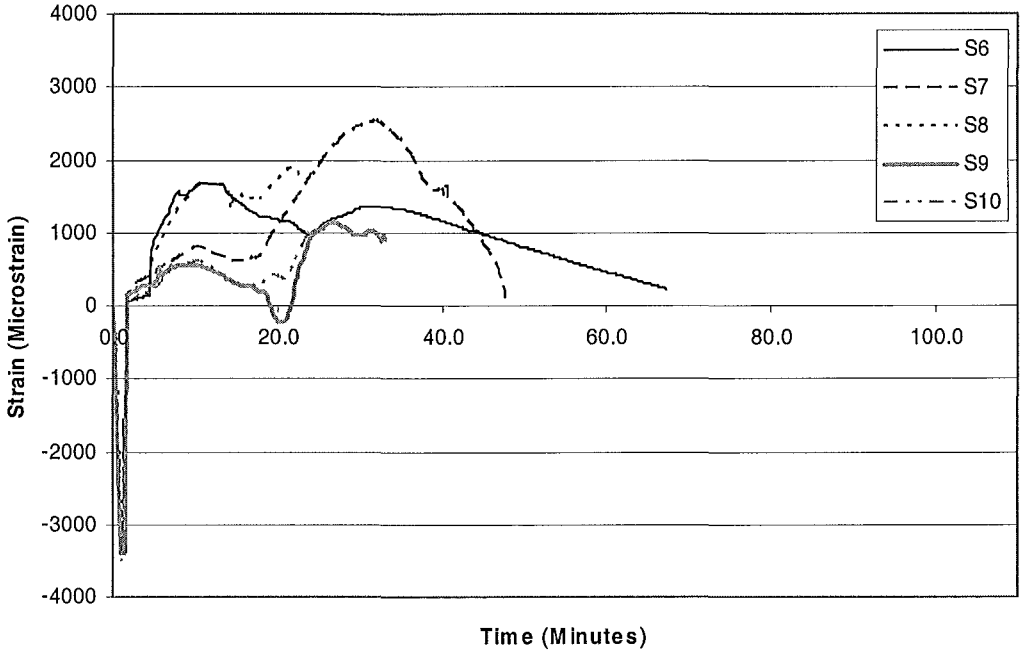

Appendix Fig. 40: Strain gauge measurements of S6-S10 in D147 flat slab.

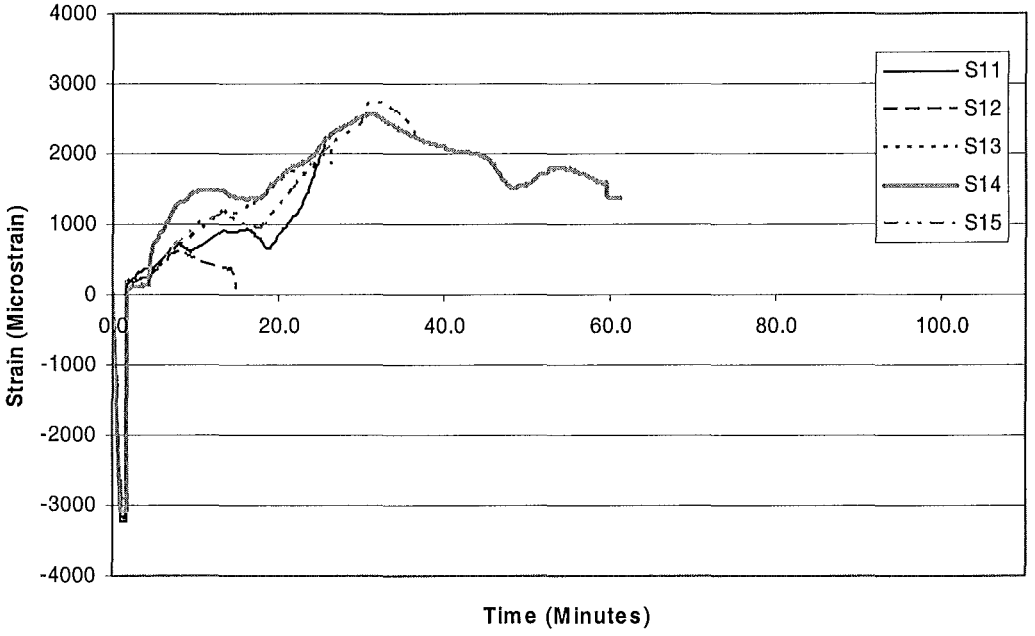

Appendix Fig. 41: Strain gauge measurements of S11-S15 in D147 flat slab.

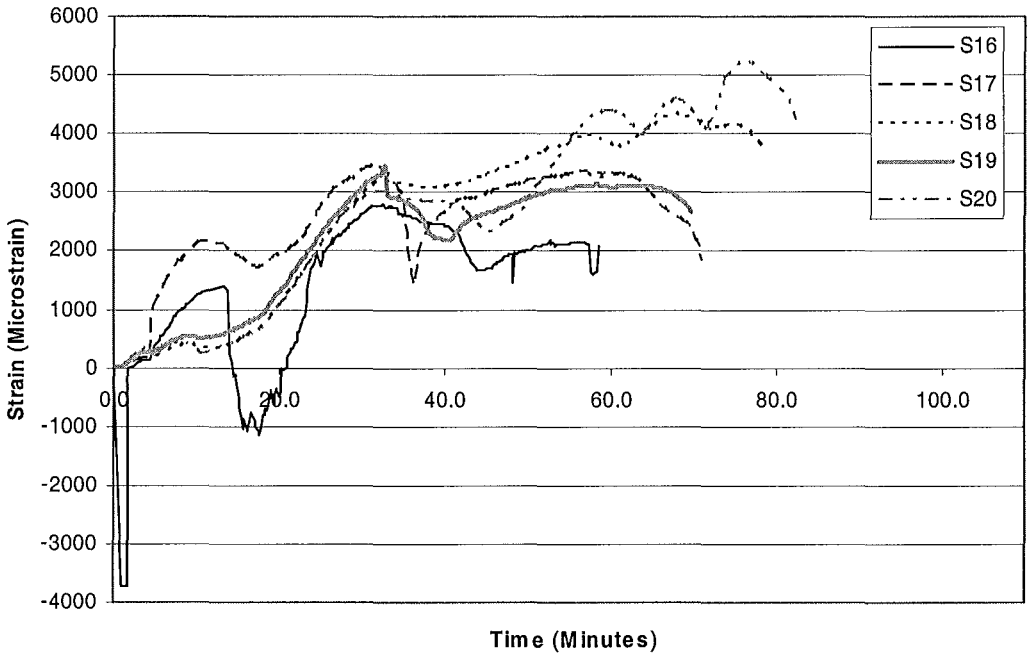

Appendix Fig. 42: Strain gauge measurements of S16-S20 in D147 flat slab.

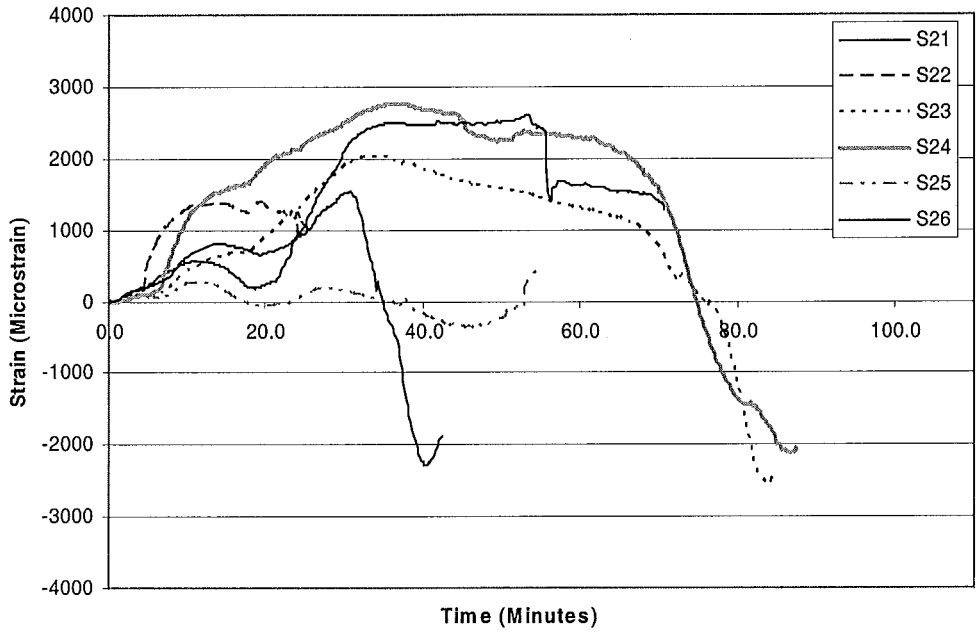

Appendix Fig. 43: Strain gauge measurements of S21-S26 in D147 flat slab.

Test 4: Hibond slab

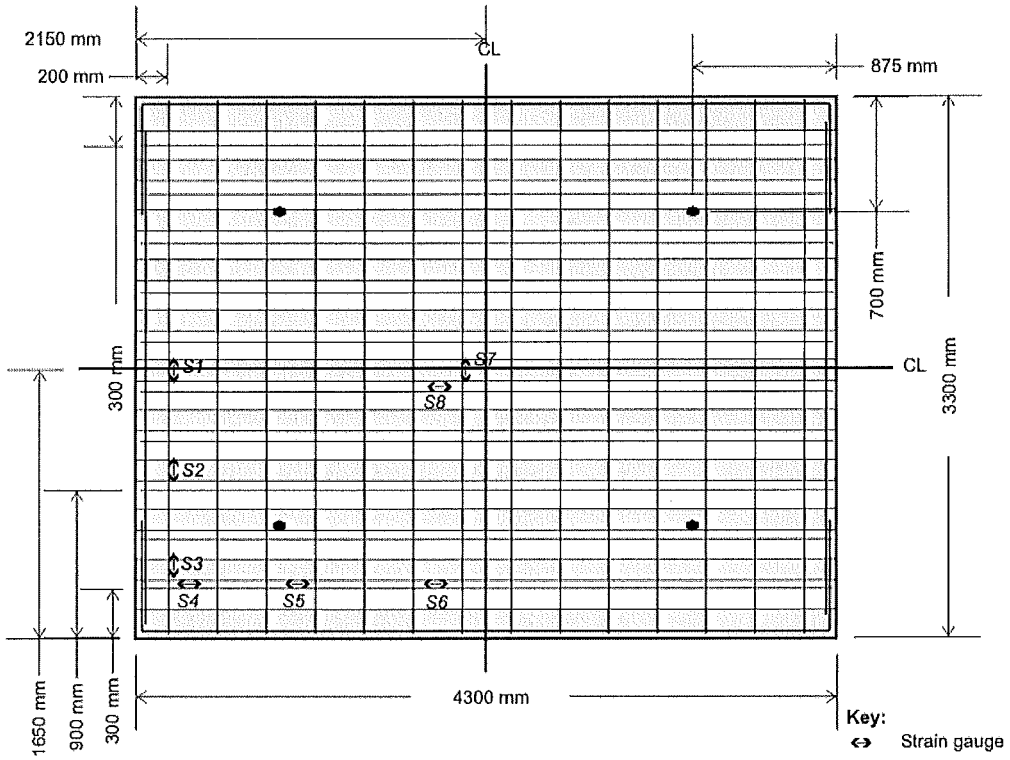

Appendix Fig. 44: Strain gauge layout in the Hibond slab.

Refer to section 6.5.5 for strain gauge data.

Test 5: Traydec slab

Strain gauges
Debonded - S1,3,4,6,7,8,14
Bonded - S2,5,9,10,11,12,13,15,16,17,18,19,20

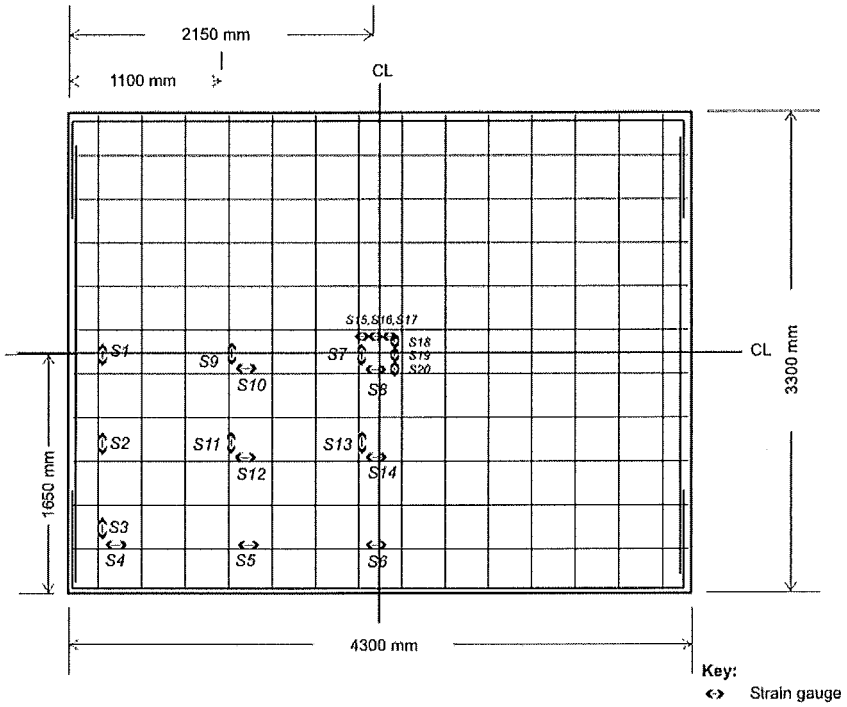

Appendix Fig. 45: Strain gauge layout in the Traydec slab.

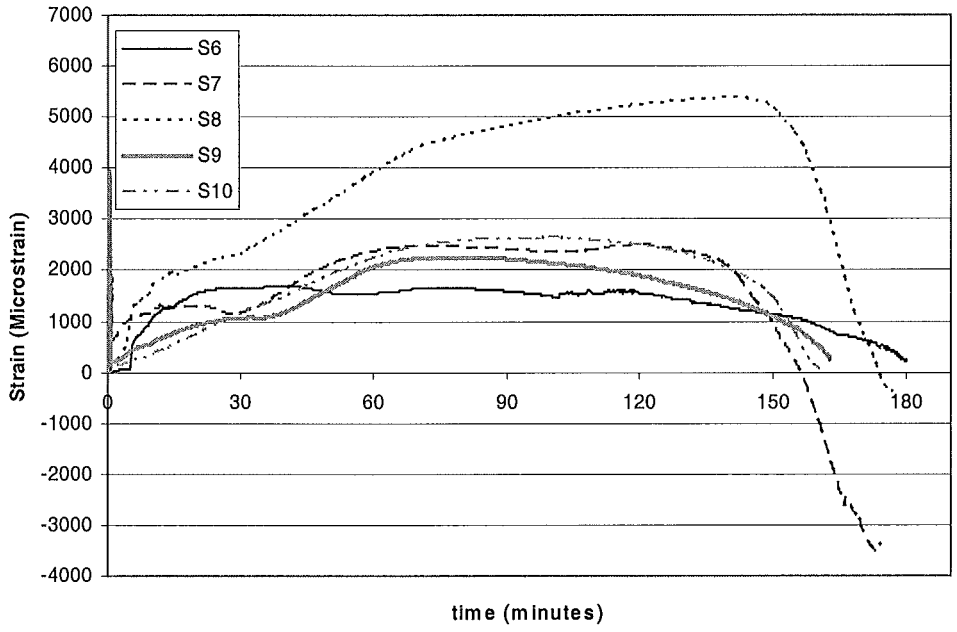

Appendix Fig. 46: Strain gauge measurements of S6-S10 in the Traydec slab.

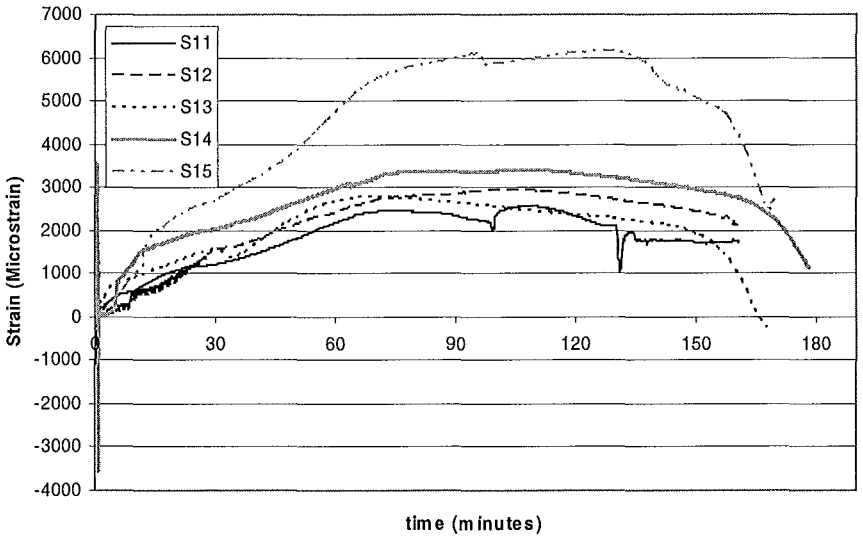

Appendix Fig. 47: Strain gauge measurements of S11-S15 in the Traydec slab.

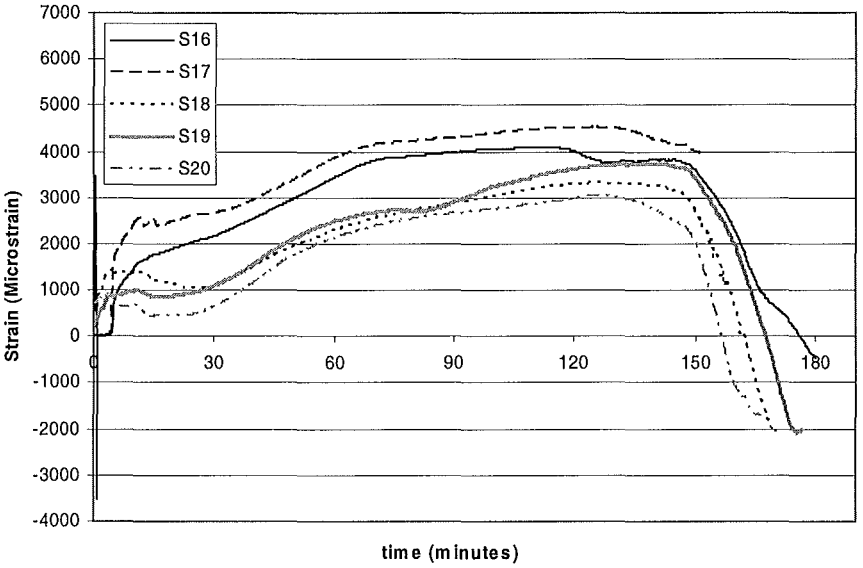

Appendix Fig. 48: Strain gauge measurements of S16-S20 in the Traydec slab.

Test 6: Speedfloor slab

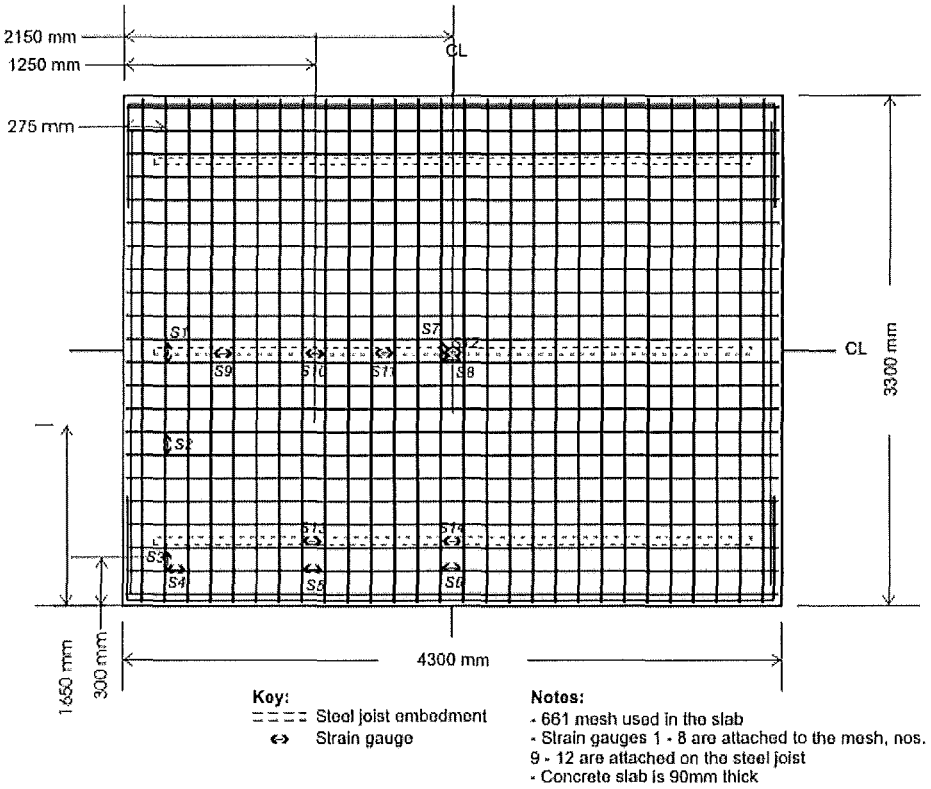

Appendix Fig. 49: Strain gauge layout in the Speedfloor slab.

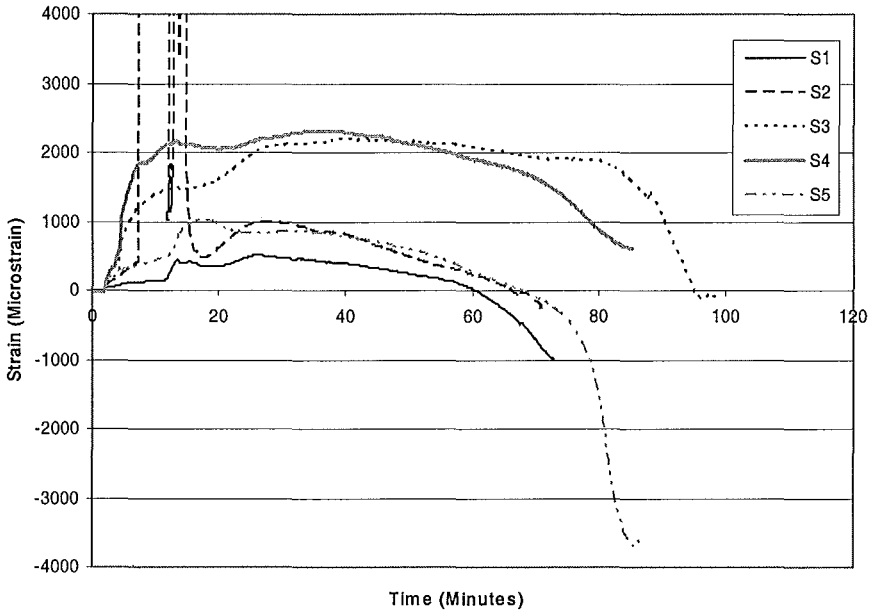

Appendix Fig. 50: Strain gauge measurements of S6-S10 in the Speedfloor slab.

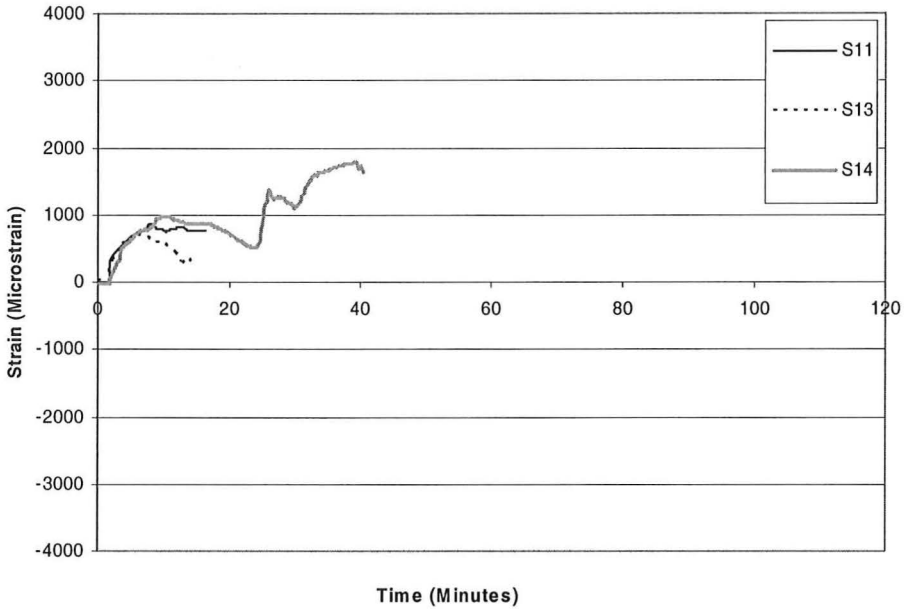

Appendix Fig. 51: Strain gauge measurements of S11-S14 in the Speedfloor slab.

Appendix 4: Photos

Construction

D147 flat slab and 661 flat slab

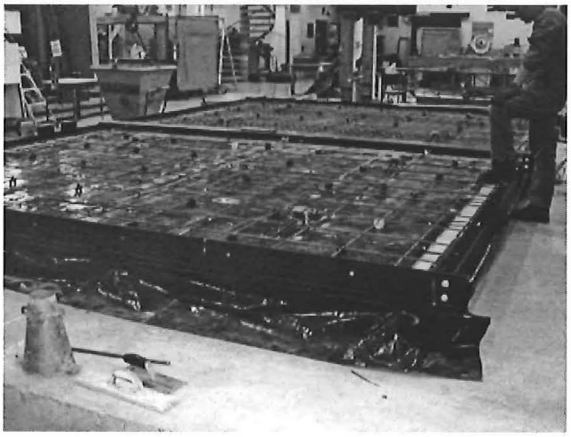

Appendix Fig. 52: View of the slabs before casting of concrete.

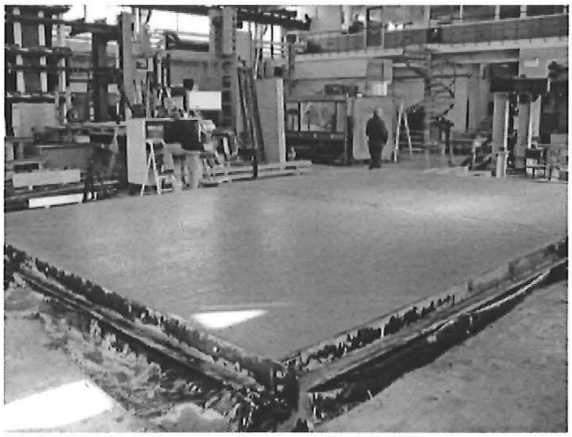

Appendix Fig. 53: Casting of slabs completed.

HD12 flat slab

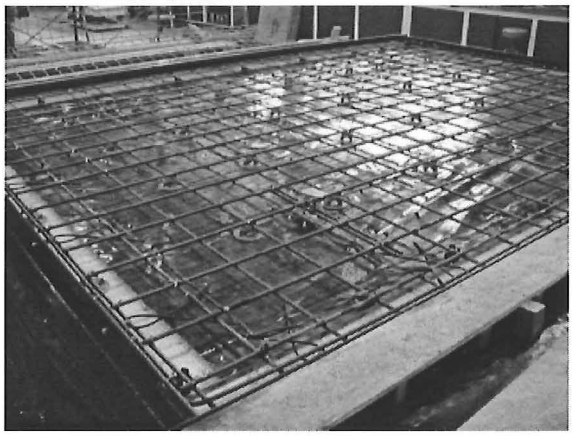

Appendix Fig. 54: View of the slab before casting of concrete.

Appendix Fig. 55: Concrete being screeded.

Hibond and Traydec slabs

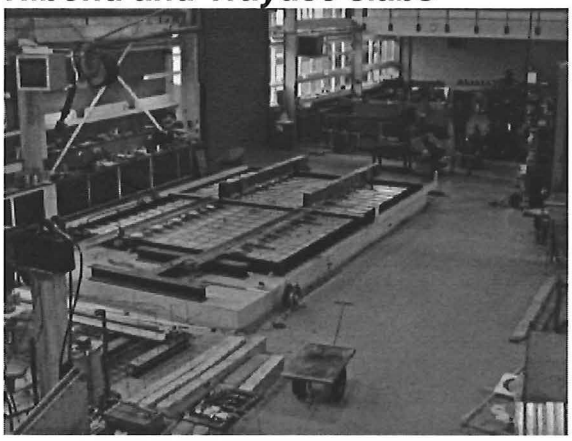

Appendix Fig. 56: View of the Hibond and Traydec slabs before casting of concrete.

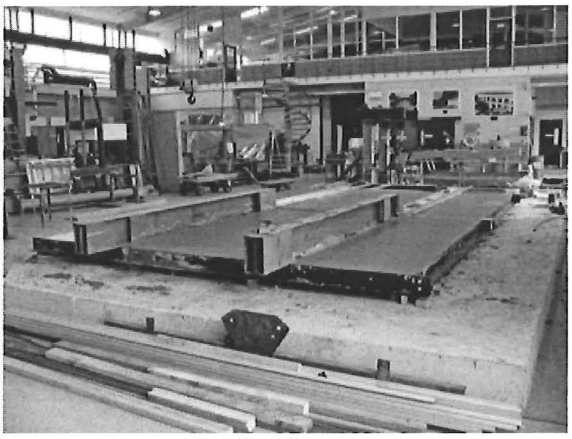

Appendix Fig. 57: Cast slabs, with the strong backs still attached.

Speedfloor slab

Appendix Fig. 58: Speedfloor joists suspended on the wooden boxing.

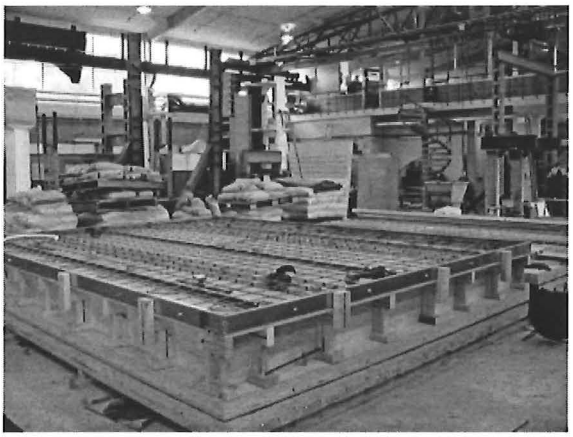

Appendix Fig. 59: Construction of Speedfloor slab completed.

Testing

Test 1: 661 flat slab

Appendix Fig. 60: Bottom view of the 661 flat slab before the test.

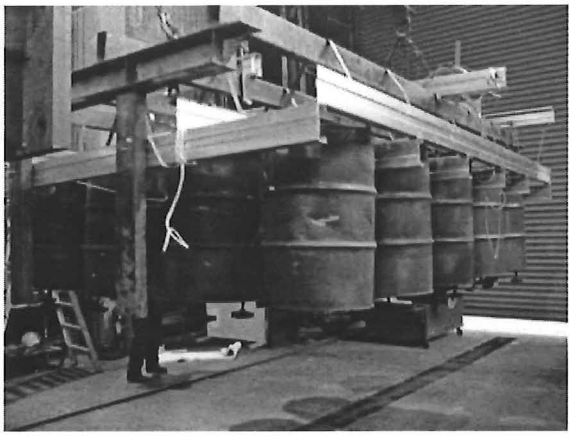

Appendix Fig. 61: Removal of drums and supporting frame after the test.

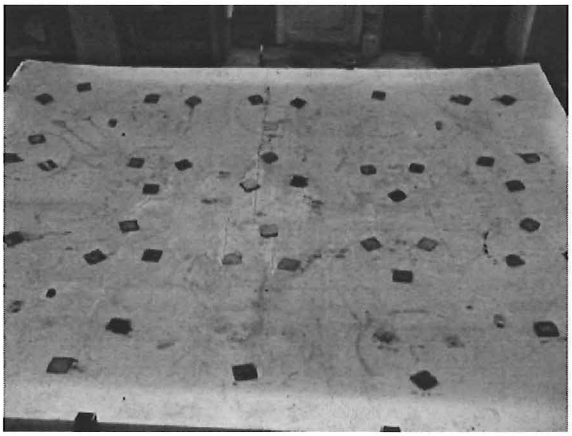

Appendix Fig. 62: Plan view of the slab after the fire test.

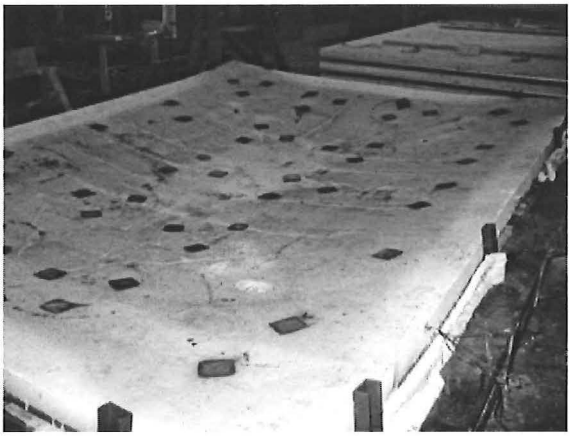

Appendix Fig. 63: Deformed shape of the slab after the fire test.

Test 2: HD12 flat slab

Appendix Fig. 64: Bottom view of the HD12 flat slab before the test.

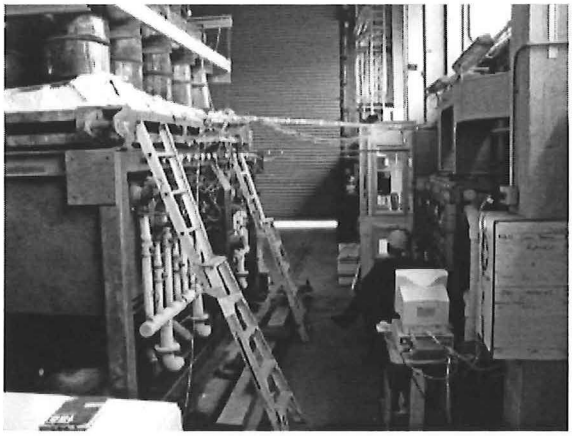

Appendix Fig. 65: Set up of the computers by the furnace for data logging and driving the furnace.

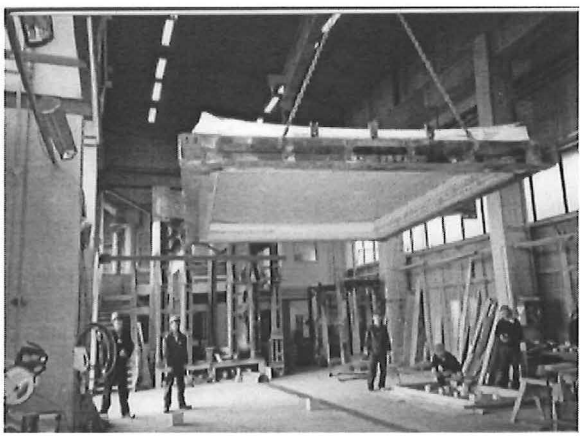

Appendix Fig. 66: Bottom view of the slab after the test.

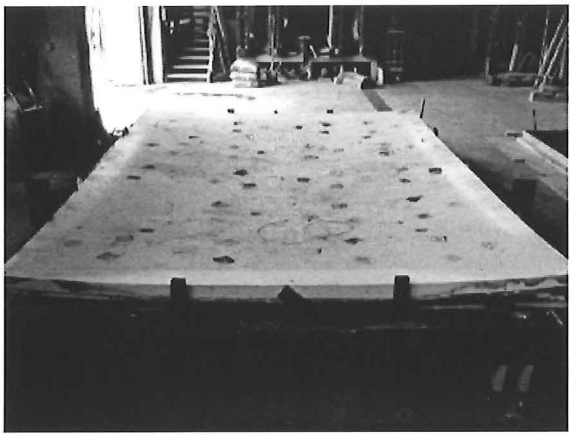

Appendix Fig. 67: Deformed shape of the slab immediately after the tests.

Test 3: D147 flat slab

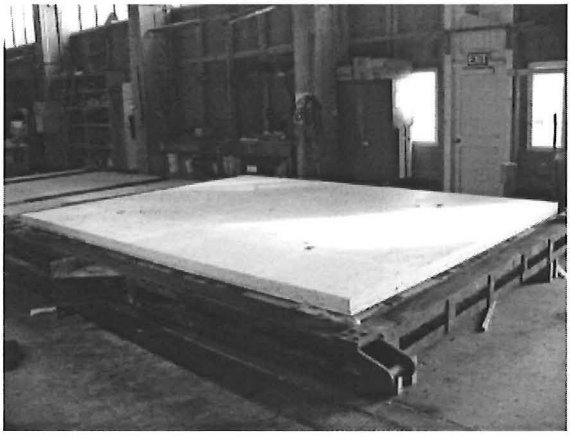

Appendix Fig. 68: Newly painted D147 flat slab, before the test.

Appendix Fig. 69: Bottom view of the slab before the test.

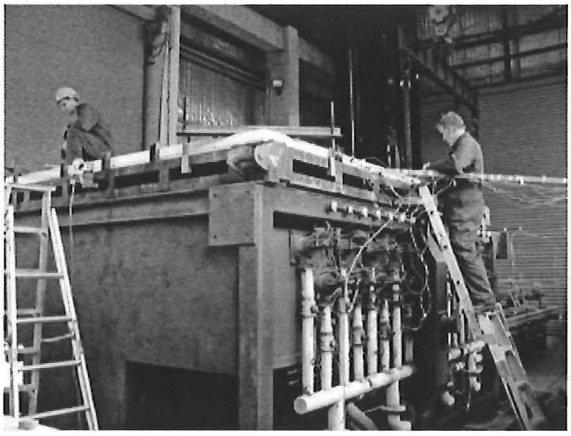

Appendix Fig. 70: Wiring of instrumentation of slab to data loggers prior to fire test.

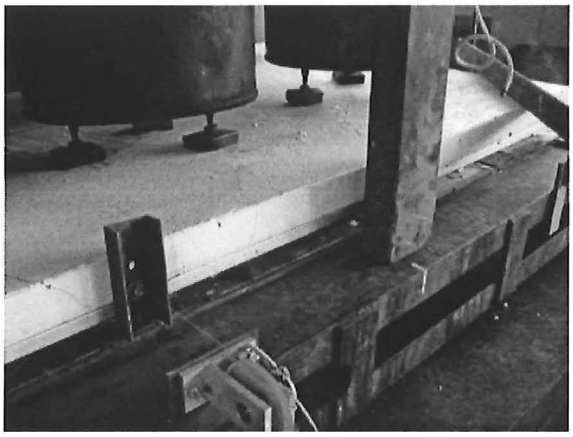

Appendix Fig. 71: Corner cracking of the slab during the fire test.

Appendix Fig. 72: Tilting of the drums due to the large deflections of the slab during the test.

Appendix Fig. 73: View of the demolished slab showing the unfractured reinforcing at midspan.

Appendix Fig. 74: View of the large surface cracks immediately after the fire test.

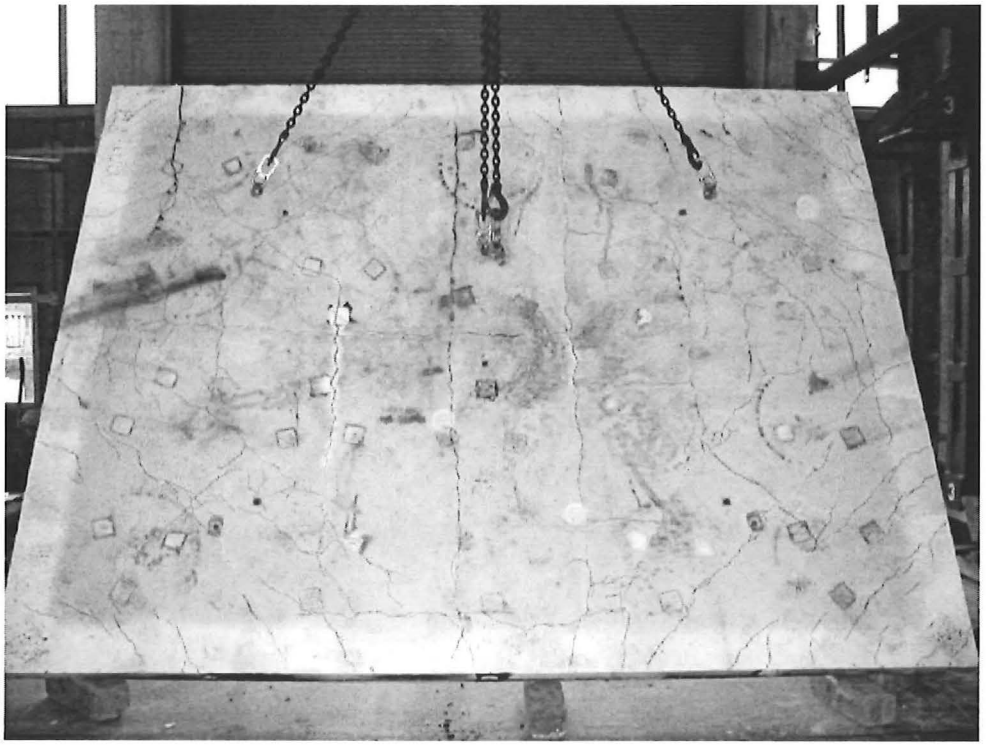

Appendix Fig. 75: Crack pattern of the top surface of the slab.

Test 4: Hibond slab

Appendix Fig. 76: Bottom view of the Hibond slab before the test.

Appendix Fig. 77: Hibond slab testing underway.

Appendix Fig. 78: Large surface crack in the longitudinal direction near the slab supports.

Appendix Fig. 79: Large surface crack in the longitudinal direction in the middle of the slab.

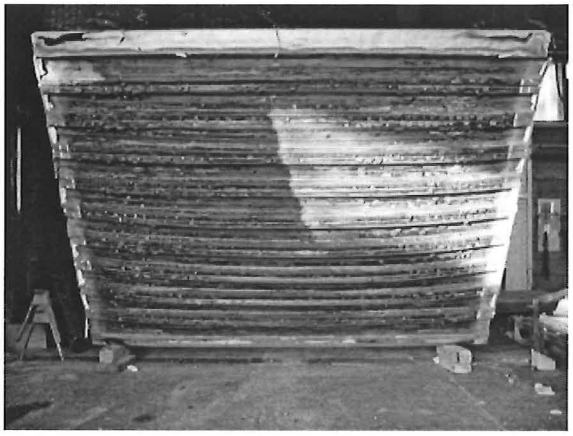

Appendix Fig. 80: View of the underside of the slab the day after the test.

Appendix Fig. 81: Holes in the steel decking due to oxidization.

Test 5: Traydec slab

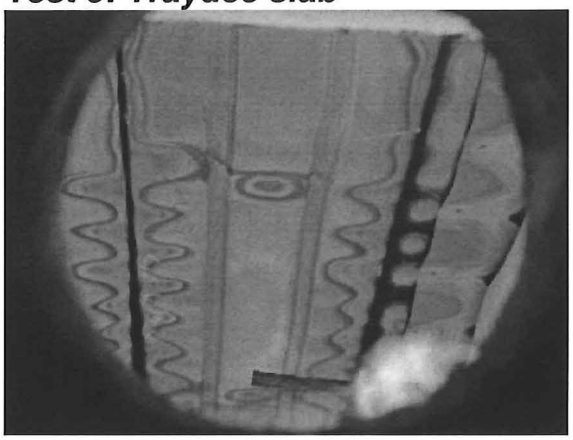

Appendix Fig. 82: Bottom view of the Traydec slab during the fire test.

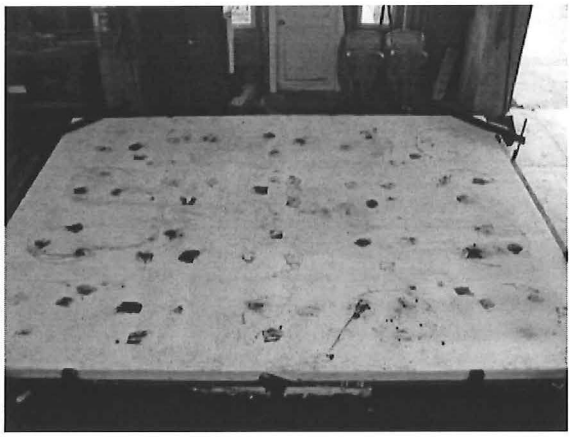

Appendix Fig. 83: Top view of the slab after the fire test, showing only small surface cracks.

Test 6: Speedfloor slab

Appendix Fig. 84: String of one of the potentiometers tied to the inserts, drilled into the slabs.

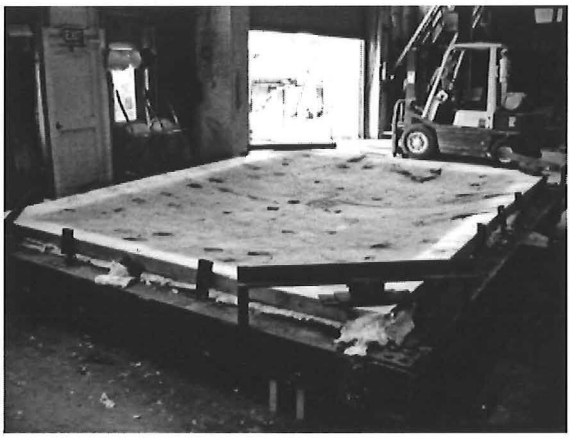

Appendix Fig. 85: Deformed shape of the slab after the test.

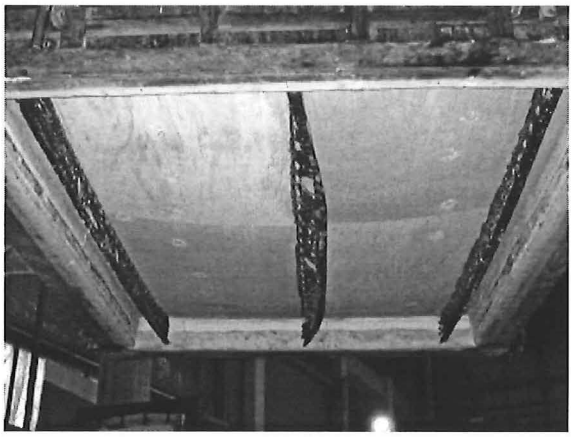

Appendix Fig. 86: Buckled centre joist of slab.

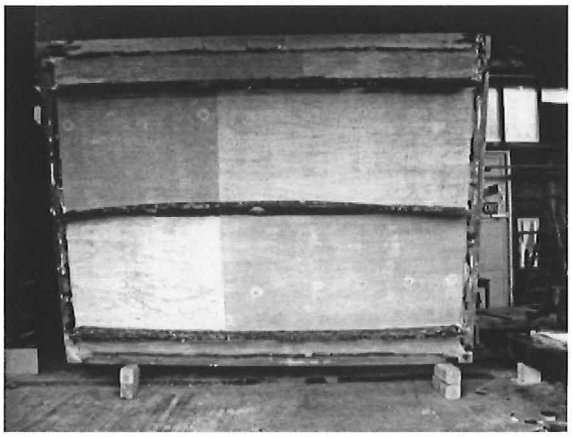

Appendix Fig. 87: Bottom view of the slab.

Miscellaneous photos

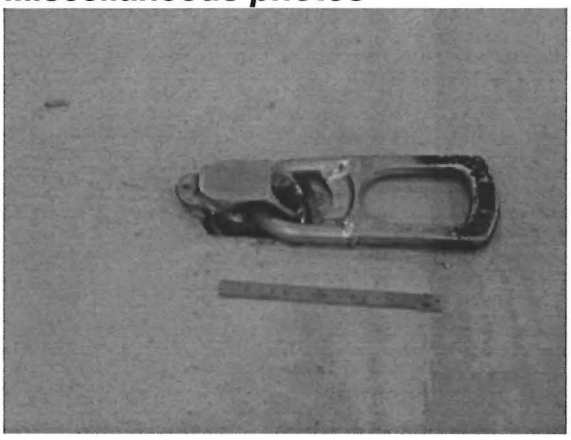

Appendix Fig. 88: View of the lifting insert recessed into the slab.

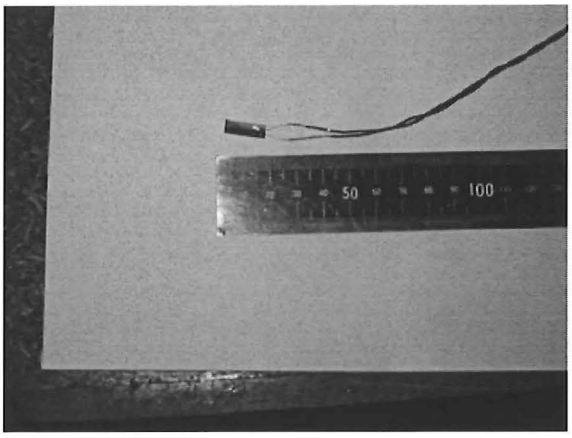

Appendix Fig. 89: High temperature strain gauge, ZFLA-6.350-11 from TML.

Appendix Fig. 90: Concrete cylinder crushing tests underway.

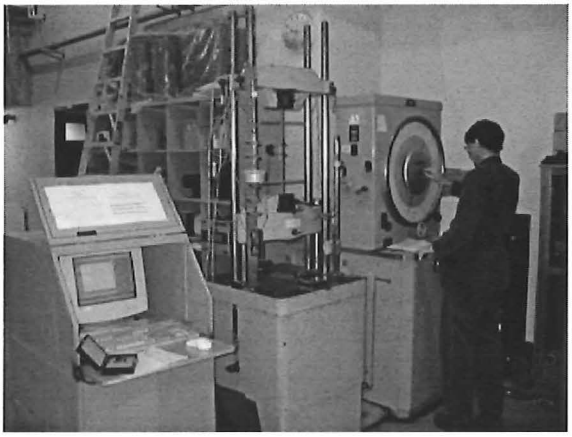

Appendix Fig. 91: Tensile tests of reinforcing steel.

FIRE ENGINEERING RESEARCH REPORTS

95/1	Full Residential Scale Backdraft	I B Bolliger
95/2	A Study of Full Scale Room Fire Experiments	P A Enright
95/3	Design of Load-bearing Light Steel Frame Walls for Fire Resistance	J T Gerlich
95/4	Full Scale Limited Ventilation Fire Experiments	D J Millar
95/5	An Analysis of Domestic Sprinkler Systems for Use in New Zealand	F Rahmanian
96/1	The Influence of Non-Uniform Electric Fields on Combustion Processes	M A Belsham
96/2	Mixing in Fire Induced Doorway Flows	J M Clements
96/3	Fire Design of Single Storey Industrial Buildings	B W Cosgrove
96/4	Modelling Smoke Flow Using Computational Fluid Dynamics	T N Kardos
96/5	Under-Ventilated Compartment Fires - A Precursor to Smoke Explosions	A R Parkes
96/6	An Investigation of the Effects of Sprinklers on Compartment Fires	M W Radford
97/1	Sprinkler Trade Off Clauses in the Approved Documents	G J Barnes
97/2	Risk Ranking of Buildings for Life Safety	J W Boyes
97/3	Improving the Waking Effectiveness of Fire Alarms in Residential Areas	T Grace
97/4	Study of Evacuation Movement through Different Building Components	P Holmberg
97/5	Domestic Fire Hazard in New Zealand	KDJ Irwin
97/6	An Appraisal of Existing Room-Corner Fire Models	D C Robertson
97/7	Fire Resistance of Light Timber Framed Walls and Floors	G C Thomas
97/8	Uncertainty Analysis of Zone Fire Models	A M Walker
97/9	New Zealand Building Regulations Five Years Later	T M Pastore
98/1	The Impact of Post-Earthquake Fire on the Built Urban Environment	R Botting
98/2	Full Scale Testing of Fire Suppression Agents on Unshielded Fires	M J Dunn
98/3	Full Scale Testing of Fire Suppression Agents on Shielded Fires	N Gravestock
98/4	Predicting Ignition Time Under Transient Heat Flux Using Results from Constant Flux Experiments	A Henderson
98/5	Comparison Studies of Zone and CFD Fire Simulations	A Lovatt
98/6	Bench Scale Testing of Light Timber Frame Walls	P Olsson
98/7	Exploratory Salt Water Experiments of Balcony Spill Plume Using Laser Induced Fluorescence Technique	E Y Yii
99/1	Fire Safety and Security in Schools	R A Carter
99/2	A Review of the Building Separation Requirements of the New Zealand Building Code Acceptable Solutions	J M Clarke

99/3	Effect of Safety Factors in Timed Human Egress Simulations	K M Crawford
99/4	Fire Response of HVAC Systems in Multistorey Buildings: An Examination of the NZBC Acceptable Solutions	M Dixon
99/5	The Effectiveness of the Domestic Smoke Alarm Signal	C Duncan
99/6	Post-flashover Design Fires	R Feasey
99/7	An Analysis of Furniture Heat Release Rates by the Nordtest	J Firestone
99/8	Design for Escape from Fire	I J Garrett
99/9	Class A Foam Water Sprinkler Systems	D B Hipkins
99/10	Review of the New Zealand Standard for Concrete Structures (NZS 3101) for High Strength and Lightweight Concrete Exposed to Fire	M J Inwood
99/12	An Analytical Model for Vertical Flame Spread on Solids: An Initial Investigation	G A North
99/13	Should Bedroom Doors be Open or Closed While People are Sleeping? - A Probabilistic Risk Assessment	D L Palmer
99/14	Peoples Awareness of Fire	S J Rusbridge
99/15	Smoke Explosions	B J Sutherland
99/16	Reliability of Structural Fire Design	JKS Wong
99/17	Heat Release from New Zealand Upholstered Furniture	T Enright
00/1	Fire Spread on Exterior Walls	FNP Bong
00/2	Fire Resistance of Lightweight Framed Construction	PCR Collier
00/3	Fire Fighting Water: A Review of Fire Fighting Water Requirements (A New Zealand Perspective)	S Davis
00/4	The Combustion Behaviour of Upholstered Furniture Materials in New Zealand	H Denize
00/5	Full-Scale Compartment Fire Experiments on Upholstered Furniture	N Girgis
00/6	Fire Rated Seismic Joints	M James
00/7	Fire Design of Steel Members	K R Lewis
00/8	Stability of Precast Concrete Tilt Panels in Fire	L Lim
00/9	Heat Transfer Program for the Design of Structures Exposed to Fire	J Mason
00/10	An Analysis of Pre-Flashover Fire Experiments with Field Modelling Comparisons	C Nielsen
00/11	Fire Engineering Design Problems at Building Consent Stage	P Teo
00/12	A Comparison of Data Reduction Techniques for Zone Model Validation	S Weaver
00/13	Effect of Surface Area and Thickness on Fire Loads	H W Yii
00/14	Home Fire Safety Strategies	P Byrne
00/15	Accounting for Sprinkler Effectiveness in Performance Based Design of Steel Buildings in Fire	M Feeney
00/16	A Guideline for the Fire Design of Shopping Centres	J M McMillan
01/1	Flammability of Upholstered Furniture Using the Cone Calorimeter	A Coles

01/2	Radiant Ignition of New Zealand Upholstered Furniture Composites	F Chen
01/3	Statistical Analysis of Hospitality Industry Fire Experience	T Y A Chen
01/4	Performance of Gypsum Plasterboard Assemblies Exposed to Real Building Fires	B H Jones
01/5	Ignition Properties of New Zealand Timber	C K Ngu
01/6	Effect of Support Conditions on Steel Beams Exposed of Fire	J Seputro
01/7	Validation of an Evacuation Model Currently Under Development	A Teo
01/8	2-D Analysis of Composite Steel - Concrete Beams in Fire	R Welsh
01/9	Contribution of Upholstered Furniture to Residential Fire Fatalities in New Zealand	C R Wong
01/10	The Fire Safety Design of Apartment Buildings	S Wu
01/11	Smoke Alarm Ownership in Relation to Socio-Economic Factors in Christchurch	N Buchanan
01/12	Accounting for Sprinkler Effectiveness in Performance Based Design of Steel Buildings for Fire	M Feeney
01/13	Equivalent Fire Resistance Ratings of Construction Elements Exposed to Realistic Fires	J Nyman
02/1	Performance of Expanded Polystyrene Insulated Panel Exposed to Radiant Heat	G Baker
02/2	A Comparison Between Predicted and Actual Behaviour of Domestic Smoke Detectors in a Realistic House Fire	D Brammer
02/3	Development of Bench-Scale Testing of Sprinkler and Smoke Detector Activation/Response Time	K S Chin
02/4	The Effect of Door Angle on Fire Induced Flow Through a Doorway	L R Clark
02/5	Implementation of a Glass Fracture Module for the BRANZ Fire Compartment Fire Zone Modelling Software	R Parry
02/6	Assessing the Feasibility of Reducing the Grid Resolution in FDS Field Modelling	N Patterson
02/7	Fire Safety Design of Ferrymead Heritage Park	M Rangi
02/8	Experimental Results for Pre-Flashover Fire Experiments in Two Adjacent ISO Compartments	L Rutherford
02/9	Measurement of Magnitude and Direction of Hot Gas Flow in a Fire Compartment with a Five-hole Probe	J Schulz
02/10	Assessment of the Current False Alarm Situation from Fire Detection Systems in New Zealand and the Development of an Expert System for Their Identifications	Y F Tu
02/11	Performance of Unprotected Steel and Composite Steel Frames Exposed to Fire	C Wastney
02/12	Experimental Fire Tests of Two-Way Concrete Slabs	L Lim

School of Engineering
University of Canterbury
Private Bag 4800, Christchurch, New Zealand

Phone 643 364-2250
Fax 643 364-2758